NEW MEXICO DEPARTMENT OF TRANSPORTATION

# RESEARCH BUREAU

Innovation in Transportation

# Advanced Statewide Calibration of MEPDG for NMDOT

## Final Report

Prepared by:
University of New Mexico
Department of Civil Engineering
Albuquerque, NM 87131

Prepared for:
New Mexico Department of Transportation
Research Bureau
7500B Pan American Freeway NE
Albuquerque, NM 87109

In Cooperation with:
The US Department of Transportation
Federal Highway Administration

**Report NM13MSC-02**

MAY 6, 2017

THIS PAGE LEFT INTENTIONALLY BLANK

# FHWA SUMMARY PAGE

| | |
|---|---|
| 1. Report No.<br>NM13MSC-02 | 2. Recipient's Catalog No. |
| 3. Title and Subtitle<br>Advanced Statewide Calibration of MEPDG for NMDOT | 4. Report Date<br>May 6, 2017 |
| 5. Author(s):<br>Rafiqul A. Tarefder, and Md Mehedi Hasan | 6. Performing Organization Report No.<br>456-01 |
| 7. Performing Organization Name and Address<br>University of New Mexico<br>Department of Civil Engineering<br>MSC01 1070<br>1 University of New Mexico<br>Albuquerque, NM 87131 | 8. Performing Organization Code<br>456A<br>9. Contract/Grant No.<br>456-391 |
| 10. Sponsoring Agency Name and Address<br>Research Bureau<br>7500B Pan American Freeway<br>PO Box 94690<br>Albuquerque, NM 87199-4690 | 11. Type of Report and Period Covered<br>Final Report<br>*April 6, 2013 – May 6, 2017*<br>12. Sponsoring Agency Code<br>New Mexico DOT |
| 13. Supplementary Notes<br>None | |

14. Abstract

The recently developed Mechanistic Empirical Pavement Design Guide (MEPDG), which is an improved and advanced methodology for the design of pavement structures, has enhanced the necessity to precisely characterize the pavement materials. A competent structural design of a pavement using MEPDG Level 1 analysis requires materials input parameters to be obtained from the laboratory test results. Currently, New Mexico Department of Transportation (NMDOT) is in the process of calibrating and implementing MEPDG. In this study, as a part of this effort, pavement materials such as subgrade, base, asphalt concrete, binder, aggregate, etc. were collected from seven selected pavement reconstruction sites in the state of New Mexico. Laboratory dynamic modulus, Fatigue Endurance Limit (FEL), dynamic shear rheometer, and resilient modulus tests were conducted on the collected materials. A database containing of all materials properties obtained from the laboratory tests has been generated and can be directly incorporated into MEPDG. Therefore, it will provide the pavement engineer and designer with valuable information for MEPDG analysis for all design level. Several field tests, which are additional to the originally proposed work, were also conducted and reported in this study. Additionally, all seven pavement sections were modeled and analyzed using the MEPDG for design Level 1, 2 and 3. Predicted distress quantities for fatigue cracking and rutting were compared among the three levels. The analysis results demonstrated that greater fatigue cracking and rutting in the Asphalt Concrete (AC) layer occurred in Level 2 and 3 compared to Level 1. The dynamic modulus of AC layer is under predicted at Level 2 and 3 resulting in higher rutting and fatigue cracking.

| | | | |
|---|---|---|---|
| 15. Key Words<br>MEPDG, Calibration, Dynamic Modulus, Fatigue Endurance Limit (FEL), Dynamic Shear Rheometer, Resilient Modulus ($M_R$) | | 16. Distribution Statement<br>*Available from NMDOT Research Bureau* | |
| 17. Security Classi. of the Report<br>None | 18. Security Classi. of this page<br>None | 19. Number of Pages<br>106 | 20. Price<br>N/A |

THIS PAGE LEFT INTENTIONALLY BLANK

**Project No. NM13MSC-02**

# ADVANCED STATEWIDE CALIBRATION OF MEPDG FOR NMDOT

Final Report
April 1, 2013 – May 6, 2017

Report Submitted to
Research Bureau
New Mexico Department of Transportation
7500B Pan American Freeway NE
PO Box 94690
Albuquerque, NM 87199-4690
(505)-841-9145
Research.bureau@state.nm.us

Prepared by
Rafiqul A. Tarefder, Ph.D., P.E.
Md Mehedi Hasan, Graduate Research Assistant

Department of Civil Engineering
MSC01 1070, 1 University of New Mexico
Albuquerque, N.M. 87131

## PREFACE

The research reported herein reviews information related to the advanced calibration of the Mechanistic-Empirical Pavement Design Guide (MEPDG). This includes the material collection, data collection, literature review, and laboratory testing needed to carry out this goal.

## NOTICE

The United States government and the State of New Mexico do not endorse products or manufacturers. Trade or manufactures' names appear herein solely because they are considered essential to the object of this report. This information is available in alternative accessible formats. To obtain an alternative format, contact the NMDOT Research Bureau, 7500B Pan American Freeway NE, PO Box 94690, Albuquerque, NM 87199-4690, (505)-841-9145.

## DISCLAIMER

This report presents the results of research conducted by the authors and does not necessarily reflect the views of the New Mexico Department of Transportation. This report does not constitute a standard or specification.

## ABSTRACT

The recently developed Mechanistic Empirical Pavement Design Guide (MEPDG), which is an improved and advanced methodology for the design of pavement structures, has enhanced the necessity to precisely characterize the pavement materials. A competent structural design of a pavement using MEPDG Level 1 analysis requires materials input parameters to be obtained from the laboratory test results. Currently, New Mexico Department of Transportation (NMDOT) is in the process of calibrating and implementing MEPDG. In this study, as a part of this effort, pavement materials such as subgrade, base, asphalt concrete, binder, aggregate, etc. were collected from seven selected pavement reconstruction sites in the state of New Mexico. Laboratory dynamic modulus, Fatigue Endurance Limit (FEL), dynamic shear rheometer, and resilient modulus tests were conducted on the collected materials. A database containing of all materials properties obtained from the laboratory tests has been generated and can be directly incorporated into MEPDG. Therefore, it will provide the pavement engineer and designer with valuable information for MEPDG analysis for all design level. Several field tests, which are additional to the originally proposed work, were also conducted in this study. Additionally, all seven pavement sections were modeled and analyzed in the MEPDG for design Level 1, 2 and 3. Predicted distress quantities for fatigue cracking and rutting were compared among the three levels. The analysis results demonstrated that greater fatigue cracking and rutting in the Asphalt Concrete (AC) layer occurred in Level 2 and 3 compared to Level 1. The dynamic modulus of AC layer is under predicted in Level 2 and 3 resulting in higher rutting and fatigue cracking.

## ACKNOWLEDGEMENTS

The authors would like to express their sincere gratitude and appreciation to Mr. Jeff Mann, Pavement Management and Design Bureau Chief, NMDOT, for being the advocate of this project and for his regular support, sponsorship, and suggestions. The University of New Mexico research team appreciates the valuable service and time from Mr. Virgil Valdez, Project Manager. His kind help in field work, material collection and so on are highly appreciated.

The UNM research team would like to thank the Project Technical Panel for their valuable suggestions during the quarterly meetings. Special thanks go to several Project Panel members namely, Naomi Gaede, Kelly Montoya, Shawn Romero, Parveez Anwar of NMDOT and James Gallegos, Materials Bureau Chief. The authors would like to thank the NMDOT's exploration crew, especially Ben Martinez.

This project is funded by the New Mexico Department of Transportation (NMDOT) Research Bureau. The research team also thank Luis Melgoza for FHWA's support. The authors would like to thank several members and personnel at UNM for their support. Special thanks to Ms. Rebekah Lucero, UNM Civil Engineering accountant.

# TABLE OF CONTENTS

# LIST OF TABLES

# LIST OF FIGURES

# INTRODUCTION

## RESEARCH NEED AND SIGNIFICANCE

The New Mexico Department of Transportation (NMDOT) uses the Mechanistic Empirical Pavement Design Guide (MEPDG[1]) Level 3 to design pavements. At Level 3, all the inputs necessary for a trial-design structure are assumed based on the available data in the MEPDG software to determine the pavement performance. MEPDG's Level 3 analyses includes uncalibrated model and unmeasured inputs; therefore, it is not known whether the field performances of the MEPDG- designed test pavement sections will perform to the level predicted. To better predict the field performance, this study proposes to collect, enhance and supplement statewide characteristic data from aggregate and asphalt binder sources for NMDOT's immediate use for the pavement design and MEPDG calibration.

The NMDOT is in the process of calibrating (Level 2 and Level 1) and implementing the new Mechanistic Empirical Pavement Design Guide (MEPDG), which requires laboratory testing and mechanical analysis of local materials. Generations of such laboratory data will enable NMDOT to optimally utilize the MEPDG in developing economical pavement recommendations. Guidance is required for the NMDOT pavement engineers to select resilient modulus values of soils, and dynamic modulus ($E^*$) values of Hot Mix Asphalt (HMA) mixes.

In addition, the fatigue performances of the NMDOT mixes and pavements are very important to the pavement designers. MEPDG predicts performance of pavements based on fatigue criteria. To ensure these predictions are correct, calibration is necessary to correlate between field performance and design predictions. Over time, the iterative calibration process will bring the theoretical or predicted pavement performance value closer to the actual measured pavement performance value.

To this end, the research approach proposed herein is developing calibration data from seven pavement sections (roadway reconstruction projects) designed by NMDOT using the MEPDG's Level 3 methodology. In particular, this proposed study will conduct laboratory tests to characterize mechanical properties and data of actual materials used, and collect data pertaining to the construction of the materials with the long term goal of calibrating the asphalt field distress performance with the MEPDG distress predictions. It is anticipated that this research project will require additional phases to continue the calibration process and adjustment of MEPDG prediction equations.

## OBJECTIVES

The primary objective of this research is to refine MEPDG predictions based on actual mechanical testing of pavement related materials and field performance at specific construction projects. The specific objectives of this study are to:

[1]MEPDG is currently termed as Pavement ME Design. However, only the term MEPDG will be used throughout the entire report to be consistent.

- Collect asphalt mixtures, binders, aggregates and subgrade soils samples from NMDOT sources, aggregate pits, etc., for selected reconstruction projects. Compact asphalt, aggregate, and subgrade soil samples to be representative of the actual field level.
- Conduct dynamic modulus tests in the laboratory for determining $E^*$ values of each HMA mix for each project.
- Determine $E^*$ master curves and shift factors of NMDOT asphalt mixes using sigmoidal functions for direct inputs of MEPDG Level 1 analysis.
- Conduct frequency sweep dynamic shear tests in the laboratory for determining shear modulus ($G^*$) and phase angle ($\delta$) of asphalt binders of New Mexico sources for direct inputs of MEPDG Level 1 analysis.
- Continue to populate the existing MEPDG's $E^*$ database with materials dynamic modulus data, mix volumetric data, and asphalt binders data to calibrate the existing $E^*$ predictive equation or to develop a new $E^*$ predictive equation of NMDOT mixes for MEPDG Level 2 analysis.
- Compact beam samples to a bulk density of 94.5 ± 0.5% of the maximum specific gravity ($G_{mm}$). Conduct fatigue tests in the laboratory for determining the Fatigue Endurance Limit (FEL) of NMDOT-designed asphalt mixes.
- Analyze the test results and evaluate the FEL value of mixes.
- Conduct resilient modulus test on the base course and subgrade soils in accordance with AASHTO T307. Determine *k*-values or coefficients of soil constitutive model used in MEPDG using regression and curve fitting.

## REPORT ORGANIZATION

This report is comprised of nine sections. Section 1 presents the research needs and objectives. Section 2 provides a comprehensive literature review of current practices and approaches of MEPDG calibration. In Section 3, construction sites selection and material collection are discussed. Section 4 presents dynamic modulus ($E^*$) specimen preparation and testing. In Section 5, evaluation of Fatigue Endurance Limit (FEL) of collected asphalt concrete mixture is discussed. Section 6 presents laboratory testing for shear modulus ($G^*$) and phase angle ($\delta$) of asphalt binders. In Section 7, laboratory resilient modulus ($M_R$) testing of base course and subgrade soils is discussed. Section 8 provides various field testing conducted on different layers of a pavement. In Section 9, conclusions are made from the findings of this research and future research recommendations are presented.

# REVIEW OF CURRENT PRACTICES

## INTRODUCTION

In this task, a thorough and comprehensive literature review is performed to identify and compile currently available literature pertaining to local calibration of MEPDG including efforts being used in various states. This review shows the most efficient and effective way to rank the tasks needed for MEPDG calibration as well as give direction on what tasks must be completed before calibration is even attempted. Some of these pre-calibration tasks are: performing sensitivity studies which provide information on important inputs and needed accuracy of testing, learning calibration techniques both specific to MEPDG and in general, learning the MEPDG models and how the program works, learning about the various pavement distress models inside MEPDG their issues, problems, and inputs, and learning about the reliability of not only the calibration itself but also the reliability of the design that is being calibrated.

## LITERATURE REVIEW

This subsection summarizes some of the most important literature for this project and present the brunt of the information essential for correctly calibrating MEPDG.
Muthadi and Kim (*1*) conducted a calibration study in North Carolina. The rutting and bottom up fatigue cracking were the two models calibrated in MEPDG version 1.0. For this study, 53 pavement sections were selected from the Long-Term Pavement Performance database (LTPP) and North Carolina Department of Transportation (NCDOT) databases. Microsoft Excel's Solver was used to calibrate the rutting model. The authors was not able to calibrate the alligator cracking model in the normal manner through calibration factors, and thus had to adjust the transfer equation to calibrate it. The error was greatly reduced after calibration to less than the global error. Both models developed were retained for use in later and more advanced calibration. Thirty of the pavements were from LTPP and 23 were from NCDOT. There was one problem with the damage values, LTPP and NCDOT measure damage in two different ways and thus the damage data was not able to be consolidated. Both rutting and fatigue cracking models were determined to be satisfactory after calibration. As is common, a split section approach was used with 80% of the sections being used to calibrate and 20% were used for validation. Trench field testing was unavailable and thus the ratios for rutting in different layers were based on the predicted values. The only questionable part of this study that may introduce error is the statistical model for fatigue. The authors theorize that this is from the different damage measurement used by NCDOT; to remedy this more advanced calibration should be done with more sections. The validation showed good fit and increased accuracy due to calibration. Chi-squared tests were used to confirm the calibration was successful.

Li et. al. (*2*) detailed the steps taken by the Washington DOT to calibrate the MEPDG version 1.0 to state conditions. The article gives detailed descriptions of preparation for calibration, needed data, inputs used to simplify calibration, results, issues, and observations they found throughout the calibration process. The authors found for calibration the following things would be needed: 1) specific traffic data, preferably one relevant axle load spectra for the state, 2) specific climate data, 3) intensive pavement structure knowledge including used binders, soil, lift depths, material, aggregates, and subgrade soils, and 4) distress data, preferably for years preceding calibration.

The calibration was broken down into 5 parts: Bench Testing, Model Analysis, Calibration, Validation, and Iteration. Bench testing is primarily used to verify that the program is correctly showing understood pavement behavior, for example the binder properties and asphalt layer thickness most influence longitudinal cracking. Model analysis is used to determine the importance of the different calibration factors and the correct order of calibration. This was done using both sensitivity analysis and elasticity analysis. Elasticity analysis determines what affect the calibration factor had on pavement distress models. Calibration was performed using certain sections of road used for calibration. Next these calibrated equations were validated with independent sections around the state. These steps were then repeated through iteration until a reasonable accuracy was achieved. Through this calibration many conclusions were found. The distress models except roughness calibrated; roughness had a bug that prevented accurate calibration. This may be fixed in newer versions of MEPDG. The authors also found that Level 1 calibration was not possible with version 1.0 of MEPDG due to processing errors.

Hoegh et. al. (*3*) used data from a Minnesota study section (MnRoad) and other sections to calibrate the rutting model in MEPDG. This is done through extensive and detailed comparison of predicted versus actual total rutting, asphalt layer rutting, and measured rutting. The approach used by the authors was to first identify sections that have enough data to contribute to the calibration, second, data was obtained for the MEPDG inputs, third, the authors ran MEPDG, and fourth, they compared predicted and actual damage, and then calibrated MEPDG. After comparing actual with predicted damage many things were found to be wrong with the rutting model. One of the issues found was that MEPDG 1.0, the version used in this study, had a bug in it that made a significant difference when using Level 2 versus Level 3 design levels. When it was looked at more closely it was found that Level 2 designs did not model the binder behavior correctly, whereas Level 3 did. Because of this bug, the investigators were forced to use Level 3 for material inputs. Further comparison found that the total rutting was consistently over predicted. What would normally be easy to correct with calibration was more difficult due to the varying degrees MEPDG would over predict base and subgrade while grossly under predicting Asphalt Concrete (AC) rutting. They found no relation between the sections that were under predicted and the sections with prediction close to the total rutting. Also, the rutting model suggested 50% of the total rutting in the subgrade and base occurred in the first month under 1% of the total traffic the pavement. This is obviously inaccurate. To help alleviate this rutting issue, the authors developed an adjusted total rutting equation. This adjustment in total rutting did help some but more adjustment was warranted. The authors suggested a new procedure for finding the total rutting. In conclusion, abnormal rutting was found, i.e., that similar sections had significantly different predicted damage. The subgrade and base had unreasonably high rutting damage in the first month. Through an adjustment to the MEPDG outputs combined with calibration, the issues in the rutting model were compensated for.

Hall et al. (*4*) summarized the initial calibration of Arkansas MEPDG. The LTPP and Pavement Management Systems (PMS) were used for most of the inputs to calibrate. Unfortunately, the authors found their data collection to be insufficient and suggested more in depth data collection for further calibration. Microsoft Excel Solver function was found to be useful to optimize alligator cracking coefficients. Of the many sites used for calibration 20% were randomly selected for validation. In Arkansas asphalt treated base was used extensively. In order to model this in MEPDG, the authors either modeled it as asphalt that is moisture sensitive or as a base that is temperature sensitive; both ways create erroneous results though. The typical transverse cracking

was not found to occur in Arkansas and the MEPDG results reflected this; however, there is transverse cracking by other means that isn't reflected in MEPDG. The authors did not calibrate transverse, longitudinal cracking, or IRI in this study. Default values of rutting in granular base were used in the calibration. The rutting models were improved by calibration; alligator cracking was not improved. This was known because the measured cracking versus predicted cracking was still statistically different.

Momin (*5*) calibrated the MEPDG to local conditions of the northeastern region of the United States. This was done by analyzing 17 pavement sections as well as data from the LTPP database. The differences were compared and coefficients developed for use in the MEPDG. The study also found a good format to follow for calibrating. It started with a literature review, then analysis of design practices followed by the MEPDG, followed by the extraction and collection of data, a "development of input data for the MEPDG along with implementation guidelines," and lastly, the calibration of the MEPDG for local conditions.

Pierce et. al. (*6*) discussed how to use existing PMS to calibrate the MEPDG program. In order to do this the author found the challenge of trying to combine two different data formats one from the PMS and the other from MEPDG. The calibration process was applied in MEPDG version 1.1. To be able to use PMS data for MEPDG calibration would save time and money for the NMDOT, construction crews, and the calibrators. The chosen state for this study was North Carolina. There were many challenges with calibration including a lack of data points, the subjective way North Carolina used to measure distress, and the limited data available to the calibrators. Despite these challenges, they were able to successfully calibrate the MEPDG. One aspect that may affect the results they found is the validity of the pavement condition collection procedures. Another aspect that may affect the results is how the cracks are measured.

Wu et. al. (*7*) compared the results from MEPDG with PMS data in Louisiana. The three modes of distress evaluated were fatigue cracking, rutting, and International Roughness Index (IRI). All of these were shown to have a strong dependency on the structure of the pavement. When comparing the PMS data over time with MEPDG fatigue cracking and IRI were sufficiently close, but rutting was over predicted. Part of this study used an optimization approach to select preliminary calibration factors for MEPDG 1.1; specifically, rutting calibration factors for two types of flexible pavements. In MEPDG, Level 3 design inputs were used and transverse cracking was neglected due to its rarity in Louisiana pavements. Rutting and IRI damage was found to follow a normal distribution whereas fatigue cracking did not. The AASHTO criterion was thought to be overly stringent and overly conservative, which agrees with previous work.

Quintus et. al. (*8*) calibrated and validated the MEPDG rutting model for MEPDG 1.0. They worked on two research projects. These projects used three phases to accomplish its objectives: first, database extension with testing, material collection, trench studies, etc., second, determination of appropriate alternative transfer functions and testing matrix to test the original and three alternative models, and third, laboratory testing, calibration, and validation. The researchers have found several things they have learned through this study which are helpful guidelines to future calibration studies.

1. A researcher can never have too much material and MRL (Materials Reference Library) is useful and should be supported by researchers.
2. The differences in residual errors for Level 3 which predicts Dynamic Modulus vs. Level 1 where Dynamic Modulus is an input are small. This means that the differences seen between actual and predicted rut that the researchers found are not caused primarily by Dynamic Modulus as originally thought. There are other parameters that influence rutting in addition to Dynamic Modulus.
3. Stress term is recommended to be implemented, but the researchers found reasonable predictions in models without a stress term.
4. Do not underestimate the value of workshops. The researchers found these as invaluable for determining ideas, concepts, and actual behavior of pavement.
5. Measurement error was found to comprise a large majority of the total error. This should be something to be aware of and looked into in future studies.
6. The depth functions in the original MEPDG were found to be reasonable, although they need thickness adjustment factors to be accurate.
7. The original MEPDG aging model showed reasonable results and needs no adjustment.

Waseem and Yuan (*9*) calibrated rutting in MEPDG done in Ontario, Canada. The main focus is on flexible and reconstructed pavements using PMS data. Longitudinal calibration was done, which is a unique feature of this study. This means that "the local calibration parameters in the three permanent deformation models were adjusted to predict the field observed rut depths over the whole life span of the pavement section". Longitudinal calibration is more accurate and comprehensive than a regular calibration adding to the ability to quantify the significance of the values. There are three models that MEPDG uses for rutting, one for HMA or AC, one for unbound granular materials, and the third for fine-grained soil. After analyzing many studies, it was found on average 57% of the rutting came from AC, 27% of the rutting came from the base layer, and 16% came from the subgrade. When comparing these values to MEPDG default models, a large disagreement was found. Instead of the aforementioned values, MEPDG gave an average of 20% rutting in AC, 12% granular base/subbase layer, and 68% in the subgrade. Obviously, this is drastically different from the empirical results. Due to this and finding contradicting studies and models, the authors decided to use the AASHTO ratios measured in 1962; which is 32% for AC, 59% in granular layers, and 9% in fine-grained soil. In calibrating MEPDG Macro-Excel files were linked with MEPDG to assist with calibration. Ten reconstructed pavement sections were used. Each pavement section was calibrated individually for the 5 calibration parameters and then the parameters were compared. There were large variations found in all parameters. For AC $B_{AC1}$ (one of the calibration parameters) the value varied from 0.162 to 0.470 this is an unexpectedly large variation. The large variation is confusing and the authors don't have a reason for such extreme variance in the local parameters. A pooled residual sum of squares minimization was performed on all 10 section but a poor fit was still seen for average values to use as the calibration parameters. In conclusion, it was found that section by section calibration was effective, but the spread of calibration parameters was large. This variation causes difficulties in implementing the calibration.

**Other Mechanistic-Empirical Design Programs Calibrations**

In addition to MEPDG specific calibrations, calibrations of other mechanistic-empirical pavement design programs in other countries were considered. As these are not specifically related to

MEPDG itself these studies were used more as general information on calibrating a design program of this complexity and were not studied in depth.

Le et. al. (*10*) analyzed and calibrated the Korean Pavement Design Guide (KPDG), which is similar to the MEPDG. The authors proposed ideas to reduce computational power to run these types of programs. One of the ways to reduce computational power is to group similar time periods based on regularity of climate and axle load magnitude characteristics. Another is to reduce the amount of points analyzed on the road to only critical points.

Saleh (*11*) calibrated the Austroads Mechanical Empirical Pavement Design, specifically the calibration and testing of the adopted Shell Fatigue Transfer Function. The calibration was done using lab testing with the suggestion of future field calibration. Calibration created a 26-27% decrease in pavement layer thickness.

Suh et. al. (*12*) described a Korean study of accelerated pavement testing (APT). More specifically, it is a use of APT to calibrate a laboratory rutting model. In APT, a full-size asphalt section is built and then a device rolls a truck wheel in a common axle configuration at a decided loading and speed. This study was conducted on a three layers AC with an AC layer of 30 cm, subbase of 30 cm, and subgrade of 180 cm. Two deflectometers were set in the pavement at 12 cm and 30 cm. The following two equations were used for calibration using the APT. The first equation is for AC and the second for aggregate.

$$\frac{\varepsilon^p}{\varepsilon^r} = \beta_{r1} 10^{0.044} N^{0.185\beta_{r2}} T^{-0.708\beta_{r3}} ACV^{0.688\beta_{r4}} \quad (1)$$

$$\frac{\varepsilon^p}{\varepsilon^r} = \beta_{r1} 10^{0.171} N^{0.159\beta_{r2}} T^{-0.603\beta_{r3}} AV^{0.116\beta_{r4}} \quad (2)$$

where $N$ is the number of load repetitions, $T$ is the temperature in °C, AV is the air void in percent, $\beta_{rj}$ are calibration factors. This equation, unlike the AASHTO 2002 equation, takes in account the AC layer temperature, the number of load repetitions, and air void ratio. The KENLAYER program was used for multilayer elastic analysis to assist in the calibration. After testing, the equation was adjusted to the following.

$$\frac{\varepsilon^p}{\varepsilon^r} = 10^{-1.85927} N^{0.3755} T^{1.5528} ACV^{-0.89602} \quad (3)$$

**MEPDG Literature**

This area of literature is important because it is essential to understand what is being calibrated. MEPDG itself needs to be understood: how the program reacts to inputs, what inputs are where, how the various pavement distresses are found, etc. In addition, the subcategory of specific distress models in MEPDG is important to know.

Newcomb and Quintus (*13*) explored pavement load response and performance relationships. Rutting and fatigue cracking were used as examples. The authors use the simplified relationship between rutting and vertical strain and fatigue cracking and bending strain to show how transfer equations relate stress and strain in the pavement to damage. The author also talks about how moduli are usually used to refine the transfer equations. Transfer equations are also known as

performance equations, performance criteria, and failure criteria. Finally, the author brings up the idea of endurance limit, a strain limit that is small enough that the load that causes that strain may be repeated infinitely without failure of the pavement. This would create a pavement that could last forever, a perpetual pavement.

Transportation Research Board (*14*) suggested the changes made to the MEPDG program up to the 0.900 version. These changes were found during the National Cooperative Highway Research Program (NCHRP) study 1-40D. The digest mainly discusses technical improvements and enhancements.

Golalipour (*15*) tested and evaluated the parameters for rutting. One of the surprising conclusions found by the author is that the shear modulus and phase angle had little correlation with rutting. This parameter has been used for years to detail the rutting susceptibility of pavement. When Superpave was developed along with modified binders, many studies found there was a poor correlation between this parameter and rutting. The multiple stress creep and recovery test has gained a lot of interest as a replacement, unfortunately it still has too many problems to become the main test for rutting. This study focuses on this test and how it can be adjusted in order for it to become a proper rutting test. To do this, the role of binder mixtures, temperature, stress level, and number of cycles effect on rutting was investigated. This study brings into question using the shear modulus and phase angle for rutting in MEPDG.

Zhou et. al. (*16*) did a validation study done in Tennessee where PMS and MEPDG results were compared using MEPDG version 1.1. The data that was not available for the materials was estimated using the Witczak model. Both roughness and rutting were evaluated. It was found that AC rutting was more accurate at Level 1 and over predicted at Level 3. The method followed for calibration prior to this study was: data was collected, then the MEPDG predicted values were found, and finally the actual damage was compared to the MEPDG predicted damage. For the climate inputs only complete climate files were used and not combination climate files. The traffic was back calculated out of Equivalent Single Axle (ESALs) that were obtained from the PMS. Nineteen sections in Tennessee were chosen for this study. Both design levels over predicted rutting, with the level combination of Level 1 and Level 2 inputs being the most overly predicted. The base and subgrade were considered the main sources of over prediction. MEPDG also under predicted roughness. In this study, MEPDG wasn't found to be sensitive enough to climate, traffic, and materials inputs.

Wen and Bhusal (*17*) investigated the possibility of using repeated loading of the indirect tensile test as a replacement of the FEL test and rutting prediction test. The test is done on a similar machine to the dynamic modulus test except the sample is turned 90 degrees. At intermediate temperatures it was found that fatigue could be found from cyclic Indirect Tension (IDT) and good results were found. The authors determined after seeing the results, that the cyclic IDT could possibly be used for rutting and fatigue in place of traditional tests such as the FEL. More validation is needed, though, to strengthen this conclusion. If it can be used for this purpose it would be a great advantage to both construction and research. One test can then be used for fatigue, rutting, thermal cracking, and moisture damage.

**Models in MEPDG**

Priest (*18*) developed an accurate model for fatigue damage. Most fatigue models are developed by adjusting a basic model by calibration or shifting to fit laboratory or field data. One of the main objectives of this study is to relate binder and thickness of layers to fatigue performance. Eight test sections from NCAT were used for this study. In this study, failure is determined to be 20% cracking of the design lane. Through literature research, the authors found that fatigue cracking is dependent on the stiffness of the pavement. All lab testing has to be shifted to some degree to match field fatigue. The authors think there is a weak correlation between laboratory tests and field performance; this is due mainly to the large variation in shifting values. If there was a strong correlation, these values would be much closer together instead the values vary from 1 to 400. After extensive literature, the authors did their own study. When this report was written three of the sections had failed, all of them had been able to survive past their design life, though. From these three sections, a fatigue transfer function was developed. The authors took a previously designed equation and simplified and calibrated it to match the results of the failed sections. The final equation is as follows:

$$N_f = k_1 * \left(\frac{1}{\varepsilon_t}\right)^{k_2} \left(\frac{1}{E}\right)^{k_3} \quad (4)$$

where $N_f$ = number of load cycles, $\varepsilon_t$ = applied horizontal tensile strain, $E$ = HMA mixture stiffness, $K_i$ = regression or calibration constants. The authors found that one model was not sufficient for fatigue cracking. They needed one model for thin pavements, one for thick, and a third for the "rich bottom" section. Using these three models removed the need for a shift factor.

Xiao et. al. (*19*) have been working on MEPDG model in the state of Arkansas. The objectives for this study are to: 1) find how the differences in distress definitions in LTPP and MEPDG affect calibration, 2) determine whether to classify longitudinal cracking in wheel path as alligator cracking, and 3) determine if the functions should be weighted to combine low, medium, and high sensitivities. The result was that the differences in LTPP and MEPDG are significant when calibrating MEPDG. Longitudinal cracking was found to be better taken as alligator cracking to have a more accurate calibration. Lastly, they found no data to suggest a weighting function was critical.

Wang et. al. (*20*) used 12 full scale test sections to characterize rutting development in subgrade using Heavy Vehicle Simulator (HVS) loading. The 12 test sections were a mixture of four soil types and 3 moisture contents. In this study, only subgrade type A-2-4 and A-4 soil types were used. The performance of the subgrade was found to be a function of soil type, moisture content, and applied stress condition. A secondary part of this study was to compare MEPDG predicted and observed rutting. MEPDG rutting model was found to have inaccuracies and the authors developed two models for the two soil types analyzed that reflected the observed rutting from the HVS testing much better. The authors surmise that with further validation and calibration these models will be an improvement over the current model. When the testing was done it was found that moisture content significantly affected deformation; the higher the moisture content the higher the deformation. Even a small change in moisture content from 18.9% to 21% moisture content dramatically affected the bearing capacity of the pavement. The finer the soil type, the more deformation was observed hence the authors determined that particle size is an important part of

rutting. The authors thought that modification is needed in MEPDG since it did not have the sensitivity to take in account soil type or stress. A relation was found between deviatoric stresses and rutting which is another factor that MEPDG does not take in account in the transfer equations. The authors determined this was another factor that needs to be in the modified model.
When developing the MEPDG transfer equation for rutting, the NCHRP 1-37A chose the Tseng-Lytton model for MEPDG. That equation is as follows:

$$\left(\frac{\varepsilon_0}{\varepsilon_r}\right) = \frac{\left(e^{(\rho)^{\beta}} * a_1 E_r^{b_1}\right) + \left(e^{\left(\frac{\rho}{10^9}\right)^{\beta}} * a_9 E_r^{b_9}\right)}{2} \tag{5}$$

$$\log \beta = -0.61119 - 0.017638 W_c$$

$$\rho = 10^9 \left\{\frac{C_0}{[1-(10^9)^{\beta}]}\right\}^{\frac{1}{\beta}} \qquad C_0 = \ln\left[\frac{\left(a_1 E_r^{b_1}\right)}{a_9 E_r^{b_9}}\right]$$

where $\varepsilon_p$ = permanent strain; $\varepsilon_o$, $\beta$, and $\rho$ = material properties; $\varepsilon_r$ = resilient strain imposed in laboratory test to obtain material properties $\varepsilon_o$, $\beta$, and $\rho$, $W_c$ = moisture content (%), $E_r$ = resilient modulus (psi); $a_1$ (=0.15), $b_1$ (= 0.0), $a_9$ (= 20.0), $b_9$ (= 0.0) = constants. From this equation it can be seen that the rutting is mainly dependent on moisture content with stress and soil type playing a very small part through the resilient modulus. Due to this, the A-4 soil rutting was over predicted and the A-2-4 soil was under predicted. This error is most likely due to the stress and soil type not taken into account and a small part from lack of calibration.

The following new permanent strain model was developed from the Uzan strain model.

$$\frac{\varepsilon_p}{\varepsilon_r} = a_1 \left(\frac{\theta}{P_a}\right)^{a_2} \left(\frac{\tau_{OCT}}{P_a} + 1\right)^{a_3} W_c^{a_4} N^{\left[b_1 \left(\frac{\theta}{P_a}\right)^{b_2} \left[\left(\frac{\tau_{OCT}}{P_a}\right)+1\right]^{b_3} W_c^{b_4}\right]} \tag{6}$$

where $W_c$ = moisture content, $N$ = number of load repetitions; $\theta$ = bulk stress ($\theta = \sigma_1 + \sigma_2 + \sigma_3$), $\tau_{OCT}$ =octahedral shear stress, $P_a$ = atmospheric pressure, $a_i$ and $b_i$ = constants. As can be seen the new permanent strain model does take in the affect stress and soil type and is adjusted by the $a_i$ and $b_i$ parameters. This model shows much more promise than the previous MEPDG model. This adjustment of the above model can create multiple models for different soil types.

Zborowski and Kaloush (*21*) did an evaluation of newer models and MEPDG's model for thermal cracking. The main focus is on rubber asphalt mixes and includes refinements to the IDT protocol, which was developed to evaluate thermal cracking resistance. A new crack depth fracture model is presented and evaluated. The model is evaluated through laboratory tests and rational from field observations, and is found to be satisfactory. Twenty-three mixes from 7 different projects with 13 conventional mixtures and 10 modified with asphalt rubber mixtures were used in this study. Part of this study, the Paris Law for Crack Propagation, was used to assist in the development of the model.

The model that MEPDG uses for thermal cracking is TCMODEL (thermal cracking model); in the authors experience it is inadequate to characterize thermal cracking. Although TCMODEL is adequate for low temperature cracking, asphalt concrete mixtures, conventional binders, and distinct or extreme pavements characteristics, it is not adequate outside of these bounds. Included in this group is modified asphalt concrete mixtures. The TCMODEL uses only the slope of creep compliance and tensile strength at -10 $^0$C from IDT tests. The reason for this is the idea that the stronger the tensile strength at these temperatures the less susceptible to thermal cracking the pavement must be. This assumption is incorrect with modified AC's because while the modified AC has poor tensile strength from IDT tests, it has exceptional thermal cracking resistance. Naturally, this brings into question the validity of using tensile strength as an indicator, and the authors theorize that total fracture energy may be a more accurate indicator. Thus the new model takes into account the total fracture energy and the IDT test is adjusted to supply this new variable. From these results and research from past years it shows that the old MEPDG thermal model gives irrational results. Furtehr, this study disproves the link between high tensile strength and thermal fracture resistance.

Huvstig (*22*) did a validation of a new rutting model in the Nordic countries. As a part of validating the model the shakedown theory was validated as well. In the shakedown theory the deformation according to loading is split into three different behavior zones depending on the applied stress. At the first level of stress there is less deformation with each loading; this is commonly considered to be compaction. The second level of stress is where the deformation is proportional to the load; this is generally considered creep. And the third level is complete collapse otherwise known as shear flow. The first limit between the first and second stress level is called the plastic shakedown limit and the second limit between the second and third stress level is called the plastic creep limit. As a part of this study, it was found that there is a strong correlation between rutting and cracking and roughness. In addition, the shear stress level was theorized to be the most important in pavement behavior. Eight road sections were chosen that are 10-20 years old LTPP roads.

It is commonly known that compaction begins happening rapidly and then evens out to a constant lower value over time. This would be fairly straightforward to predict except that over the course of the study the roads showed stress that would go beyond the plastic shakedown and plastic creep limit. This means that for these instances in time the pavement would not act in a predictable way. Surprisingly, the data showed that even the failure limit was exceeded, however, the pavement did not actually fail. Therefore, the authors theorized that the material had been plasticized. When the LTPP sections were evaluated, the permanent deformation was mostly in the unbound materials. The following equation is the model used in MEPDG for permanent deformation.

$$\frac{\varepsilon_p}{\varepsilon_r} = a_1 * N^{a2} * T^{a3} \quad (7)$$

where $\varepsilon_p$ = permanent strain, $\varepsilon_r$ = resilient strain of the asphalt material, $N$ = Number of load repetitions, $T$ = temperature and $a_i$ = non – linear regression coefficients.

**Sensitivity Studies**

Sensitivity studies are essential because these are the studies that guide material and data collection. Sensitivity studies look at how "sensitive" a computer program or design equation is

to percent changes in inputs. These studies show which parameters have a large effect on the outputted distresses and which parameters have insignificant affect. Obviously, this is important in determining where the focus should be in data collection, material collection, and testing.

Li et. al. (*23*) did a sensitivity analysis on a typical axle load spectra found in Washington State. The focus of the sensitivity analysis was on longitudinal cracking, alligator cracking, rutting, and IRI. Transverse cracking was ignored as it was found that Axle Load Spectra (ALS) had no effect on it. MEPDG was found to under predict damage when compared to actual damage. Annual average daily truck traffic and annual growth rate changes affected the performance of the pavement more than ASL did. The three main conclusions found were, 1) one typical ALS could be used to represent all of Washington State Department of Transportation (WSDOT) in MEPDG, 2) MEPDG is moderately sensitive to ALS for WSDOT pavement designs, and 3) MEPDG needs to be calibrated for Washington State conditions.

Sumee (*24*) did a thesis that explores the sensitivity of MEPDG to New Mexico inputs by advanced statistical methods. This study is conducted in three parts; first, the author collected New Mexico specific data from LTPP and NMDOT, second, the author ran a basic sensitivity analysis that changed one parameter at a time, and third, the author took the most sensitive variables from the previous step and did advanced statistical analysis to determine sensitivity with interactions between the parameters. The first step was in order to find the ranges, distributions, and means of New Mexico parameters. The second step was to minimize time and computational need for the advanced statistical analysis, the most significant parameters were chosen according to MEPDGs' sensitivity. The third step was done using both parametric and non-parametric statistical analysis. It was found that the traffic inputs such as AADTT (annual average daily truck traffic) and percent of truck traffic in the design lane were significant parameters for all forms of pavement distress evaluated. It was also determined that rutting, both surface and total, was the most severe and prevalent pavement distress in New Mexico. Rutting was determined to be highly sensitive to both AADTT, percent of trucks in design lane, and the bottom AC layer thickness. IRI, longitudinal cracking, and alligator cracking were found to be highly sensitive to bottom AC thickness. The MEPDG outputs were sensitive to HMA parameters such as thickness, percent air voids, binder content, and Performance Grade (PG) of binder. Longitudinal and transverse cracking was found to be especially sensitive to base course, material type, modulus, and thickness. The water table depth did not affect any of the parameters strongly so all output parameters were deemed insensitive to this. The other parameters that had little to no effect on the outputs were operational speed and design lane width. Due to time constraints, not all parameters were able to be checked in this study. The parameters examined in this study were AC mix properties, AC thickness, base thickness, ground water table depth, operational speed, traffic inputs especially AADTT, base material properties, and subgrade type. Rutting was found to be sensitive to the most parameters, which leads the author to conclude that the MEPDG rutting model is in severe need of calibration for New Mexico. After the research had been accomplished, the author discussed the limitations of this study and what should be done in future MEPDG sensitivity studies. First, the author admits there is a lack of data for this study and that further studies should find more data on the ranges and distributions of the input parameters. Secondly, individual sieve analysis results were not covered in this study and thus the changes in gradations need to be taken into account. Also, dynamic modulus, creep compliance, and tensile strength parameters would greatly enhance the

accuracy of future studies. Finally, given the sensitivity seen to traffic parameters it is essential for future studies to have as accurate as possible traffic data, particularly for the AADTT.

Diefenderfer (*25*) determined the sensitivity of the MEPDG outputs to HMA and binder inputs as well as data collection. In order to do this, the author modeled two roads, an interstate and primary road. It was found that rutting fatigue between the three levels was different but not statistically significant. The fatigue for the primary route was over predicted. It was also found that fatigue error was always greater than distress error for all predictions. The study identified the different sensitivities of different failures for the Level 1, 2, and 3 MEPDG analyses. The author recommended further calibration as well as local calibration and verification of rutting and fatigue predictive models.

El-Badawy (*26*) did a compilation of literature review on sensitivity studies and a study of his own to find how the different inputs affect the predicted damage. The factors were found for longitudinal cracking, alligator cracking, and rutting. The results of this study are from a single layer HMA. From the literature review, it was found that base and subbase type and thickness had little to no effect on HMA rutting. Two structures were analyzed: a 6 in HMA, with a 10 in A-1-b base, and A-6 subgrade, and a similar section except the HMA was split into three subsections. MEPDG version 0.7 was used for this study. It was found that a thicker HMA helps prevent alligator cracking and subgrade rutting. AC fatigue was affected by both base and HMA properties. The AC rutting was found to be based only on HMA. Changing the volumetric properties in the upper and lower AC sub-layers had a small effect on rutting, especially when compared to the intermediate sub-layer. In the case of longitudinal and fatigue cracking, reducing the percent air voids affected the amount of damage more than increasing the binder content. Lastly, in the case of alligator, cracking a change of binder content in the bottom AC sub-layer was more effective in improving performance than decreasing air voids.

Orobio and Zaniewski (*27*) studied the sensitivity of material properties inputs in MEPDG. The authors used a space-filling approach with Latin Hypercube method to pick the values and Standardized regression coefficients to compare the values along with Gaussian Stochastic processes and metamodels to evaluate and categorize relative importance. It was decided to purely use Level 3 inputs in MEPDG, which may limit the applicability of the study. Because of the methods used for this study, all variables could be tested concurrently, which saves time and computing need. The properties tested that had significant affect were binder content, as-built air voids, Poisson's ratio, surface shortwave absorption of asphalt layers, and resilient modulus of the subgrade. Two structures were evaluated: Structure 1, had 3 AC layers on top of a permeable asphalt treated base, on top of subgrade; thus there were 5 layer inputs, 3 for the asphalt layers, 1 for the base, and the last for subgrade properties. Structure 2 had 4 layers, a dense graded AC on top of an aggregate base, on top of an aggregate subbase, and lastly the subgrade.

The evaluated parameters for Structure 1 are:

1) Layer 1-surface shortwave absorptive, effective binder content, air voids, total unit weight, Poisson's ratio, thermal conductivity, and heat capacity
2) Layer 2-effective binder content, air voids, total unit weight, Poisson's ratio, thermal conductivity, and heat capacity

3) Layer 3-effective binder content, air voids total unit weight, Poisson's ratio, thermal conductivity, and heat capacity
4) Layer 4-effective binder content, air voids, total unit weight, Poisson's ratio, thermal conductivity, and heat capacity
5) Layer 5- Poisson's ratio, coefficient of lateral pressure, modulus, average tensile strength at 14 $^0$F, and mix coefficient of thermal contraction.

For structure 2 the following input parameters were studied:

1) Layer 1-surface shortwave absorptive, effective binder content, air voids, total unit weight, Poisson's ratio, thermal conductivity, and heat capacity.
2) Layer 2-Poisson's ratio, coefficient of lateral pressure, and modulus.
3) Layer 3-Poisson's ratio, coefficient of lateral pressure, and modulus.
4) Layer 4-Poisson's ratio, coefficient of lateral pressure, modulus, average tensile strength at 14 °F, and mix coefficient of thermal contraction.

It was found that 13 of the 30 input parameters for Structure 1 had a significant impact on IRI; 6 of which were negatively affecting (when the parameter got larger the damage got smaller). Eleven of the 30 parameters had a significant effect on rutting, 5 of which are negative. And 13 out of 30 had a significant effect on cracking. For structure 2, 9 out of 18 were found to be significant for IRI, 10 were significant for rutting, and 7 were significant for cracking.

Surprisingly, Poisson's ratio had a significant impact on some of the damage. This is interesting because Poisson's ratio is normally determined to be insignificant and thus a default parameter is used in design. This study also clearly shows that the structural and material properties can have a significant effect on the MEPDG outputs and pavement performance. In conclusion, the IRI was found to be most affected by resilience modulus and as-built air voids. Rutting was most affected by Poisson's ratio and resilient modulus. Cracking was most affected by as-built air voids, resilient modulus of the subgrade, and effective binder content. The author believes that MEPDG could be vastly improved if it was integrated with statistical software. If this was done, the statistical analysis used in the study would be more available. One drawback to this study was its limitation to Level 3 inputs neglects the impact of the Dynamic Modulus of AC, which is a critical value for advanced calibration.

Schwartz et al. (*28*) did a final report for a full sensitivity study done on MEPDG. A one to one and global sensitivity were done on most of the input parameters for MEPDG. This study was accomplished on 5 pavement types, 5 climates, and 3 traffic levels. The evaluated inputs were general traffic inputs such as AADTT and design speed, layer thickness', material properties, groundwater depth, and geometric parameters such as lane width. Twenty-five to thirty-five parameters were chosen through conventional wisdom and the one-to-one sensitivity analysis. In this study a normalized sensitivity index was used to compare the parameters. The normalized sensitivity index (NSI) was defined as "the percentage change of predicted distress relative to its design limit caused by a given percentage change in the design input." This essentially means the sensitivity becomes a ratio of percentage change of the parameter vs. percentage change of the distress, with the limits of the parameter being the range for that climate and material, and the limit of the distress was from 0 to the maximum allowable distress. The bound surface layer such as the HMA was consistently the most sensitive parameter for all types of pavements. There were three steps accomplished in this study: first, a one-to-one sensitivity analysis was done to determine

which parameters were important enough to be included in the intensive global sensitivity analysis, second, the important parameters were put through a global sensitivity analysis, and third the results were compared with previous studies. The global sensitivity was accomplished both through an ANN (artificial neural network) and RSM (response surface method).

For just HMA the following trends were seen:

1. The HMA properties were the most consistently sensitive parameters.
2. Subgrade and base properties were not as consistently sensitive parameters.
3. The longitudinal cracking, alligator cracking, and AC rutting saw more sensitivity in their input parameters than seen in the IRI and thermal cracking parameters.
4. The sensitive design inputs for thermal cracking had very little overlap with the sensitive design inputs for longitudinal cracking, alligator cracking, AC rutting, total rutting, and IRI. This is to be expected as MEPDG has thermal cracking as mainly a response to climate.
5. Thermal cracking did not occur in MEPDG with the correct binder. Thus the binder had to be adjusted to test the sensitivity of this distress.

Additionally, shortwave absorption was found to be a sensitive input, however, there is little research in this area on testing for this parameter and how to accurately input it. In conclusion for all pavements:

1. 10,000 ANN evaluations show very well-defined single peaks.
2. Bound surfaces had the highest sensitivities.
3. Sensitivities did not vary across the climates, but magnitude of the severity of the distress did vary.

In conclusion for HMA:

1. HMA properties, being the bound surface, were the only consistently highest sensitivities. These were Dynamic Modulus, Thickness, Shortwave absorptions, and Poisson's Ratio.
2. Longitudinal cracking, alligator cracking, and AC rut sensitivities were higher than IRI and thermal cracking sensitivities.
3. The sensitivity of air voids and effective binder content are beyond the sensitivity of these values when considered purely in their effect on Dynamic Modulus.
4. Little to no thermal cracking was seen with the correct binder.
5. Thermal conductivity and heat capacity were found to be sensitive parameters for longitudinal cracking and to a lesser extent to alligator cracking and AC rutting. It also might be a sensitive parameter for granular layers, but MEPDG does not allow this input. Note that these properties are difficult to test for and quantify.
6. Moderately stiff foundations with HMA were sensitive to operational speed for longitudinal cracking and AC rutting; this is most likely from interactions with Dynamic Modulus aging over time in the model though.

In addition to the above conclusions, there were some surprising conclusions that the author did not expect to encounter:

1. Poisson's ratio was a highly sensitive parameter.
2. HMA unit weight was a highly sensitive parameter.

The authors do not know why these results were found. The Poisson's ratio sensitivity is concerning due to the fact that this is difficult to quantify and is usually a default value.

Cooper et. al. (*29*) did a sensitivity study on MEPDG. The sensitivity analysis was done at three levels low, medium, and high with 5 input parameters: traffic level, HMA thickness, dynamic modulus, base course thickness, and subgrade type. A full factorial design was done using the statistical analysis software PROC FACTEX. To maintain simplicity, the authors analyzed a basic three-layer system with base, subgrade, and HMA. The HMA was varied through three types of typical Louisiana mixtures. After the analysis was completed, the following results were obtained:

1. Combined parameters had more affect than non-combined.
2. Traffic Level was the main factor in all types of distresses analyzed.
3. In IRI, the second most determining factor was HMA thickness and the third was subgrade strength. For combined affects, first was traffic combined with HMA thickness, second was traffic combined with dynamic modulus, and third was base thickness and subgrade type.
4. In fatigue cracking, second single factor was HMA thickness and third was base thickness. The combination factors was first traffic and HMA thickness, second was traffic and base thickness, and third was traffic and subgrade.
5. Total rutting was secondly affected by HMA thickness and thirdly dynamic modulus. The combined factors were, first, traffic and HMA thickness, secondly, traffic and subgrade type, and thirdly, traffic and base thickness.
6. For AC rutting, dynamic modulus was second most affective and third was HMA thickness. For combined affect first was traffic and dynamic modulus and second was traffic and HMA thickness.
7. Top down or longitudinal cracking was secondly affected by base course and thirdly by dynamic modulus, and the combination was firstly, traffic and base thickness and secondly, base thickness and subgrade type.

The longitudinal cracking function was brought into question by the authors due to the fact that MEPDG bases it on a traditional model that gives the base course thickness more affect than would be expected in the field.

# SITES SELECTION AND MATERIAL COLLECTION

## INTRODUCTION

Appropriate pavement reconstruction sites selection and adequate material collection is a major tenant of this study. Seven pavement reconstruction sites from various districts in the state of New Mexico were selected for this project. Enough materials were collected from different layers of the pavement site during their construction to conduct the necessary laboratory testing requirements.

## CONSTRUCTION SITES

In order to calibrate MEPDG for New Mexico, it requires construction projects from around the state. It was decided to have at least one construction project per district to fully represent the variety of material and construction techniques in the different areas of the state. Seven pavement reconstruction sites were chosen for this study. Each construction site had a representative station within the project where the majority of the material collection and field testing was accomplished. This was done to ensure that when calibrating there was one set of data inputs for one set of pavement distress. Originally, testing and material collection was done over an area of 2-3 miles. After considering the consequences of a large area with varying material and distress conditions, it was determined that the testing and material areas be confined to a 500-700 foot section. Table 1 summarizes the various construction sites with the mile post (MP) and control number.

**TABLE 1 Selected pavement sites**

| Construction sites | Control No. | Station No. | Mile post |
|---|---|---|---|
| US54N | CN 2100250 | 150+00 | 132.5 |
| US54S | CN G3A92 | 100+00 | 95.2 |
| US285 | CN5100411 | 186+00 | 251.4 |
| I-25 | A301010 | 1319+00 | 219.3 |
| US491 | 6100783 | 2452+50 | 28.1 |
| NM14 | S100140 | 281+00 | Between NM14 and the Southbound I-25 off ramp |
| NM47 | 3100300 | 163+00 | NM 47 just before the Melina road (South bound) |

A brief description of each reconstruction sites is discussed below.

### US54N CN 2100250

This construction site is located in the southern part of New Mexico approximately 20 minutes north of Carrizozo on US54 and covers mile posts 130-146. The aggregates were from a nearby pit for base course and asphalt concrete. They were both a SPIII mix design with 1% versabind. The Reclaimed Asphalt Pavement (RAP) used for this pavement site was from milling the road on

the US54 South. Warm Mix Asphalt (WMA) was laid in two lifts of 3 in. each for a total depth of 6 in. The subgrade and base course both have the same AASHTO classification with the subgrade being an A-2-4 and the base course being an A-1-b. The main MP of concern for this site is MP 132.5. The majority of the field testing and material collection was done at this point. This station is 150+00, which might be of use to future researchers as the signs for the stations may be left on the fence by the constructed road.

**US54S CN G3A92**

This reconstruction site is in the southern part of New Mexico, approximately 25 minutes south of Carrizozo on US54. This project consisted of realigning the one-way highway from MP 94.23 to 107.10. As such, the old highway was milled and used as RAP for the base course and HMA on the new road. The entire section was constructed as a new pavement structure from the subgrade up.

The construction was done as follows:

a. Subgrade was tested and the estimated *R*-value was obtained and checked for compliance, and the soil was then either replaced with borrow or compacted to 100% for a depth of 6 in.
b. Base course was laid by first laying a 3 in. lift of virgin aggregate and then a 3 in. lift of RAP. The two layers were then mixed in the field to an assumed mix ratio of 50/50 RAP and virgin aggregate.
c. HMA was laid in two lifts of 3 inches each for a total depth of 6 inches.

**US285 CN5100411**

This reconstruction site is located at the intersection of US285 and I-40 at Clines Corners. This pavement work consisted of redoing the entire intersection as well as reconstruction of a little more than 3 miles on US285 north of Clines Corners. The chosen section was at station 185+00, 500 feet from the end of the project. This puts the section as far as reasonably possible away from the bridges and ramps. The pavement consisted of a subgrade being A-6 with geofiber reinforcement, 6 in. base being A-1-a and 6.5 in. SPIII HMA that was done in two lifts as well.

**I-25 CN A301010**

This reconstruction site is located on Interstate-25 (I-25) at Rio Bravo in district 3 about 8 miles to the south of Albuquerque. It was essentially a roadway reconstruction work and covered MP from 216.25 to 220. It involved reconstruction of two lanes in each direction of north bound and south bond lane with provisions to addition of future lanes. The existing roadway and shoulders were excavated to accommodate new surfacing. The subgrade was then compacted to the desired level before placing a 6 in. untreated base course over the full width of roadway and shoulders in one lift. After the base course was laid, the WMA was laid in two lifts of 3 inches for a total depth of 6 inches. The WMA had a RAP content of 15% and was SPIII. What is interesting in this project is that they also placed another 2 inches of WMA with PG 76-22 after the second lift of WMA was laid. This lift of WMA had also a RAP content of 15%. Finally, 5/8 in. of open-graded friction course (OGFC) was laid.

**US491 CN 6100783**

This pavement reconstruction site is on US491 by Sheep Spring, New Mexico, covering MP 15.03 to 37. It involved the construction of two more lanes two change the single lane road to a two lanes road. The subgrade and base course both have the same AASHTO classification with the subgrade being an A-2-4 and the base course being an A-1-b. The HMA was laid in two lifts of 3 in. each for a total depth of 6 in. The top lift had no RAP content, however, the bottom lift contained 15% RAP. The aggregate and the base course were from a nearby pit.

**NM14 CN S100140**

This was the sixth pavement reconstruction site chosen for this calibration study. The pavement site is located at a crossing south of Santa Fe at the Interstate 25 and Cerrillos Road (NM 14). The subgrade soil was classified as A-2-4 while the base course was A-1-b according to AASHTO soil classification system. After the 6 in. base course was laid, the HMA was laid in two lifts of 3 in. for a total depth of 6 in. The HMA had no RAP content and was SPIII.

**NM47 CN 3100300**

This was the last pavement reconstruction site selected for this calibration study. The pavement site is located on NM47 about 20 miles to the south of Albuquerque. It covered MP from 31.0 to 32.8. The subgrade and base course both have the same AASHTO classification with the subgrade being an A-2-4 and the base course being an A-1-a. The HMA was laid in two lifts of 3 in. for a total depth of 6 in. The HMA had a RAP content of 15% and was SPIII.

## MATERIAL COLLECTION

Material collection is a major task of this study in that the materials will be tested and some stored for later evaluation. All materials used on the chosen road section were collected from each construction project with the aid of NMDOT. This includes material from each pavement layer from the road being constructed (subgrade, hot mix, base course) and material that is mixed together or laid into the pavement structure such as aggregates, additives, geogrid, geotextile, etc. From the literature review, the researchers know that lack of material for future testing is one of the avoidable problems in calibration studies. Once the road is built, it is next to impossible to obtain true to field materials and so the quantities for materials may seem excessive but when compared to the risk of not having enough material to run all the tests, the larger amounts are necessary. Figure 1 shows the materials collection from the field. Table 2 shows a generalized idea of the amounts and materials needed for this project. Several important issues that were observed in the field were documented in APPENDIX E.

**FIGURE 1 Material collection from the field**

**TABLE 2 Recommended material**

| Material | Unit Size | Number of Units |
|---|---|---|
| Binder | 1 gallon buckets | 7-10 |
| HMA/WMA mix | 1 20-30lb bags | 75-90 |
| HMA/WMA aggregates (sand, Fines, coarse, RAP etc) | 1 40-50lb bags | 3 each aggregate |
| Subgrade | 1 40-50 lb bags | 20-30 bags |
| Base | 1 40-50 lb bags | 5-10 |
| HMA cores | 1 4 or 6 inch Cores | 2-3 |
| Geosynthetics/Geogrid | Sheet/Roll | 3ft X 4 ft piece/one fifth |

## SUMMARY

- Seven pavement reconstruction sites were selected for this study.
- Sufficient materials were collected from the selected pavement sites to conduct the necessary laboratory tests.

# DYNAMIC MODULUS TESTING

## INTRODUCTION

Dynamic modulus ($|E^*|$) is an essential input parameter in the MEPDG software. It is used to characterize the HMA or WMA for pavement structural design. Therefore, determination of $|E^*|$ in the laboratory is imperative. In this study, the $|E^*|$ of AC mixture collected from various construction sites was determined. Mastercurves were constructed for each of collected AC mixture. The mastercurve parameters were also determined for MEPDG implementation. The details of the test and the results are discussed in the following sections.

## SAMPLE PREPARATION

The plant collected HMA or WMA mix was heated in an oven at 149 °C (300 °F) for less than an hour and then compacted in gyratory compactor at 138 °C (280 °F) following AASHTO T 312-07 (*30*) test standard. Compaction pressure of 600 kPa (87 psi) was used. Height of sample and number of gyrations were controlled for target air void. Cylindrical samples of 6 in. (150 mm) diameter and 6.75 in. (170 mm) height were prepared. The sample was cut into 4 in. (100 mm) diameter and 6 in. (150 mm) height cubes using a laboratory saw as shown in Figure 2.

**FIGURE 2 Sample preparation**

## LABORATORY TESTING

The $|E^*|$ tests were conducted using the AASHTO T 342-11 (*31*) test standard. All the samples were checked for surface waviness and perpendicularity. Prior to testing, the sample was conditioned at 21 °C for at least two hours. The test was performed at five different temperatures (-10, 4, 21, 37 and 54 °C) and six different frequencies (0.1, 0.5, 1, 5, 15 and 25 Hz). The test sample placement is shown in Figure 3, which also shows the two Linear Variable Displacement Transducers (LVDTs) clamped on it. Three replicate samples were prepared and tested for each type of mixture.

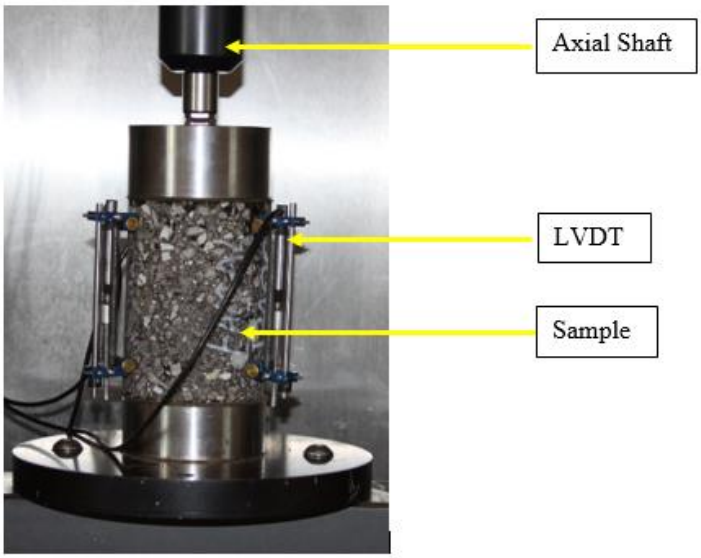


**FIGURE 3 Dynamic modulus test setup**

## CONSTRUCTION OF MASTERCURVE

The time-temperature superposition principle has been applied on the dynamic modulus data collected from the laboratory tests conducted at different temperatures and frequencies. This principle allows us to move horizontally the dynamic modulus data at different temperatures on the loading time scale or loading frequency scale to produce one smooth curve dependent only on loading frequency or time (*32*). The amount by which dynamic modulus data is shifted to fit in a smooth curve at a reference temperature is referred to as shift factor. Shifting is achieved by dividing the loading time in the time domain or multiplying the loading frequency in the frequency domain by the shift factor to get the reduced time or reduced frequency. The smooth curve that is developed by shifting the dynamic modulus data is referred to as the mastercurve. The function that is predominantly used for developing mastercurve for dynamic modulus data is the sigmoid function (*32*). Equation 8 represents the sigmoid function.

$$\log|E^*| = \delta + \frac{(\alpha)}{1+e^{\beta+\gamma\left[\log f + a_1(T_R - T) + a_2(T_R - T)^2\right]}} \tag{8}$$

where $\alpha$, $\beta$, $\gamma$, $a_1$ and $a_2$ are the curve fitting parameters for the master curve, $f$ is the frequency of loading, $T_R$ is the reference temperature, and $T$ is any temperature other than the reference temperature. Three samples were prepared and tested for each construction site. Table 3 summarizes the mixes on which the dynamic modulus test was conducted. This table provides information about the mix type, maximum specific gravity, RAP content, air void content and asphalt content

**TABLE 3 Summary of the tested mixes and specimens**

| Construction Site | Control No. | Mix Type | SP Gradation | Specified Binder PG | Used Binder PG | % RAP | No. of Tested Specimen | Spec ID | Max. Specific Gravity ($G_{mm}$) | Bulk Specific Gravity ($G_{mb}$) | Air void | Asphalt Content (%) |
|---|---|---|---|---|---|---|---|---|---|---|---|---|
| US54N | CN 2100250 | WMA | SP-III | 70-22 | 64-28 | 25 | 3 | 1 | 2.452 | 2.329 | 5.0 | 4.7 |
| | | | | | | | | 2 | | 2.330 | 5.0 | |
| | | | | | | | | 3 | | 2.330 | 5.0 | |
| US54S | CN G3A92 | HMA | SP-III | 70-22 | 64-28 | 25 | 3 | 1 | 2.459 | 2.310 | 6.0 | 5.2 |
| | | | | | | | | 2 | | 2.318 | 5.7 | |
| | | | | | | | | 3 | | 2.309 | 6.0 | |
| US285 | CN5100411 | HMA | SP-III | 64-28 | 58-28 | 35 | 3 | 1 | 2.521 | 2.372 | 6.0 | 5.1 |
| | | | | | | | | 2 | | 2.371 | 6.0 | |
| | | | | | | | | 3 | | 2.370 | 6.0 | |
| I-25 | A301010 | WMA | SP-III | 76-22 | 70-22 | 15 | 3 | 1 | 2.597 | 2.441 | 6.0 | 4.9 |
| | | | | | | | | 2 | | 2.444 | 5.9 | |
| | | | | | | | | 3 | | 2.446 | 5.8 | |
| US491 (*BL) | 6100783 | HMA | SP-III | 70-22 | 70-22 | 15 | 3 | 1 | 2.441 | 2.312 | 5.3 | 4.8 |
| | | | | | | | | 2 | | 2.302 | 5.7 | |
| | | | | | | | | 3 | | 2.309 | 5.1 | |
| US491 (*TL) | 6100783 | HMA | SP-III | 70-22 | 70-22 | 0 | 3 | 1 | 2.435 | 2.308 | 5.2 | 4.7 |
| | | | | | | | | 2 | | 2.306 | 5.3 | |
| | | | | | | | | 3 | | 2.304 | 5.4 | |
| NM14 | S100140 | HMA | SP-III | 64-28 | 64-28 | 0 | 3 | 1 | 2.496 | 2.343 | 6.0 | 5.1 |
| | | | | | | | | 2 | | 2.367 | 5.2 | |
| | | | | | | | | 3 | | 2.373 | 5.0 | |
| NM47 | 3100300 | HMA | SP-III | 70-22 | 70-22 | 15 | 3 | 1 | 2.444 | 2.307 | 5.6 | 5.1 |
| | | | | | | | | 2 | | 2.307 | 5.6 | |
| | | | | | | | | 3 | | 2.297 | 6.0 | |

*BL = Bottom Layer and *TL = Top Layer

Figure 4 shows how the mastercurve is developed from the laboratory test data. The mastercurve was developed at 70 °F reference temperature for the AC mixture collected from US54N construction site and was shown in Figure 5. It can be seen that the |*E**| increases with increase in frequency of loading, which is expected.

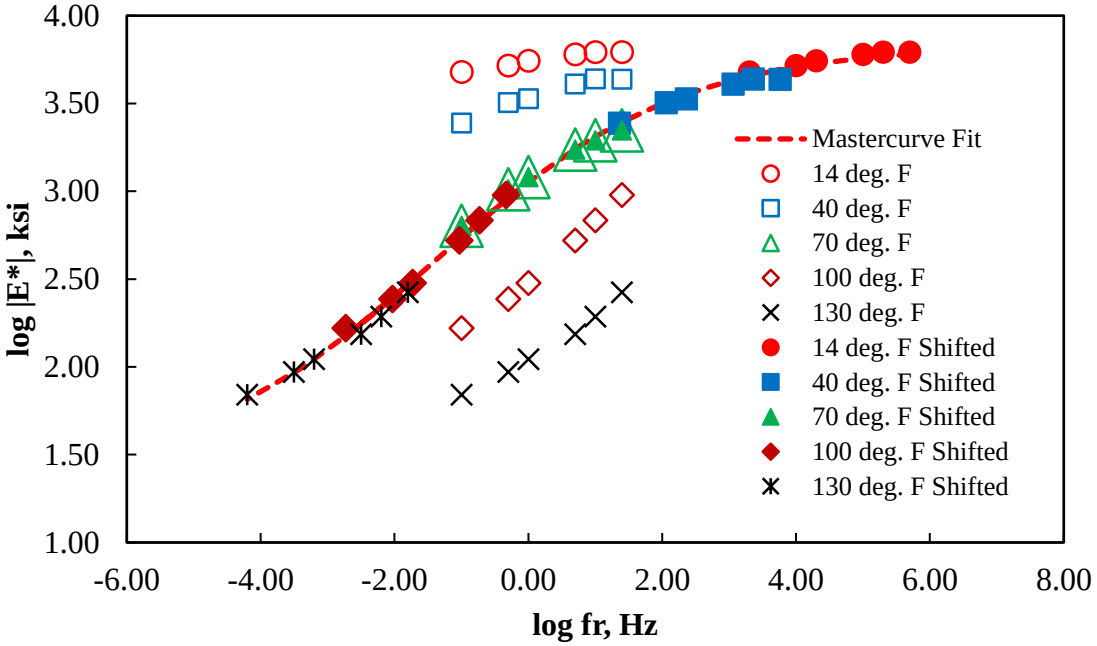


**FIGURE 4 Development of mastercurve**

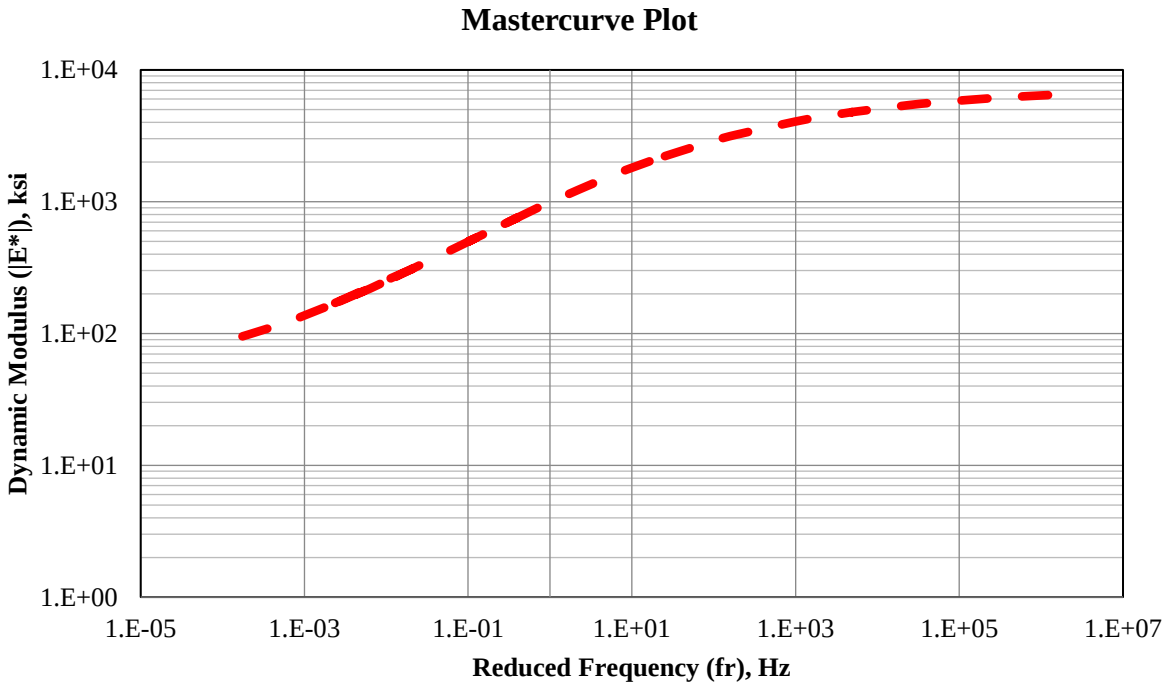


**FIGURE 5 Developed mastercurve for US54N mix**

Figure 6 illustrates the mastercurves of all AC mixtures collected and tested for this study. From this Figure, it is observed that AC mix of NM47 shows higher dynamic modulus value at low, medium as well as higher frequency levels than the other mixes. This is attributed to the high PG binder grade and the RAP content in the mix. On the other hand, AC mixture of US491 top layer shows the lowest dynamic modulus values compare to the other mixes.

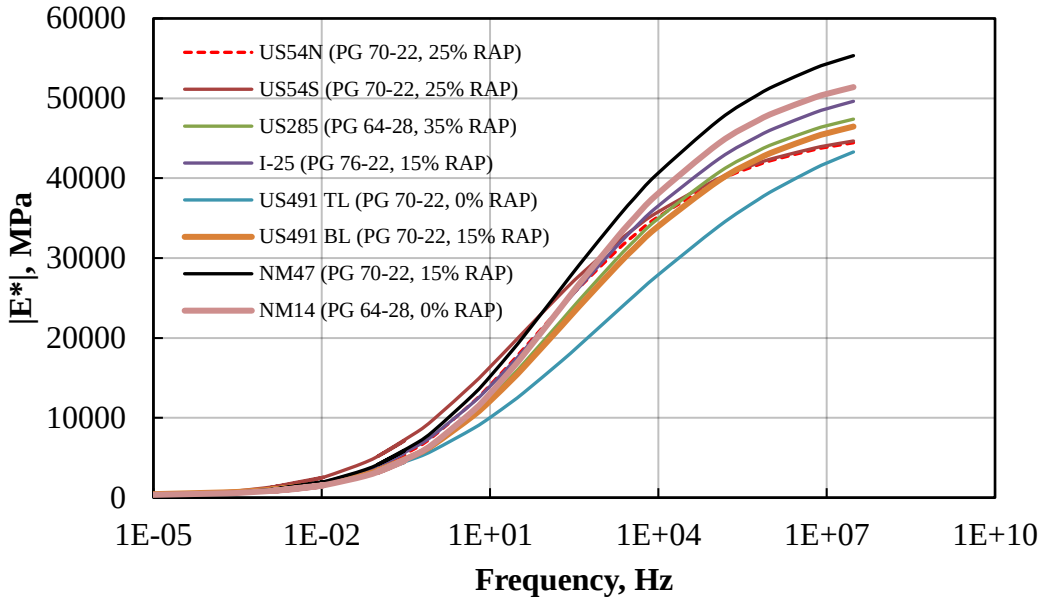


**FIGURE 6 Developed mastercurves for all mixes**

Table 4 summarizes the average master curve fitting parameters at 70 °F reference temperature for all the AC mixtures tested in this research project. APPENDIX A presents the |*E**| data summary sheet for all the AC samples tested in this study.

**TABLE 4 Summary of the mastercurve fitting parameters**

| Construction Site | Unit System | Reference Temperature | α | β | δ | γ |
|---|---|---|---|---|---|---|
| US54N | \|E*\| in ksi | 70 °F | 2.4369 | -0.7599 | 1.3907 | -0.5511 |
| US54S | \|E*\| in ksi | 70 °F | 2.5511 | -1.0173 | 1.2813 | -0.5051 |
| US285 | \|E*\| in ksi | 70 °F | 2.3353 | -0.5226 | 1.5292 | -0.5234 |
| I-25 | \|E*\| in ksi | 70 °F | 2.6384 | -0.7760 | 1.2513 | -0.4826 |
| US491 (BL) | \|E*\| in ksi | 70 °F | 2.6392 | -0.6089 | 1.2280 | -0.4017 |
| US491 (TL) | \|E*\| in ksi | 70 °F | 2.3433 | -0.5226 | 1.5144 | -0.5151 |
| NM14 | \|E*\| in ksi | 70 °F | 2.4757 | -0.3595 | 1.4988 | -0.5798 |
| NM47 | \|E*\| in ksi | 70 °F | 2.7397 | -0.7826 | 1.3269 | -0.4873 |

## SUMMARY

- Dynamic modulus test was conducted on various asphalt concrete mixtures and mastercurves were constructed for each mixture.
- Higher RAP content and PG binder grade results in higher dynamic modulus at all frequency level.
- A database of $|E^*|$ values for the collected AC mixtures has been populated that can be integrated in MEPDG.

# FATIGUE ENDURANCE LIMIT (FEL) TESTING

## INTRODUCTION

Fatigue Endurance Limit (FEL) is another important input parameter in the MEPDG design software. Therefore, determination of FEL is essential in the laboratory. The FEL of the AC mixture is determined using the beam fatigue test. Fatigue damage occurs in asphalt pavement due to repeated tensile strain at the bottom of AC under traffic loading. If the developed strain value is below the threshold value, FEL, no fatigue damage occurs. Previous studies have shown that FEL varies from 70 to 400 micro-strain ($\mu\varepsilon$) based on mixture variability (*33*). Until now, the fatigue endurance limit of AC is determined by conducting laboratory fatigue testing using the Four-Point Bending (4PB) test. The number of loading cycles to failure is related to applied tensile strain to determine the FEL. This is called the phenomenological approach, because the relationship is purely empirical and does not explain the fundamentals of fatigue failure. Previous research showed that fatigue failure occurred after a sample achieved 50% reduction in stiffness. In this study, the FEL of AC samples collected from various construction sites were determined using traditional failure approach that employs the $\varepsilon$-$N$ relationship. A fatigue life of 50 million cycles was used to predict the micro-strain level, which is equivalent to the fatigue endurance limit.

## SAMPLE PREPARATION

Beam samples are prepared in the laboratory using HMA mixture collected from the field. HMA mixtures are heated to 150 °C for no more than one hour (to avoid aging) and are then compacted using a Geotechnical Consulting Test System (GCTS) beam compactor, shown in Figure 7. The compactor is capable of fabricating two test specimens (18″ x 6″ x 3″) in less than five minutes. Figure 7 also shows freshly compacted HMA mixtures within the heated molds and those which have been previously compacted. Once cooled, the compacted HMA specimens are then cut into two beams (15″ x 2.5″ x 2.0″) using a GCTS stone-cutting saw. The maximum specific gravity ($G_{mm}$) of the loose AC mixture was determined by using the AASHTO T 209 (*34*) standards. Bulk specific gravity ($G_{mb}$) and air voids were determined in accordance with AASHTO T 166 (*35*)and AASHTO T 269 (*36*) test standards respectively. Those beam samples which contain 5.5 ± 0.5% air voids have been tested.

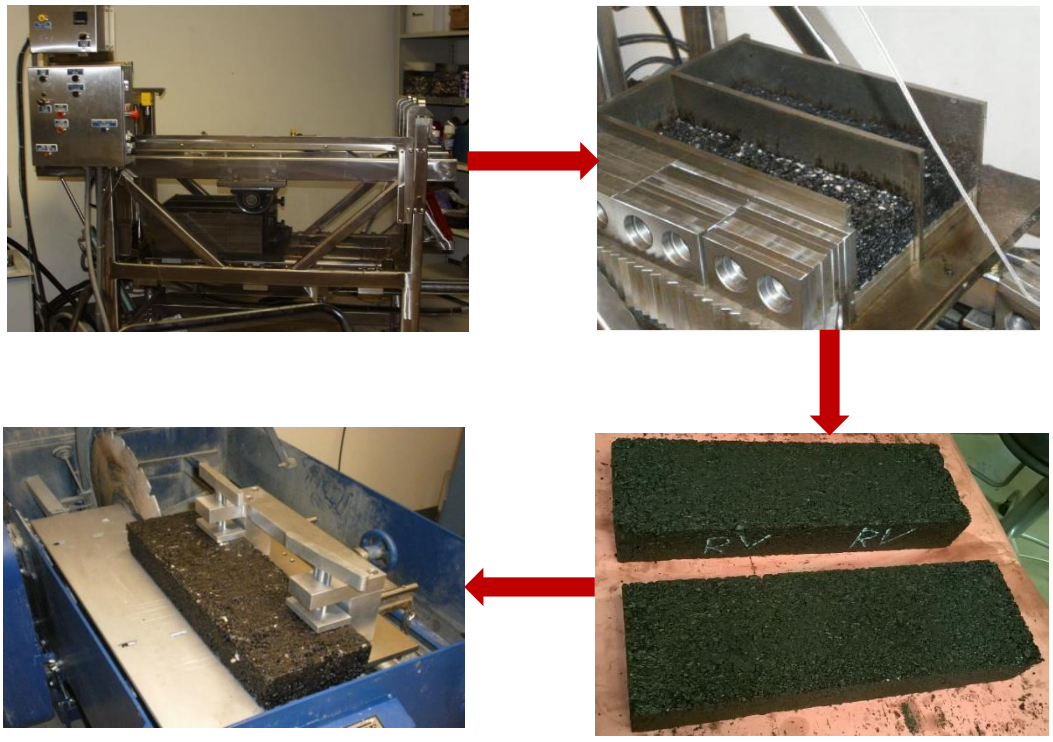

**FIGURE 7 Sample preparation**

## LABORATORY TESTING

A beam fatigue test was conducted according to AASHTO T 321-07 (*37*) standard. Figure 8 illustrates a schematic of the test setup. Using the deflection history, load response history, and geometry of test specimen, the maximum strain and stress in the specimen was calculated using Eq. (9) and Eq. (10) respectively.

$$\varepsilon = \frac{12\,h\,\delta}{3L^2 - 4a^2} \tag{9}$$

$$\sigma = \frac{P\,L}{b\,h^2} \tag{10}$$

where ε = maximum strain, σ = maximum stress, $P$ = load applied by actuator at time $t$, $b$ = average specimen width and $h$ = average specimen height, $\delta$ = deflection at center of beam at time $t$, $a$ = distance between inside clamps and $L$ = distance between outside clamps.

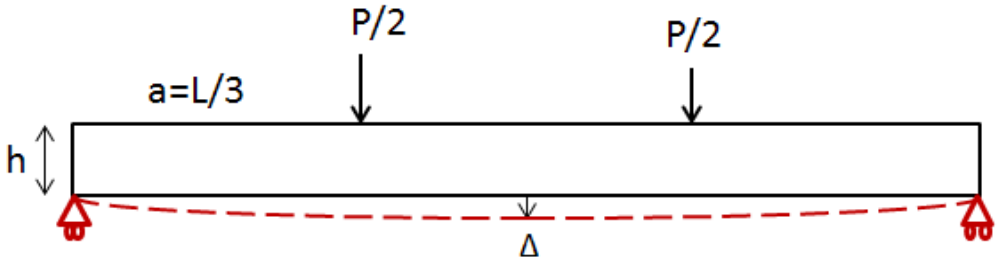


**FIGURE 8 Schematic of the four-point beam fatigue test**

Sample's flexural stiffness ($E$) is then calculated using σ and ε data recorded from each cycle.

$$E = \frac{\sigma}{\varepsilon} \tag{11}$$

Here the traditional approach is used in fatigue analysis of AC in accordance with the AASHTO T 321-07 (*35*) Standards. Loading was done using a sinusoidal waveform at a frequency of 10 Hz at a fixed temperature of 20 °C. One replicate sample was tested at each strain level. Cyclic loading of the beam sample induced tension at the bottom section where microcracking and subsequent macrocracking propagated to the top of the beam. This behavior, in essence, simulated field fatigue cracking due to traffic loading. Fatigue testing was conducted at strain levels varying from 400–800 $\mu\varepsilon$, from which a $\varepsilon$-$N$ relationship was developed. The test setup is shown in Figure 9. Under cyclic loading, the AC beam endured damage induced cyclic loading (displacement control). Dissipated energy generated at the initial phase of applying load and the stiffness of the sample decreased very sharply. Microcracks developed at the second stage of damage when the stiffness of asphalt sample decreased linearly. Finally, the stiffness dropped suddenly due to visible macro crack formation.

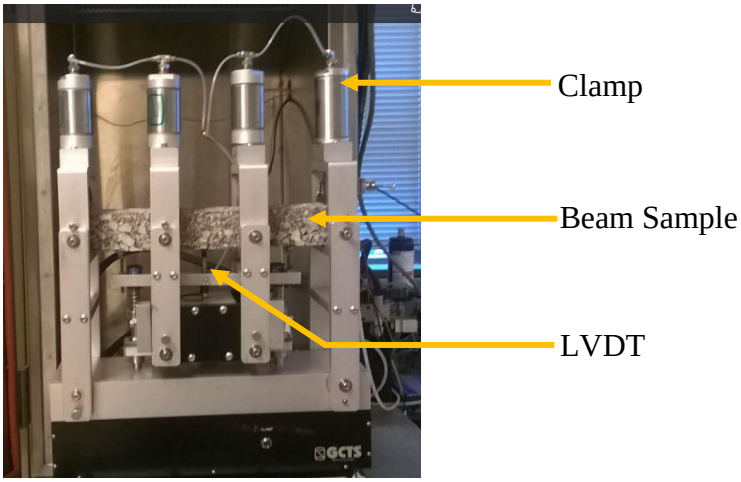


**FIGURE 9 Beam fatigue test apparatus**

## RESULTS AND DISCUSION

As mentioned earlier the test was conducted at four different strain levels ranges from 200 to 800 micro-strain ($\mu\varepsilon$). Several beams were also tested at 150 microstrain level. Two replicate beam samples were tested at each strain level. Figure 10 exhibits beam fatigue test results for the asphalt concrete sample of US54N at 800 micro-strain level. It is seen from Figure 10 that the stiffness of the materials decreases with increases in number of cycles. The reduction in stiffness is associated with plastic deformation and the formation and propagation of microcrack in the sample. Fatigue failure occurs when the stiffness of the materials reduces to 50% of its initial stiffness.

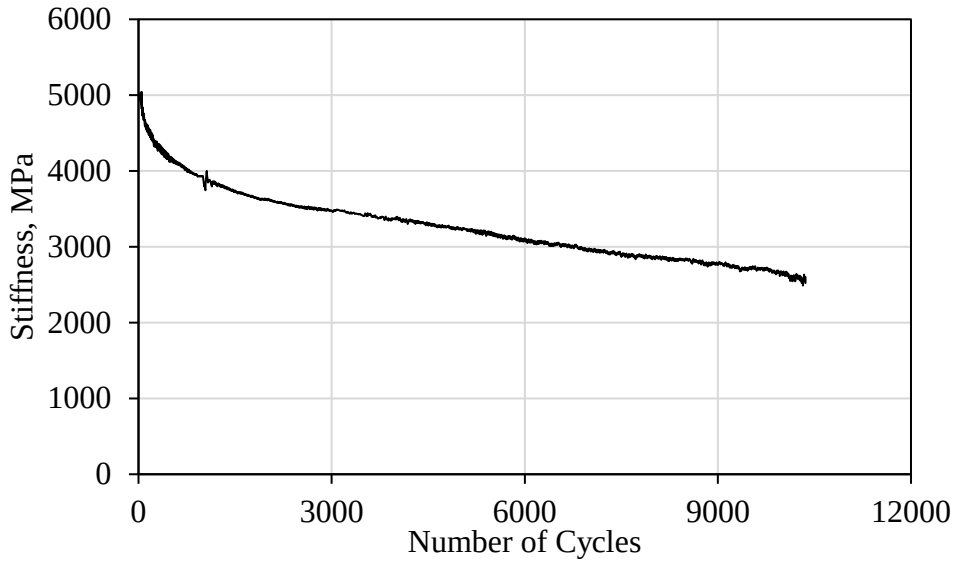


**FIGURE 10 Load cycles versus stiffness of AC of US54N at 800 microstrain**

The beam fatigue test results for US 54N AC mixture are shown in Table 5. It shows the applied strain levels, measured initial stiffness ($E$) and the number of cycles at failure of each test ($N_f$). It can be observed that the $N_f$ decreases with an increase in strain value. The $\varepsilon$-$N_f$ curve in log-log scale has been plotted in Figure 11. It shows that the curve becomes a straight line. The best fit curve is a power function.

**TABLE 5 Beam fatigue test results for US54 N**

| Construction Site | Applied strain (με) | E (Mpa) | $N_f$ |
|---|---|---|---|
| US54N | 800 | 5477 | 8400 |
| | 800 | 5920 | 7850 |
| | 600 | 6526 | 107100 |
| | 600 | 6100 | 50480 |
| | 400 | 9630.79 | 211510 |
| | 400 | 7254 | 140010 |
| | 200 | 8972 | 5874396 |
| | 200 | 5896 | 3597865 |
| | 150 | 6955 | 19875623 |

A fatigue life of 50 million cycles was used to predict the micro-strain level which was equivalent to the fatigue endurance limit. Based on the finding of the study, it can be concluded that the FEL of AC collected from US54N was 121 με.

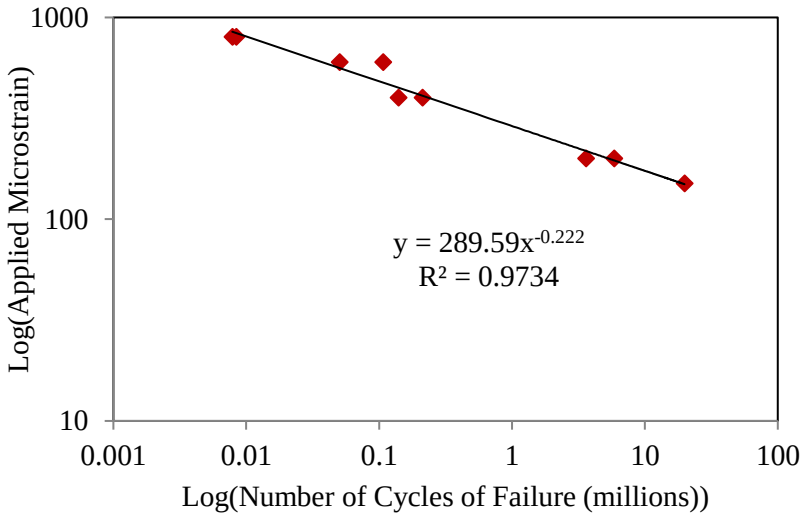


**FIGURE 11 Log-log $\varepsilon$-$N_f$ curve of US54 N AC mixture**

The beam fatigue test results for US54S AC mixture are shown in Table 6. It shows the applied strain levels, measured initial stiffness ($E$) and the number of cycles at failure of each test ($N_f$). It can be observed that the $N_f$ decreases with an increase in strain value. The $\varepsilon$-$N_f$ curve in log-log scale has been plotted in Figure 12. It shows that the curve becomes a straight line. The best fit curve is a power function.

**TABLE 6 Beam fatigue test results for US54 S**

| Construction Site | Applied strain (με) | E (Mpa) | $N_f$ |
|---|---|---|---|
| US54 S | 800 | 5900 | 9104 |
| | 800 | 5920 | 8690 |
| | 600 | 6273 | 61141 |
| | 600 | 6100 | 40000 |
| | 400 | 5612 | 120000 |
| | 400 | 7254 | 180000 |
| | 200 | 6520 | 6652310 |
| | 200 | 5896 | 7597865 |

A fatigue life of 50 million cycles was used to predict the micro-strain level, which was equivalent to the fatigue endurance limit. Based on the finding of the study, it can be concluded that the FEL of AC collected from US54S was 130 $\mu\varepsilon$.

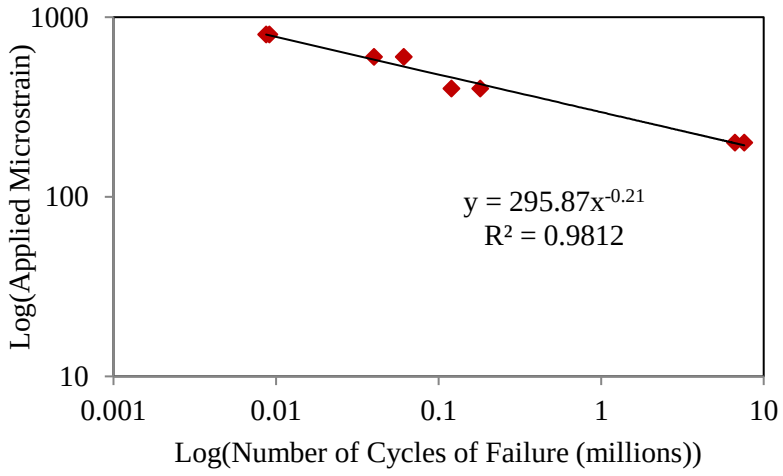


**FIGURE 12 Log-log $\varepsilon$-$N_f$ curve of US54 S AC mixture**

The beam fatigue test results for US 285 AC mixture are shown in Table 7. It shows the applied strain levels, measured initial stiffness ($E$) and the number of cycles at failure of each test ($N_f$). It can be observed that the $N_f$ decreases with an increase in strain value. The $\varepsilon$-$N_f$ curve in log-log scale has been plotted in Figure 13. It shows that the curve becomes a straight line. The best fit curve is a power function.

**TABLE 7 Beam fatigue test results for US285**

| Construction Site | Applied strain (με) | E (Mpa) | $N_f$ |
|---|---|---|---|
| US285 | 800 | 5439 | 19180 |
| | 800 | 5600 | 21000 |
| | 600 | 7660 | 42020 |
| | 600 | 7000 | 40000 |
| | 400 | 6508 | 295101 |
| | 400 | 6254 | 320000 |
| | 200 | 7272 | 3208701 |
| | 200 | 7072 | 3808701 |

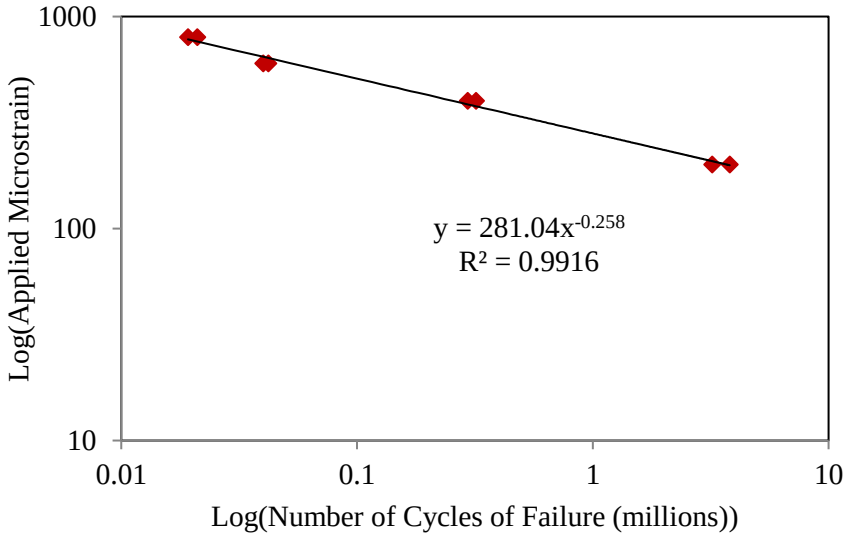


**FIGURE 13 Log-log $\varepsilon$-$N_f$ curve of US285 AC mixture**

A fatigue life of 50 million cycles was used to predict the micro-strain level, which was equivalent to the fatigue endurance limit. Based on the finding of the study, it can be concluded that the FEL of AC collected from US285 was 103 $\mu\varepsilon$.

The beam fatigue test results, figure and estimated FEL of other AC mixture have been documented in APPENDIX B.

Table 8 presents the determined FEL value of all the AC mixtures selected for this study. As can be seen from this table, FEL value varies from 100 to 150 micro-strain. The FEL value was found to be higher for US491 top layer AC mixtures compared to the other mixtures. Because the US491 top layer has no RAP content. The lowest FEL was found for US285 AC mixture. The higher RAP content is attributed to lower the fatigue performance of the mix.

**TABLE 8 Determined FEL value of all mixtures**

| Construction Site | Grade Specified | Aggregate Type | Measured FEL |
|---|---|---|---|
| US54N | 70-22 | SP III with 25% RAP (WMA) | 121 |
| US54S | 70-22 | SP III with 25% RAP (HMA) | 130 |
| US285 | 64-28 | SP III with 35% RAP (HMA) | 103 |
| I-25 | 76-22 | SP III with 15% RAP (WMA) | 117 |
| US 491 (BL) | 70-22 | SP III with 15% RAP (HMA) | 137 |
| US 491 (TL) | 70-22 | SP III with 0% RAP (HMA) | 140 |
| NM 14 | 64-28 | SP III with 0% RAP (HMA) | 119 |
| NM 47 | 70-22 | SP III with 15% RAP (HMA) | 133 |

## SUMMARY

- FEL test was conducted on various asphalt concrete mixtures and FEL value was determined for each mixture.
- FEL of collected AC mixture varies from 100 to 150 micro-strain.
- Higher RAP content significantly lower the fatigue performance of a mixture.
- A database of FEL values for the collected AC mixtures has been populated that can be integrated in MEPDG.

# CHARACTERIZATION OF RHEOLOGICAL PROPERTIES

## INTRODUCTION

Dynamic shear modulus ($G^*$) and phase angle (δ) of asphalt binder are another two essential input parameters in MEPDG. Asphalt binder was collected from each construction sites and frequency sweep dynamic shear rheometer (DSR) test was conducted on both unaged (virgin) and Rolling Thin Film Oven (RTFO) aged binder to determine the dynamic shear modulus (G*) and phase angle (δ) of the asphalt binder. The details of the test procedure and results are discussed herein.

## DSR TESTING

Asphalt binders are viscoelastic. This means they simultaneously act like an elastic solid (deformation due to loading is recoverable – it is able to return to its original shape after a load is removed) and viscous liquids (deformation due to loading is non-recoverable – it cannot return to its original shape after a load is removed). The DSR is capable of quantifying both elastic and viscous properties. The test measures the dynamic shear modulus or complex modulus, $G^*$ and phase angle ($\delta$) of asphalt binders under a continuous sinusoidal loading using a dynamic shear rheometer and parallel plate test geometry. Figure 14 shows the DSR test device.

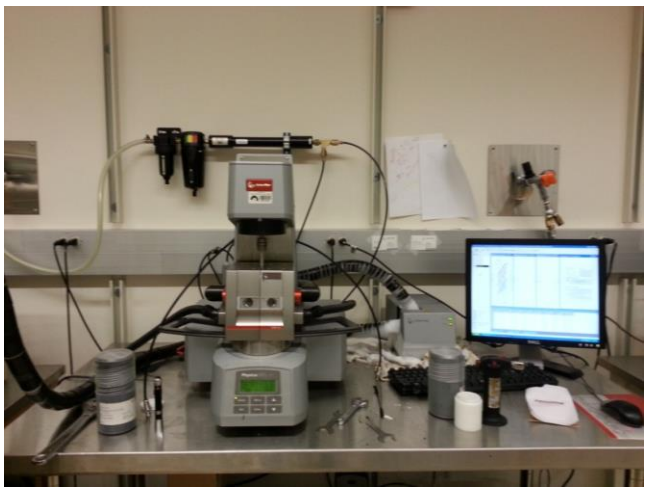

**FIGURE 14 Dynamic shear rheometer**

### Sample Preparation

First the collected unaged asphalt binder is taken into a can with loosely fitted cover and heated until the binder is sufficiently fluid to pour. Then the binder is poured into a 25 mm diameter mold as shown in Figure 15.

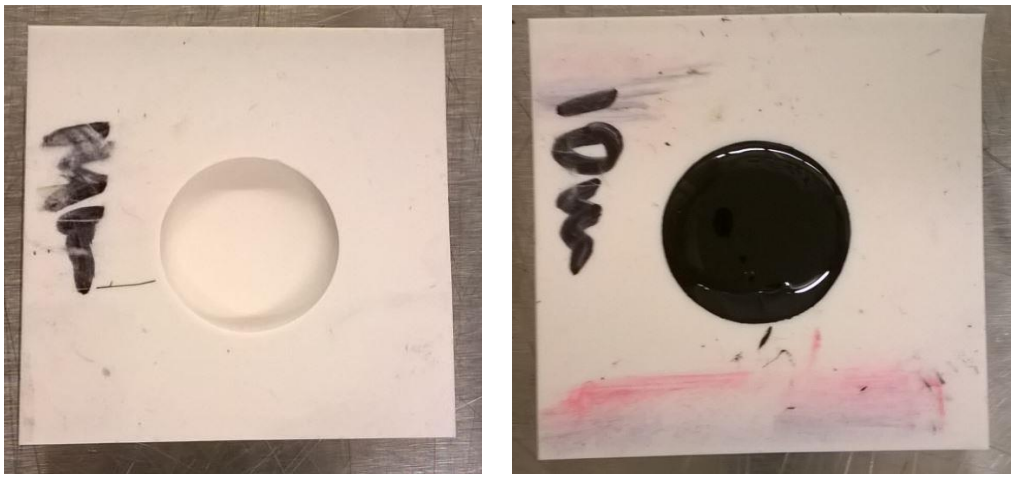

(a) Mold (b) Mold filled with sample

**FIGURE 15 Sample preparation for DSR test**

## Laboratory Testing

The test was conducted using the unaged binders collected from all the construction sites. US54N, US54S and NM14 pavement sites used PG 64-28 binder, and PG 58-28 was used in Clines Corners construction sites. Whereas, PG 70-22 binder was used in I-25 Rio Bravo, US491 top and bottom layer and NM47 pavement sites. The $G^*$ and δ were measured at seven different temperatures (40, 55, 70, 85, 100, 115 and 130 °F) and at different loading frequency. During the test, the asphalt binder sample was subjected to shear stress at frequencies ranging from 1 rad/s to 100 rad/s with 5 measuring points per decade in log scale. At each temperature, $|G^*|$ values were tested at 11 different frequencies (1, 1.58, 2.51, 3.98, 6.31, 10, 15.8, 25.1, 39.8, 63.1, and 100 Hz). At each temperature the binders stiffness ($G^*$) and phase angle (δ) values at different frequency were recorded. A thinner sample (1 mm) with a diameter plate (25 mm) was used so that the phase angle (δ) becomes measurable. All the tests were conducted following the AASHT0 T 315-09 (*38*) test protocol within the linear viscoelastic range under strain-controlled mode.

## Results and Discussion

### *a) PG 64-28 Binder*

Figure 16 shows the complex shear modulus at different temperatures for unaged PG 64-28 binder collected from US54N, US54S and NM14 construction sites. It can be observed that the $G^*$ value of the asphaltic material increases with loading frequency. For example, at 21.1 °C, the $G^*$ increases from 148 kPa to 4030 kPa due to the increase in frequency from 1 to 100 rad/sec. It is expected as increases in frequency cause less deformation to asphaltic material. However, G* value decreases with the increase of temperature as fluidity of asphalt increases with temperature. At the highest temperature, 54.5 °C, the $G^*$ increases from 542 Pa to 34600 Pa due to the increase in frequency from 1 to 100 rad/sec. At the lowest temperature, 4.4 °C, the $G^*$ increases from $3.7 \times 10^6$ Pa to $43 \times 10^6$ Pa due to the increase in frequency from 1 to 100 rad/sec.

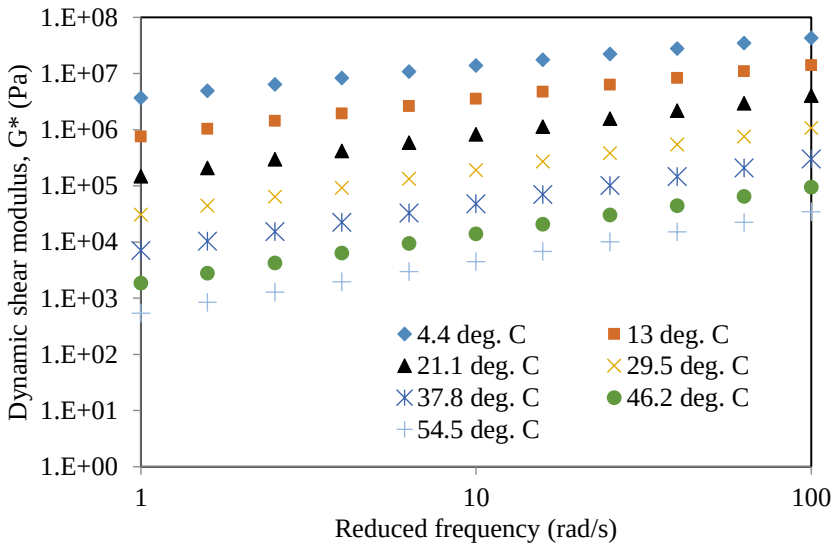


**FIGURE 16 Complex shear modulus vs. frequency plot at different temperatures**

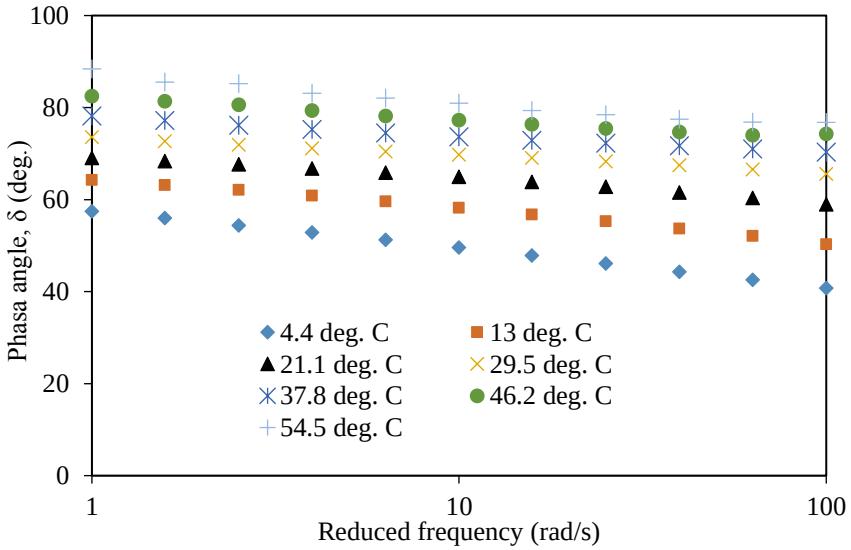


**FIGURE 17 Phase angle vs. frequency plot at different temperatures**

Figure 17 shows the phase angle (δ) at different temperatures for unaged PG 64-28 binder collected from US54N, US54S and NM14 construction sites. It can be observed that the phase angle (δ) value of the asphaltic material decreases with loading frequency. For example, at 21.1 °C, the phase angle decreases from 69.1º to 59.0º due to the increase in frequency from 1 to 100 rad/sec. It is expected as increases in frequency cause less deformation to asphaltic material and it starts to behave like an elastic material. However, δ value increases with the increase of temperature as fluidity of asphalt increases with temperature and its viscous property becomes more prominent.

*b) PG 58-28 Binder*

Figure 18 shows the complex shear modulus at different temperatures for unaged PG 58-28 binder collected from US285 Clines Corners construction site. It can be observed that the *G** value of the

asphaltic material increases with loading frequency. For example, at 21.1 °C, the *G** increases from 87 kPa to 2860 kPa due to the increase in frequency from 1 to 100 rad/sec. It is expected as increases in frequency cause less deformation to asphaltic material. However, *G** value decreases with the increase of temperature as fluidity of asphalt increases with temperature. At the highest temperature, 54.5 °C, the *G** increases from 200 Pa to 19700 Pa due to the increase in frequency from 1 to 100 rad/sec. At the lowest temperature, 4.4 °C, the *G** increases from $2.7x10^6$ Pa to $34x10^6$ Pa due to the increase in frequency from 1 to 100 rad/sec.

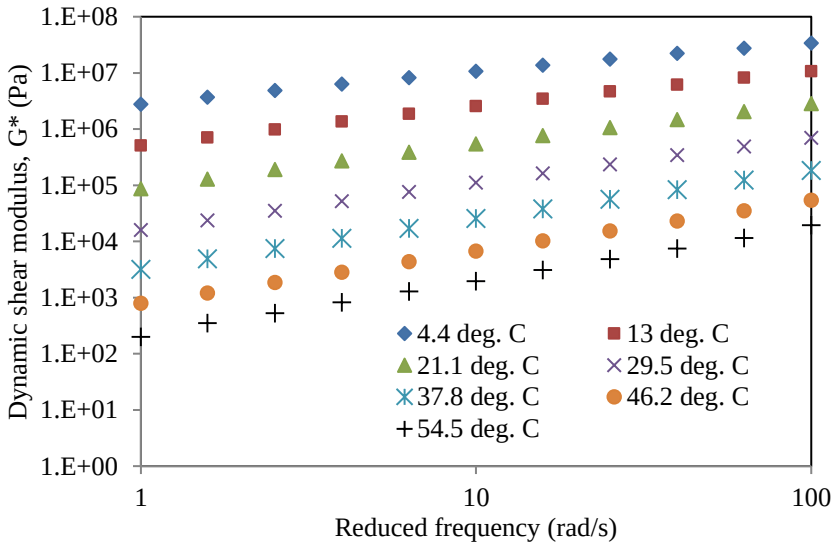


**FIGURE 18 Complex shear modulus vs. frequency plot at different temperatures**

Figure 19 shows the phase angle (δ) at different temperatures for unaged PG 58-28 binder collected from US285 Clines Corners construction site. It can be observed that the phase angle (δ) value of the asphaltic material decreases with loading frequency. For example, at 21.1 °C, the phase angle decreases from 73.7º to 61.5º due to the increase in frequency from 1 to 100 rad/sec. It is expected as an increase in frequency causes less deformation to asphaltic material and it starts to behave like an elastic material. However, δ value increases with the increase of temperature as fluidity of asphalt increases with temperature and its viscous property becomes more prominent.

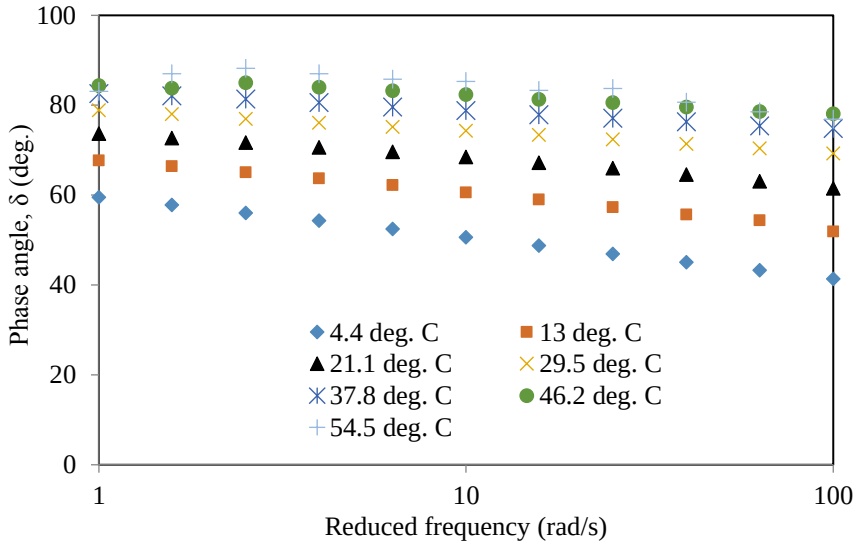


**FIGURE 19 Phase angle vs. frequency plot at different temperatures**

*c) PG 70-22 Binder*

Figure 20 shows the complex shear modulus at different temperatures for unaged PG 70-22 binder collected from I-25 Rio Bravo construction sites. It can be observed that the *G** value of the asphaltic material increases with loading frequency. For example, at 21.1 °C, the *G** increases from 348 kPa to 3530 kPa due to the increase in frequency from 1 to 100 rad/sec. It is expected as an increase in frequency causes less deformation to asphaltic material. However, *G** value decreases with the increase of temperature as fluidity of asphalt increases with temperature. At the highest temperature, 54.5 °C, the *G** increases from 158 Pa to 55400 Pa due to the increase in frequency from 1 to 100 rad/sec. At the lowest temperature, 4.4 °C, the *G** increases from $3.84 \times 10^6$ Pa to $2.26 \times 10^7$ Pa due to the increase in frequency from 1 to 100 rad/sec.

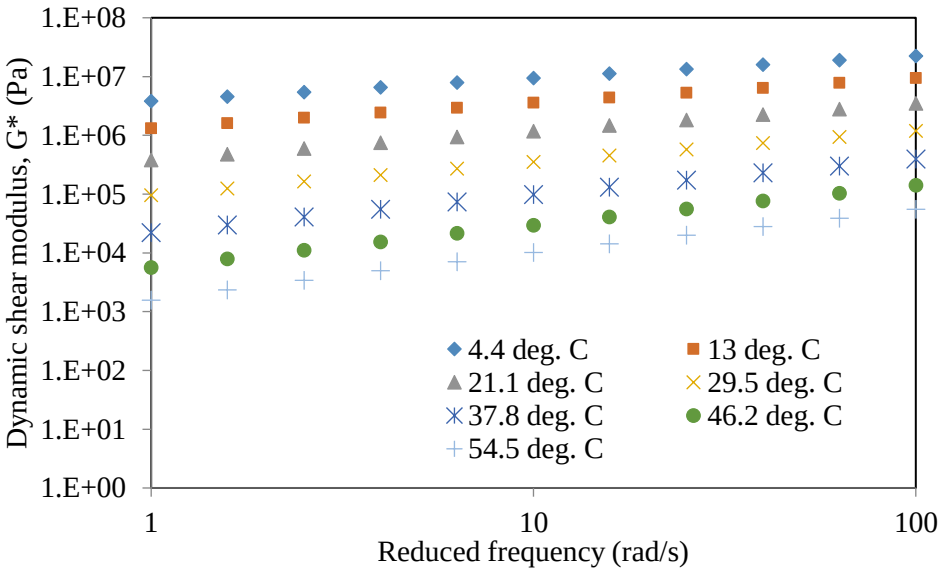


**FIGURE 20 Complex shear modulus vs. frequency plot at different temperatures**

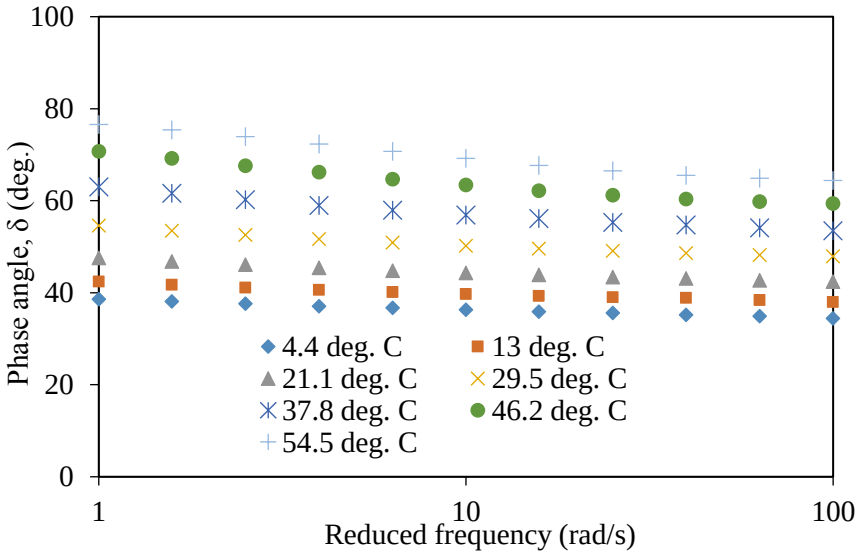


**FIGURE 21 Phase Angles vs. frequency plot at different temperatures**

Figure 21 shows the phase angle (δ) at different temperatures for unaged PG 64-28 binder collected from I-25 Rio Bravo construction sites. It can be observed that the phase angle (δ) value of the asphaltic material decreases with loading frequency. For example, at 21.1 °C, the phase angle decreases from 47.6º to 42.4º due to the increase in frequency from 1 to 100 rad/sec. It is expected as increases in frequency cause less deformation to asphaltic material and it starts to behave like an elastic material. However, δ value increases with the increase of temperature as fluidity of asphalt increases with temperature and its viscous property becomes more prominent.

## DSR TEST ON RTFO AGED BINDER

The DSR test was conducted on the RTFO aged binder collected from various construction sites. Rolling The RTFO test simulates the short-term aging of asphalt binder experienced during the manufacturing and placement processes. Therefore, this test is important in investigating and predicting early age HMA pavement behavior and distresses.

### Sample Preparation for RTFO Test

- A can of binder with a loosely fitted cover is put inside the oven and heated up until fluid enough to pour.
- Four bottles (as shown in Figure 22) are taken and 25 gm of virgin binder is poured into each bottle.
- Immediately after pouring the binder into the bottle, the bottle should be turned to a horizontal position and rotate gently for at least one full rotation to make a thin film over its wall.
- The bottles are then allowed to cool in the cooling rack for a minimum of 60 minutes and a maximum of 180 minutes.
- Then the bottles are placed in the RTFO oven and the door is closed.

- The assembly is rotated at a rate of 15 ± 0.2 r/min at 163± 0.5°C and the air flow is set at 4000 ± 200 mL/min.

The sample preparation and RTFO equipment are shown in Figure 23.

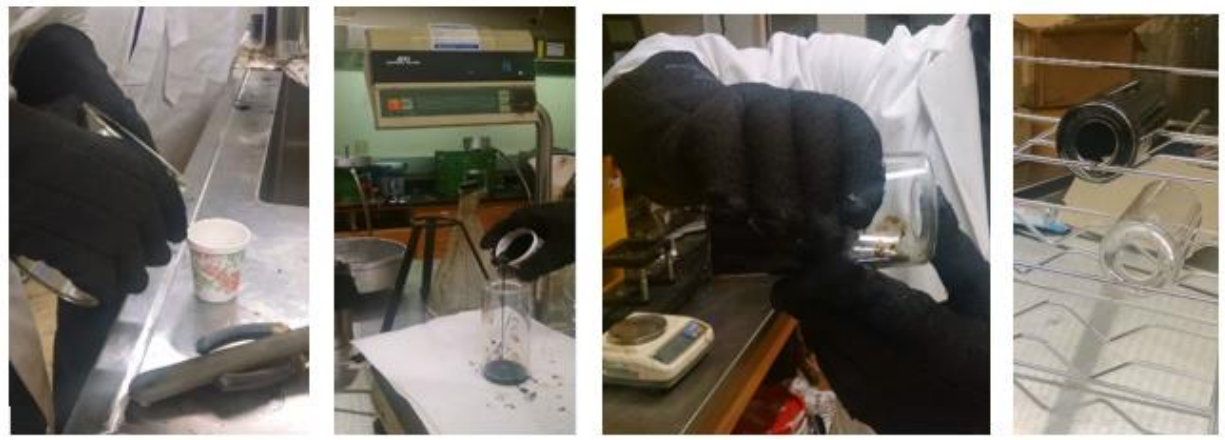

**FIGURE 22 Sample preparation for RTFO test**

**FIGURE 23 RTFO equipment**

**Laboratory Testing**

The DSR test was conducted on the RTFO aged binder. The $G^*$ and δ were measured at seven different temperatures (40, 55, 70, 85, 100, 115 and 130 °F) and at different loading frequency. During the test, the asphalt binder sample was subjected to shear stress at frequencies ranging from 1 rad/s to 100 rad/s with 5 measuring points per decade in log scale. At each temperature, $|G^*|$ values were tested at 11 different frequencies (1, 1.58, 2.51, 3.98, 6.31, 10, 15.8, 25.1, 39.8, 63.1, and 100 Hz). At each temperature, the binder stiffness ($G^*$) and phase angle (δ) values at different frequency were recorded. A thinner sample (1 mm) with a diameter plate (25 mm) was used so

that the phase angle (δ) becomes measurable. All the tests were conducted following the AASHT0 T 315-09 (*38*) test protocol within the linear viscoelastic range under strain-controlled mode.

**Results and Discussion**

*a) PG 64-28 Binder*

Figure 24 shows the complex shear modulus at different temperatures for RTFO aged PG 64-28. It can be observed that the *G** value of the asphaltic material increases with loading frequency. For example, at 21.1 °C, the *G** increases from 372 kPa to 6870 kPa due to the increase in frequency from 1 to 100 rad/sec. It is expected as an increase in frequency causes less deformation to asphaltic material. However, *G** value decreases with the increase of temperature as fluidity of asphalt increases with temperature. At the highest temperature, 54.5 °C, the *G** increases from 1.59 kPa to 73 kPa due to the increase in frequency from 1 to 100 rad/sec. At the lowest temperature, 4.4 °C, the *G** increases from $6.8 \times 10^6$ Pa to $56 \times 10^6$ Pa due to the increase in frequency from 1 to 100 rad/sec.

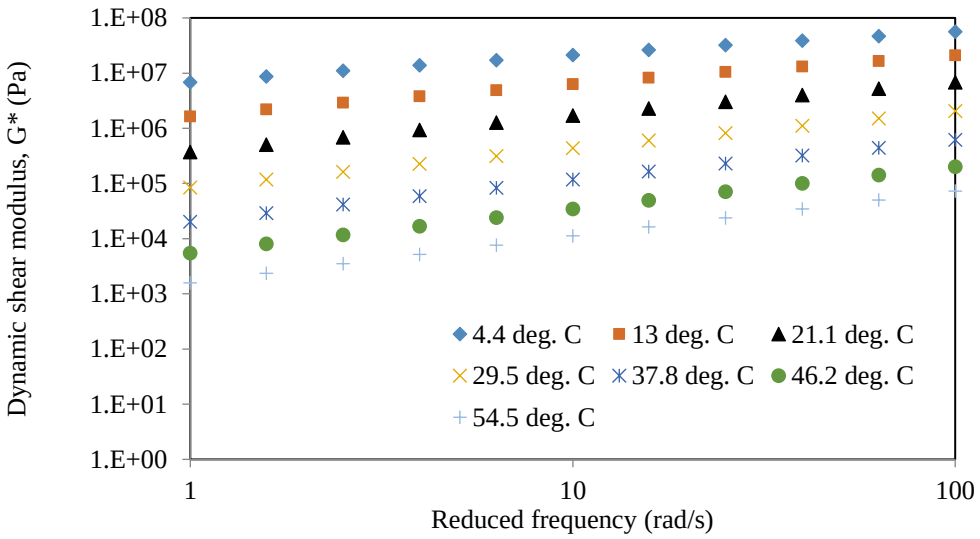


**FIGURE 24 Complex shear modulus vs. frequency plot at different temperatures**

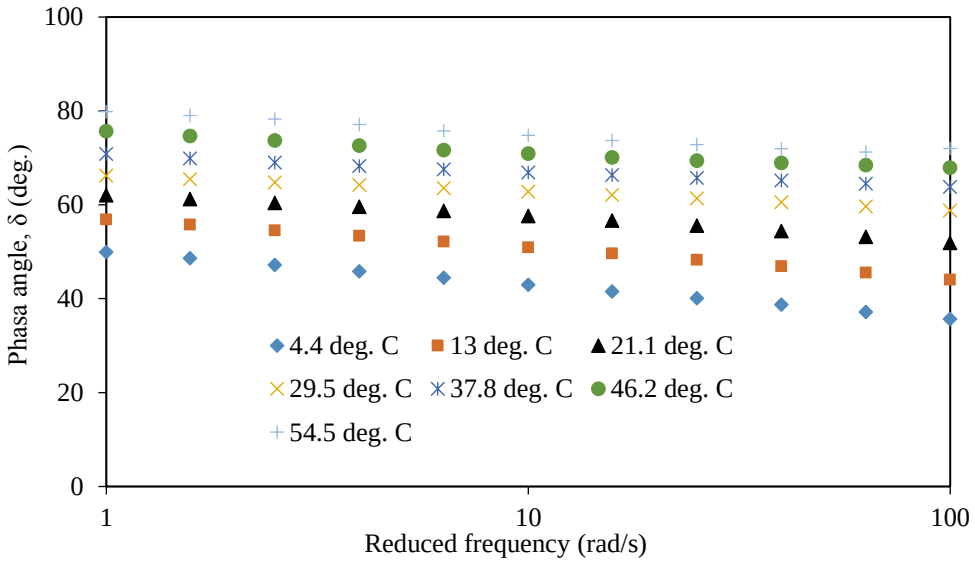


**FIGURE 25 Phase angle vs. frequency plot at different temperatures**

Figure 25 shows the phase angle (δ) at different temperatures for RTFO aged PG 64-28 binder. It can be observed that the phase angle (δ) value of the asphaltic material decreases with loading frequency. For example, at 21.1 °C, the phase angle decreases from 62.0º to 51.9º due to the increase in frequency from 1 to 100 rad/sec. It is expected as an increase in frequency causes less deformation to asphaltic material and it starts to behave like an elastic material. However, δ value increases with the increase of temperature as fluidity of asphalt increases with temperature and its viscous property becomes more prominent.

*b) PG 58-28 Binder*

Figure 26 shows the complex shear modulus at different temperatures for RTFO aged PG 58-28 binder. It can be observed that the *G** value of the asphaltic material increases with loading frequency. For example, at 21.1 °C, the *G** increases from 227 kPa to 4840 kPa due to the increase in frequency from 1 to 100 rad/sec. It is expected as an increase in frequency causes less deformation to asphaltic material. However, *G** value decreases with the increase of temperature as fluidity of asphalt increases with temperature. At the highest temperature, 54.5 °C, the *G** increases from 656 Pa to 46500 Pa due to the increase in frequency from 1 to 100 rad/sec. At the lowest temperature, 4.4 °C, the *G** increases from $5.19 \times 10^6$ Pa to $4.49 \times 10^7$ Pa due to the increase in frequency from 1 to 100 rad/sec.

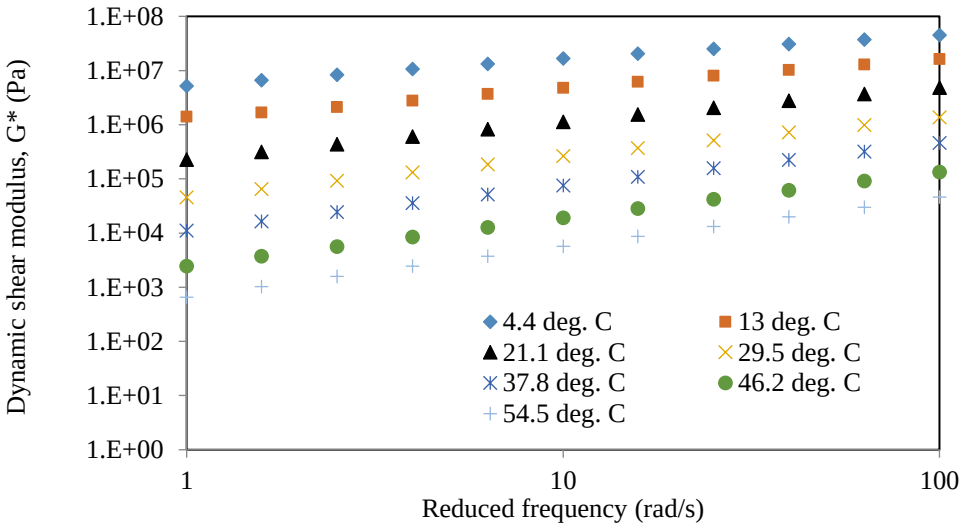


**FIGURE 26 Complex shear modulus vs. frequency plot at different temperatures**

Figure 27 shows the phase angle (δ) at different temperatures for RTFO aged PG 58-28 binder collected from US285 Clines Corners construction site. It can be observed that the phase angle (δ) value of the asphaltic material decreases with loading frequency. For example, at 21.1 °C, the phase angle decreases from 65.7º to 53.7º due to the increase in frequency from 1 to 100 rad/sec. It is expected as an increase in frequency causes less deformation to asphaltic material and it starts to behave like an elastic material. However, δ value increases with the increase of temperature as fluidity of asphalt increases with temperature and its viscous property becomes more prominent.

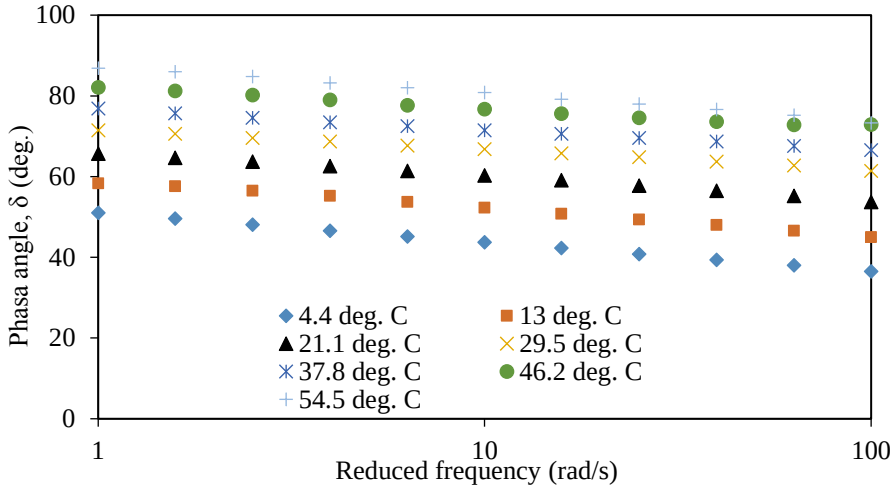


**FIGURE 27 Phase angle vs. frequency plot at different temperatures**

*c) PG 70-22 Binder*

Figure 28 shows the complex shear modulus at different temperatures for RTFO aged PG 70-22 binder collected from I-25 Rio Bravo and US491 construction sites. It can be observed that the *G** value of the asphaltic material increases with loading frequency. For example, at 21.1 °C, the *G** increases from 606 kPa to 4630 kPa due to the increase in frequency from 1 to 100 rad/sec. It is

expected as increases in frequency cause less deformation to asphaltic material. However, G* value decreases with the increase of temperature as fluidity of asphalt increases with temperature. At the highest temperature, 54.5 °C, the *G** increases from 3500 Pa to 92000 Pa due to the increase in frequency from 1 to 100 rad/sec. At the lowest temperature, 4.4 °C, the *G** increases from $5.05x10^6$ Pa to $2.61x10^7$ Pa due to the increase in frequency from 1 to 100 rad/sec.

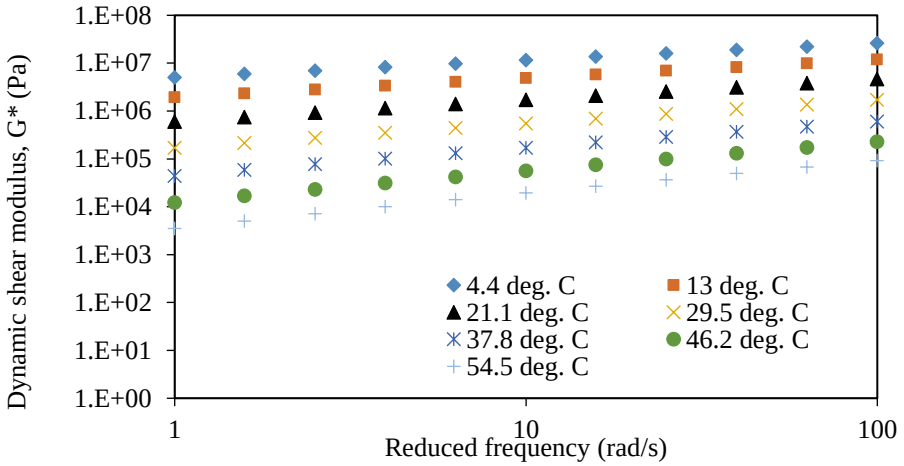


**FIGURE 28 Complex shear modulus vs. frequency plot at different temperatures**

Figure 29 shows the phase angle (δ) at different temperatures for RTFO aged PG 70-22 binder collected from I-25 Rio Bravo and US491 construction sites. It can be observed that the phase angle (δ) value of the asphaltic material decreases with loading frequency. For example, at 21.1 °C, the phase angle decreases from 43.3º to 39.1º due to the increase in frequency from 1 to 100 rad/sec. It is expected as increases frequency causes less deformation to asphaltic material and it starts to behave like an elastic material. However, δ value increases with the increase of temperature as fluidity of asphalt increases with temperature and its viscous property becomes more prominent.

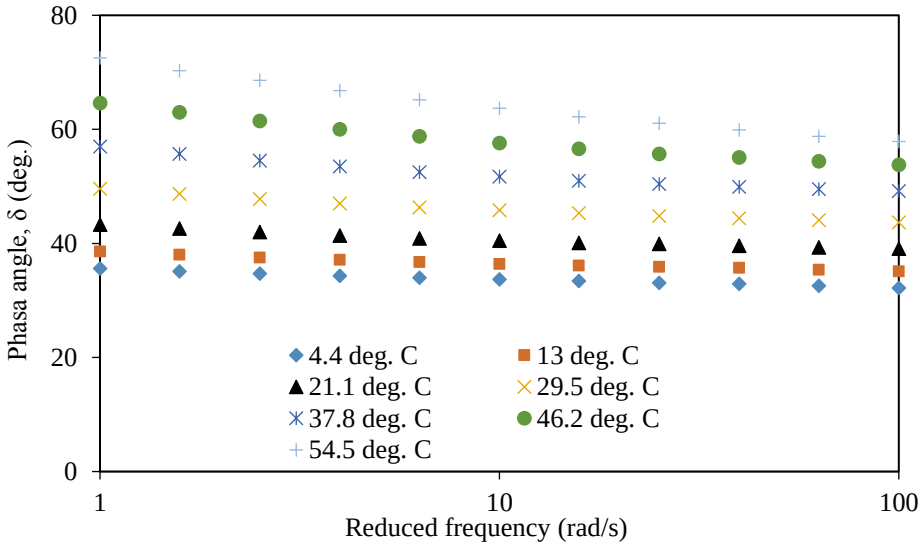


**FIGURE 29 Complex shear modulus vs. frequency plot at different temperatures**

**SUMMARY**

- Determination of dynamic shear modulus ($G^*$) and phase angle ($\delta$) of asphalt binder using DSR test have been demonstrated in this section.
- It is observed that that the $G^*$ value of the asphaltic material increases with loading frequency and decreases with temperature.
- It is also observed that the phase angle ($\delta$) value of the asphaltic material decreases with loading frequency and increases with temperature.
- A summary of the dynamic shear modulus and phase angle of unaged asphalt binder test results have been presented in APPENDIX C that can be directly employed in MEPDG analysis for design Level 1, 2 as well as Level 3.

# RESILIENT MODULUS TEST OF BASE AND SUBGRADE

## INTRODUCTION

Resilient modulus ($M_R$) of unbound layer is one of the critical input parameters in the MEPDG design software. It has been widely used for characterizing the non-linear stress-strain behavior of subgrade, sub-base and base materials subjected to traffic loadings in the design of pavements. Therefore, determination of $M_R$ is essential in laboratory. The details of the test procedure and results are discussed herein.

## SAMPLE PREPARATION

Base and subgrade materials were collected from various construction site. Optimum moisture content of the material was determined by Proctor Test using ASTM D 2216 (*39*) and ASTM D 698 (*40*) test protocols respectively. Prior to the compacting, water was added to the sample to achieve optimum moisture content using ASTM D 698 (*40*) test standard. The samples diameter was 4 in. (100 mm) for both the base and subgrade materials. The heights of the samples were taken at least twice of the diameter.

**FIGURE 30 Sample preparation**

The sample was compacted in eight layers using dynamic impact compaction by modified proctor effort of 56000 ft-lbf/ft$^3$. A total of 27 impact blows in each of the 8 layers was applied to prepare the 4 in. (100 mm) diameter sample. Figure 30 shows a prepared sample and the mold which was used to make sample.

## LABORATORY TESTING

$M_R$ test for subgrade and base materials was conducted in accordance with AASHTO T 307-99 (*41*) test sequence. This method measures the elastic modulus of untreated base and subgrade material. A repeated axial cyclic stress of fixed magnitude was applied to a cylindrical sample. During testing, the sample was subjected to a dynamic cyclic stress and a static confining pressure by means of a pressure chamber. The total recoverable axial deformation of the sample was measured and used to calculate the $M_R$ value as shown in the following equation.

$$M_R = \frac{S_{cyclic}}{\varepsilon_r} \tag{12}$$

where $S_{cyclic}$ is the applied cyclic axial stress and $\varepsilon_r$ is the resilient axial strain. The test setup is shown in Figure 31. The sample was confined in the pressure chamber and external LVDT was used. The vertical deformation ratio of the two LVDTs was monitored for accurate measurement. Three replicate samples of subgrade and base materials were prepared in the laboratory for each of the construction sites. The properties of the subgrade and base materials are shown in Table 9.

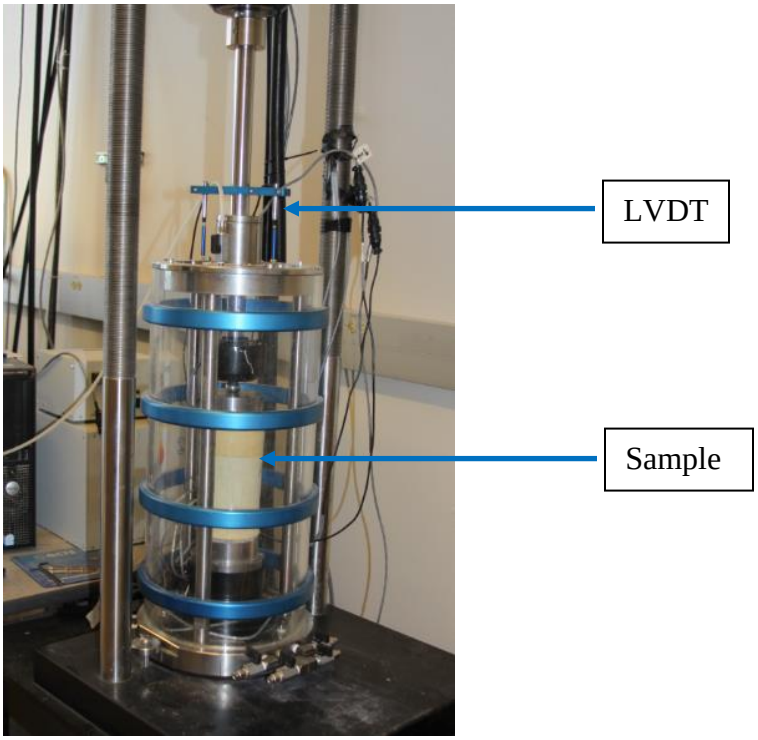


**FIGURE 31 Resilient modulus test setup**

**TABLE 9 Properties of subgrade and base material**

| | | % Passing | | | | | | | | |
|---|---|---|---|---|---|---|---|---|---|---|
| **Material type** | **Construction sites** | **#4** | **#10** | **#40** | **#200** | **Liquid limit** | **Plasticity Index** | **AASHTO soil class** | **Optimum moisture content** | **Dry density, lb./ft$^3$** |
| Subgrade | US54 N | 74.1 | 63.1 | 45.6 | 14.8 | - | NP | A-2-4 | 13.8 | 114.5 |
| | US54 S | 99.3 | 98.2 | 93 | 34 | - | NP | A-2-4 | 9.8 | 117.5 |
| | US 285 | 97.8 | 97 | 93 | 55.7 | 31 | 13 | A-6 | 11.9 | 106.2 |
| | I-25 Rio Bravo | 95.3 | 82.7 | 41.1 | 2 | - | NP | A-2-4 | 9.1 | 123.2 |
| | US491 | 96.4 | 94 | 87.2 | 25 | - | NP | A-2-4 | 10.1 | 119.3 |
| | NM 14 | 87 | 78.5 | 60 | 11 | - | NP | A-2-4 | 11 | 118.4 |
| | NM 47 | 53 | 43 | 23 | 3 | - | NP | A-2-4 | 7.2 | 125.3 |
| Base | US54 N | 53.7 | 42.1 | 26.9 | 10.3 | - | NP | A-1-b | 6.5 | 128.2 |
| | US54 S | 39.5 | 26.9 | 13.5 | 2.1 | - | NP | A-1-a | 7 | 133.5 |
| | US 285 | 43.5 | 27.5 | 13.1 | 4.8 | - | NP | A-1-a | 6.7 | 131.5 |
| | I-25 Rio Bravo | 50 | 38.2 | 18.3 | 2 | - | NP | A-1-b | 8.4 | 129.8 |
| | US491 | 59 | 42 | 17 | 2 | - | NP | A-1-b | 7.8 | 130.6 |
| | NM 14 | 52 | 35 | 14 | 3 | | NP | A-1-b | 6.9 | 128.9 |
| | NM 47 | 44 | 36 | 14 | 2 | - | NP | A-1-a | 5.6 | 134.3 |

## RESULTS AND DISCUSSION

Since the unbound materials, such as base, subgrade materials exhibit stress dependent behavior (*42*), the following stress dependent constitutive model recommended by MEPDG has been used to fit the laboratory tested values:

$$M_R = k_1 p_a \left( \frac{\theta}{p_a} \right)^{k_2} \left( \frac{\tau_{oct}}{p_a} + 1 \right)^{k_3} \quad (13)$$

where $M_R =$ Resilient modulus of unbound layer material,

$p_a =$ Atmospheric pressure (14.7 psi)

$\theta =$ Bulk stress $= \sigma_1 + \sigma_2 + \sigma_3)$

$\sigma_1, \sigma_2$, and $\sigma_3$ = principal stresses and $\sigma_2 = \sigma_3$

$\sigma_d$ = deviator stress = $\sigma_1$ - $\sigma_3$

$\tau_{oct} =$ Octahedral shear stress $(= \frac{\sqrt{2}}{3} |\sigma_1 - \sigma_3|)$, and $k_1, k_2, k_3$ = regression constants

Three replicate samples were prepared for each type of subgrade and base materials and tested at optimum moisture content following AASHTO T 307-99 (*41*) test standard. The pertinent material constants ($k_1$, $k_2$, and $k_3$) were evaluated for both the subgrade and base course materials. Table 10 presents the regression coefficients determined from the laboratory test for the subgrade soils.

**TABLE 10 MEPDG model's parameter for subgrade materials**

| Construction sites | AASHTO soil class | Specimen No. | k1 | k2 | k3 | $R^2$ |
|---|---|---|---|---|---|---|
| | | 1 | 883 | 0.5799 | 0.0687 | 0.89 |
| US54 N | A-2-4 | 2 | 835 | 0.6006 | 0.2487 | 0.82 |
| | | 3 | 850 | 0.5582 | 0.1665 | 0.88 |
| | | 1 | 1278 | 0.36 | 0.1285 | 0.96 |
| US54 S | A-2-4 | 2 | 1269 | 0.3281 | 0.1345 | 0.93 |
| | | 3 | 1198 | 0.2231 | 0.566 | 0.96 |
| | | 1 | 905 | 0.6305 | -2.553 | 0.91 |
| US 285 | A-6 | 2 | 901 | 0.5707 | -2.422 | 0.93 |
| | | 3 | 934 | 0.5384 | -2.365 | 0.91 |
| | | 1 | 862 | 0.1249 | 1.037 | 0.98 |
| US491 | A-2-4 | 2 | 842 | 0.0803 | 1.199 | 0.87 |
| | | 3 | 860 | 0.0958 | 1.101 | 0.88 |
| | | 1 | 556 | 0.2449 | 2.081 | 0.92 |
| NM14 | A-2-4 | 2 | 543 | 0.1928 | 2.076 | 0.74 |
| | | 3 | 558 | 0.2685 | 1.97 | 0.93 |
| | | 1 | 616 | 0.1108 | 2.352 | 0.94 |
| NM47 | A-2-4 | 2 | 774 | 0.2166 | 1.84 | 0.88 |
| | | 3 | 714 | 0.2 | 2.21 | 0.94 |

From Table 10 it is observed that the value of $k_1$ and $k_2$ is found to be positive for each type of subgrade materials. Coefficient $k_1$ is directly proportional to resilient modulus, so it is a positive value. Coefficient $k_2$ should also be positive because bulk stress includes the effect of confine pressure and the materials get compacted more with increase in bulk stress. This is known as stiffening or hardening effect. Coefficient $k_3$ may be positive or negative depending upon the material type. The fine grained soils generally exhibit stress softening that is resilient modulus value decreases with increase in octahedral shear stress. The softening effect may be caused due to the shear deformation in the materials developed by the increase in octahedral shear stress. Coefficient $k_3$ is negative for these types of materials. As can be seen from Table 10, the coefficient $k_3$ is found to be positive for the subgrade soils of every construction sites except for the US285 subgrade soils which is clay (A-6) type of soils. Figure 32 shows the $M_R$ value of subgrade soils of US54N and US285 construction sites. It can be seen from the Figure that the $M_R$ value of subgrade soils of US54N increases with an increase in deviator stress whereas a decreasing trend of the $M_R$ value with an increase in deviator stress is observed in the US285 subgrade soils.

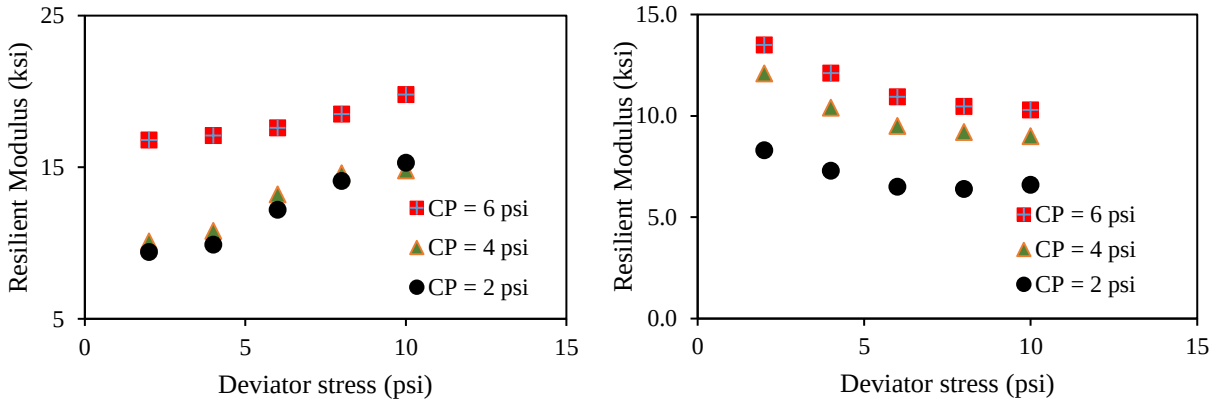


a) US 54 N b) US 285

**FIGURE 32 Resilient modulus with deviator stress**

Figure 33 demonstrates the resilient modulus of US54N and I-25 Rio Bravo subgrade soils with bulk stress. As can be seen from this Figure, the $M_R$ value increases with increase in bulk stress.

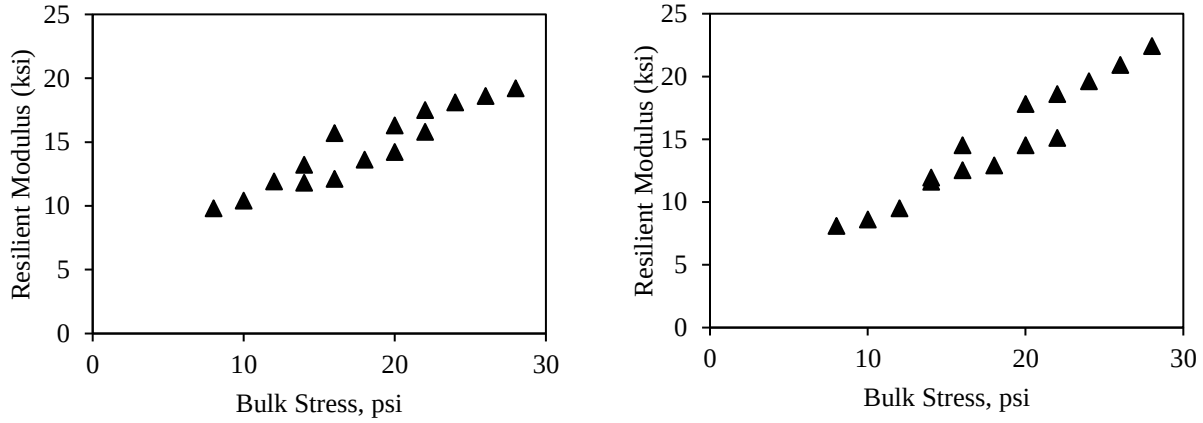


a) US 54 N b) I-25 Rio Bravo

**FIGURE 33 Resilient modulus with bulk stress**

Table 11 summarizes the regression coefficients determined from the laboratory test for the base materials. It is obvious from the table that all the coefficients ($k_1$, $k_2$ and $k_3$) are found to be positive. It implies that the resilient modulus value of base materials increases with increase in deviator stress, bulk stress as well as octahedral shear stress. Figure 34 illustrates the $M_R$ value of US54N and US54S base materials with deviator stress. As can be seen from this Figure that the $M_R$ value increases with an increase in deviator stress. This is expected for base course, as an increase in deviator stress causes reorientation (not like cohesive soils which shows shear deformation) of granular particles letting more compaction, also known as hardening effect. Shear deformation is unlike in base course due to particle interlocking.

**TABLE 11 MEPDG model's parameter for base materials**

| Construction sites | AASHTO soil class | Specimen No. | k1 | k2 | k3 | $R^2$ |
|---|---|---|---|---|---|---|
| | | 1 | 902 | 0.1969 | 0.8321 | 0.96 |
| US54N | A-1-b | 2 | 988 | 0.1022 | 1.239 | 0.96 |
| | | 3 | 964 | 0.2229 | 0.8494 | 0.98 |
| | | 1 | 888 | 0.4058 | 0.5893 | 0.86 |
| US54S | A-1-a | 2 | 924 | 0.3467 | 0.6968 | 0.90 |
| | | 3 | 926 | 0.3573 | 0.6604 | 0.89 |
| | | 1 | 888 | 0.2137 | 1.236 | 0.95 |
| US285 | A-1-a | 2 | 984 | 0.1721 | 1.246 | 0.91 |
| | | 3 | 951 | 0.1832 | 1.268 | 0.90 |
| | | 1 | 1042 | 0.4568 | 0.4136 | 0.97 |
| I-25 | A-1-b | 2 | 908 | 0.4411 | 0.5579 | 0.95 |
| | | 3 | 989 | 0.4254 | 0.5451 | 0.98 |
| | | 1 | 840 | 0.3816 | 0.1676 | 0.99 |
| US491 | A-1-b | 2 | 840 | 0.3178 | 0.4601 | 0.97 |
| | | 3 | 939 | 0.3423 | 0.3162 | 0.98 |
| | | 1 | 955 | 0.518 | 0.3214 | 0.98 |
| NM14 | A-1-b | 2 | 983 | 0.4584 | 0.3779 | 0.98 |
| | | 3 | 955 | 0.4894 | 0.3641 | 0.98 |
| | | 1 | 983 | 0.503 | 0.308 | 0.95 |
| NM47 | A-1-a | 2 | 960 | 0.5293 | 0.2773 | 0.95 |
| | | 3 | | | | |

Figure 35 demonstrates the resilient modulus of US54N and US54S base materials with bulk stress. As can be seen from this Figure, the $M_R$ value increases with an increase in bulk stress. Confinement increases with an increase in bulk stress resulting in higher $M_R$ value.

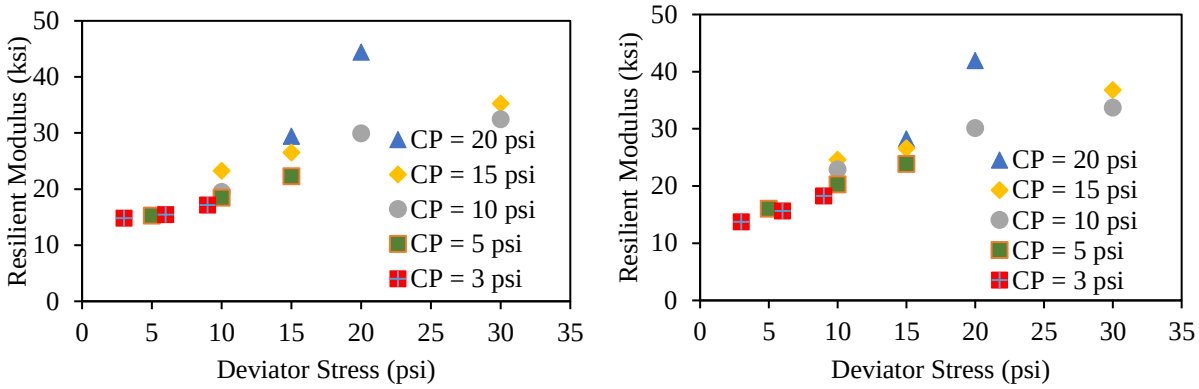


a) US54N b) US54S

**FIGURE 34 Resilient modulus with deviator stress.**

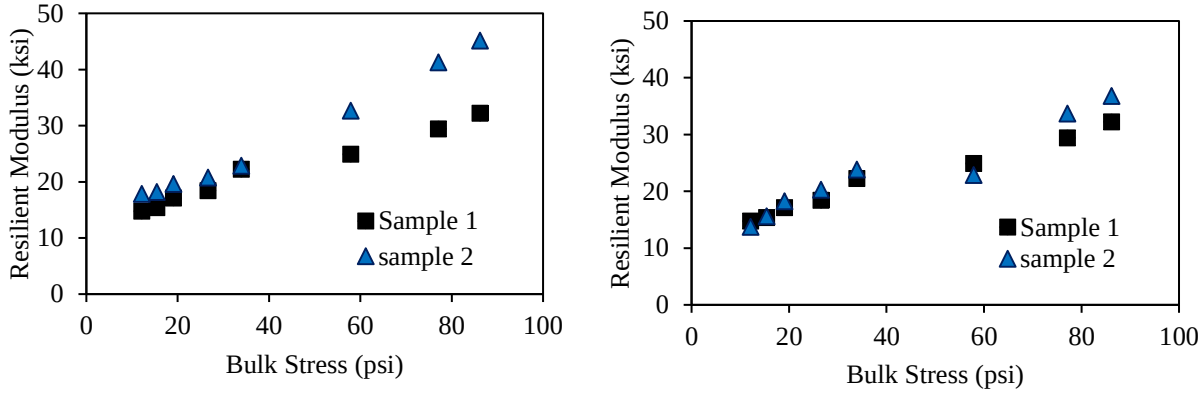


c) US54N d) US54S

**FIGURE 35 Resilient modulus with bulk stress**

## SUMMARY

- The $M_R$ of the subgrade and base materials increase with deviator and bulk stress. The $M_R$ of the fine grained cohesive soil, however, decreases with an increase in octahedral shear stress.
- The $M_R$ of the base materials are found to be increased with octahedral shear stress.
- The materials gradation and the $M_R$ test results are summarized in APPENDIX D and can be directly employed in MEPDG analysis for design Level 1, 2 as well as Level 3.

THIS PAGE LEFT INTENTIONALLY BLANK

# FIELD TESTING

## INTRODUCTION

Several field tests which are additional to the originally proposed work were conducted in this study. These tests give us a field comparison for the laboratory values obtained, an idea of the spatial uniformity in the horizontal and vertical direction, water content, density, compaction, and other useful information. The tests that were performed were Dynamic Cone Penetrometer (DCP) testing, Falling-weight Deflectometer Testing (FWD), and Clegg Hammer or Impact Hammer (CIH) testing. The test procedure, location and results are discussed in the following sections.

## DYNAMIC CONE PENETROMETER (DCP) TEST

DCP testing device is shown in Figure 36. It consists of a rod with a standard sliding weight called hammer attached to the top and a disposable cone tip to penetrate the soil on the bottom. The weight of the hammer is 8 kg and it slides on a 16 mm driving rod. The tip has an included angle of 60 degrees and a diameter at the base of 20 mm. The hammer is lifted up and dropped from a standard height of 575 mm which causes the cone at the bottom of the device to be forced into the ground (*43*). The weight is dropped multiple times till there are enough blows to determine the soil characteristics or the cone has reached a depth of interest. With each blow, the new depth of the device is recorded. The depths and corresponding blow numbers are then plotted in Microsoft Excel where a best linear fit is applied. The slope is considered the DCP value and is usually measured in mm/blow or in./blow.

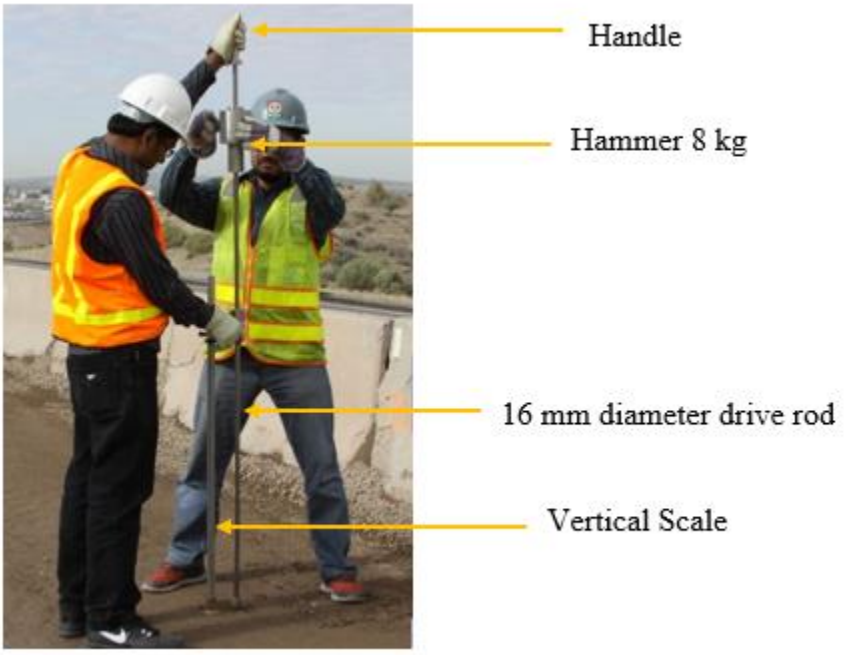


**FIGURE 36 DCP testing device**

Field DCP test was conducted on the compacted subgrade soils of all the chosen construction sites. Twenty test points were selected at five foot apart as shown in Figure 37 except for US54N, US54S and US285 where only 5 test points were selected.

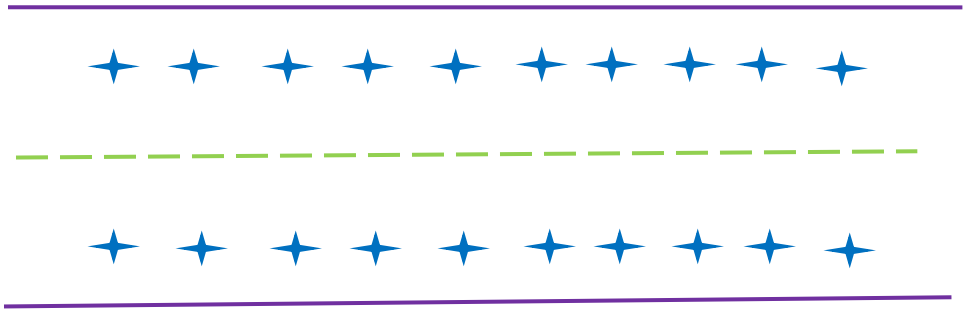

**FIGURE 37 DCP testing schematic**

Twenty blows were applied on each of the twenty test locations. The DCP value was determined from the depths and corresponding blow numbers plot. Figure 38 shows one DCP test results conducted on I-25 construction site at 217.3 MP. The slope of the DCP plot is used in MEPDG Eq. (14) to estimate the $M_R$ value of the subgrade soil.

$$M_R = 2555\left(\frac{292}{DCP^{1.12}}\right)^{0.6} \tag{14}$$

where the DCP value is in mm/blow and the $M_R$ value is in psi.

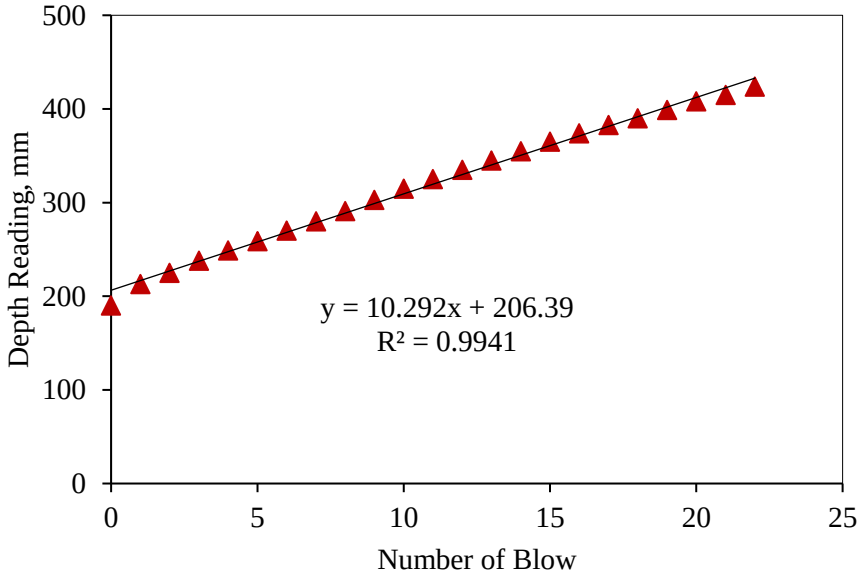


**FIGURE 38 DCP test results**

**Results and Discussions**

The $M_R$ value of the compacted subgrade soils of each construction sites was evaluated employing Eq. (14). Figure 39 shows the $M_R$ values with standard deviation of all the subgrade soils obtained from DCP value. It is observed from Figure 39, the US285 subgrade soils show the highest $M_R$ value. Even though the US285 has a clay type of soil, it is showing higher $M_R$. The reason is that the test was conducted during the winter and the temperature was around 15 °F. The water may have frozen, producing a stronger material than when at higher temperatures. The obtained $M_R$ values of all the selected subgrade soils vary from 17000 to 46000 psi.

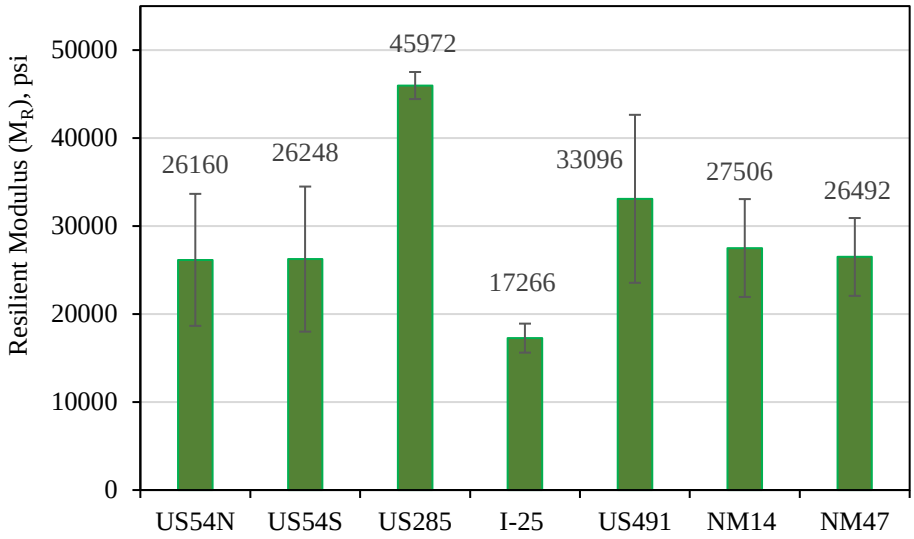


**FIGURE 39 $M_R$ value obtained from DCP test**

**CLEGG IMPACT HAMMER (CIH) TEST**

In the CIH testing device a hammer of weight 4.5 kg is attached to an acceleration measuring device. The hammer is dropped from a specified height of 450 mm one or two times in order to create a pre-disturbed area for the hammer to hit. This is done because before the seating blows there is loose soil and excessive variability on the contact surface not related to the impact value of the soil. According to the test standard, four drops of the hammer are performed at one testing spot. All of the blows are recorded and analyzed. The value obtained from the measuring device attached to the hammer is the deceleration in units of 10's of gravities or *g*. The standard for this test is ASTM D 5874-02 (*44*). Figure 40 shows the CIH testing device.


**FIGURE 40 CIH testing device**

**Results and Discussions**

Twenty-two CIH tests were conducted directly on the compacted subgrade and base course materials of all the pavement sites in a pattern as shown in Figure 42. Four drops were done at each spot and the highest value was taken as the correct impact value. The test was performed every five feet. The highest impact value was used to determine the resilient modulus of subgrade as well as the base course materials employing the following empirical relationship (*45*).

$$M_R = 0.088 * (CIV)^2 \quad (15)$$

where *CIV* is the Clegg Impact Value and $M_R$ value is in MPa.

Figure 41 demonstrates the resilient modulus of subgrade soils and Figure 42 illustrates the resilient modulus of base materials obtained from the CIH test. It is observed from these figures that the CIH obtained resilient modulus of subgrade soils vary from 10000 psi to 23000 psi and 10000 psi to 30000 psi for the base materials.

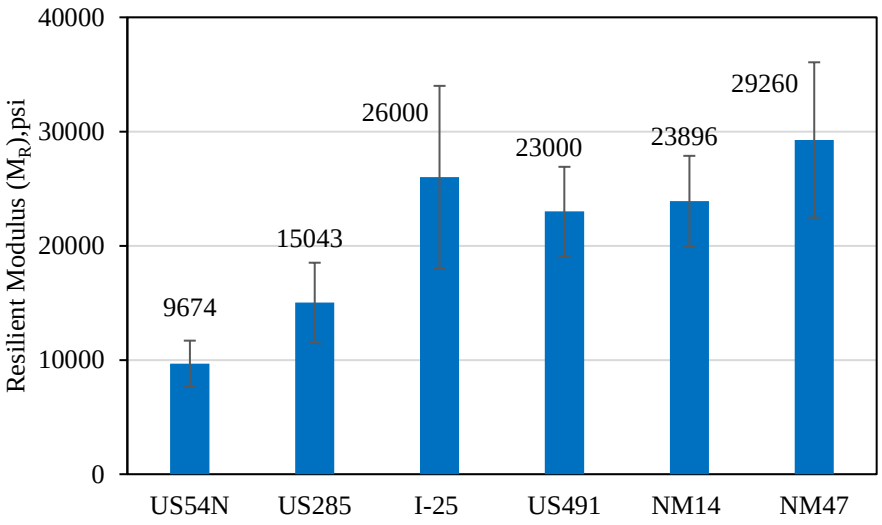


**FIGURE 41 $M_R$ value of base materials obtained from CIH test**

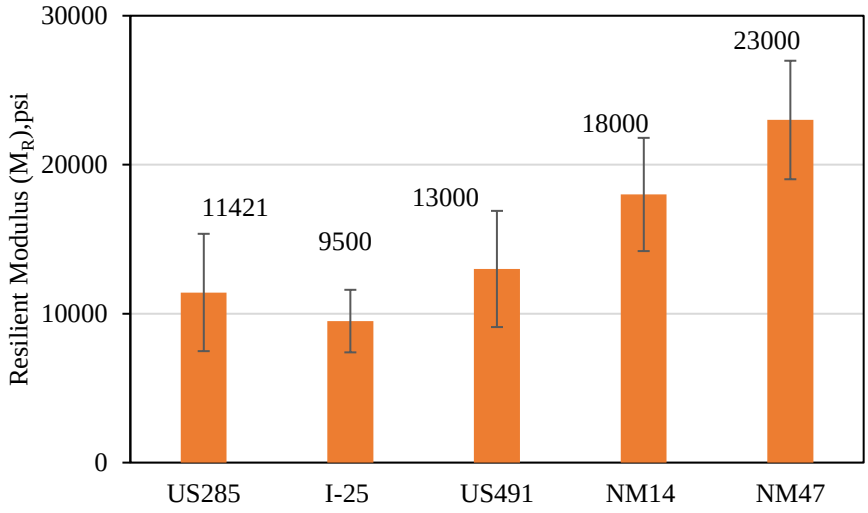


**FIGURE 42 $M_R$ value of subgrade soils obtained from CIH test**

## FALLING WEIGHT DEFLECTOMETER (FWD) TEST

FWD is a nondestructive test which is used to determine the moduli of the pavement layers. An impact load is applied on the surface by dropping a weight (usually, 9-16 kips) and transmitted to the AC through a circular steel plate. The pavement surface deflects vertically forming a deflection basin. Surface deflections are measured through geophones locating at different distances from loading point. The measured vertical deformation at different radial points, pavement geometry and applied load are provided into the backcalculation software as input and the stiffness of different layers are determined using backcalculation algorithm based on linear and non-linear elastic analysis. Figure 43 shows FWD testing device.

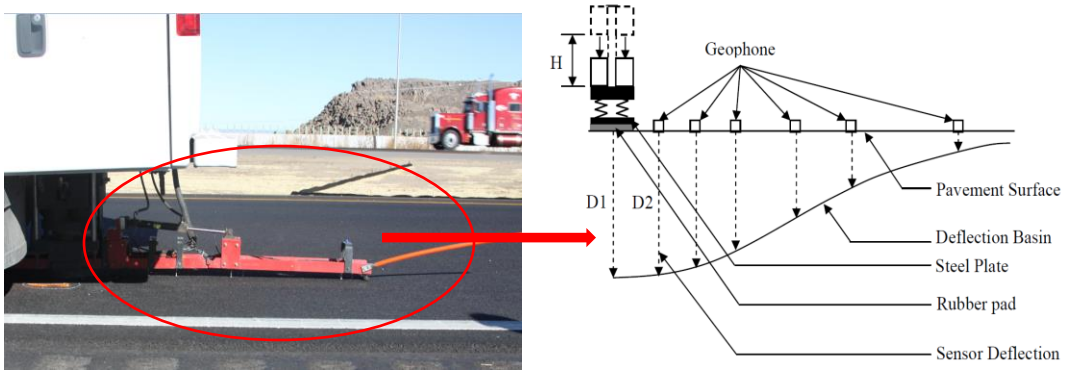


**FIGURE 43 FWD testing**

**Results and Discussions**

FWD test was conducted on the compacted subgrade and base as well as AC layer of the selected pavement. The test was performed at three load levels, such as 9, 12, and 16 kips. Layer modulus values were determined from the deflection of the layer caused by the load. These calculations were accomplished using a computer program that analyzes and manipulates the data according to inputs and engineering judgment of the analyzer. Figure 44 shows the backcalculated AC layer modulus obtained from the FWD test for 9 kip load for all the pavement sites. In Figure 44, the highest modulus was found for US54S AC layer whereas the lowest modulus was for US491.

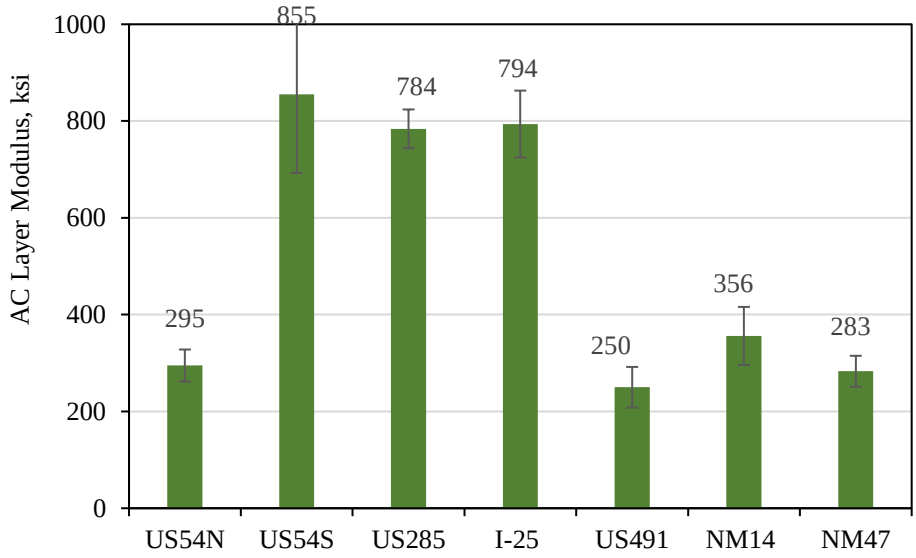


**FIGURE 44 AC layer modulus from FWD test**

Figure 45 illustrates the subgrade and base modulus of all the pavement sites for FWD test conducted on the final AC layer for 9 kip load. It is seen from this Figure that the subgrade soils

modulus vary from 16 ksi to 41 ksi. The highest subgrade modulus was found for I-25 and the lowest for NM47 and US491.

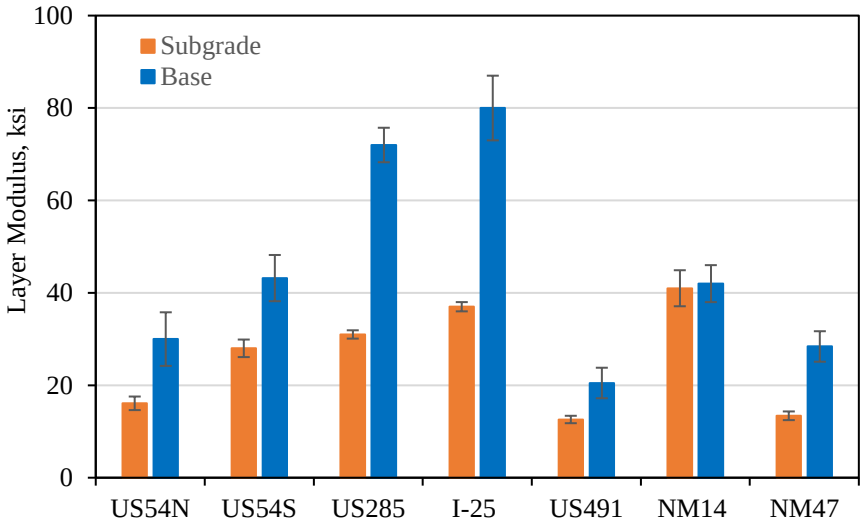


**FIGURE 45 Unbound layer modulus from FWD test**

As mentioned earlier, the FWD test was also conducted directly on the compacted subgrade soils. Figure 46 shows the subgrade modulus of various pavement sites obtained from the FWD test carried out on the subgrade soils for 9 kips load. It is observed from Figure 45 that the highest subgrade modulus was found for US54S and the lowest for US285. Overall the modulus value varies from 15 ksi to 24 ksi.

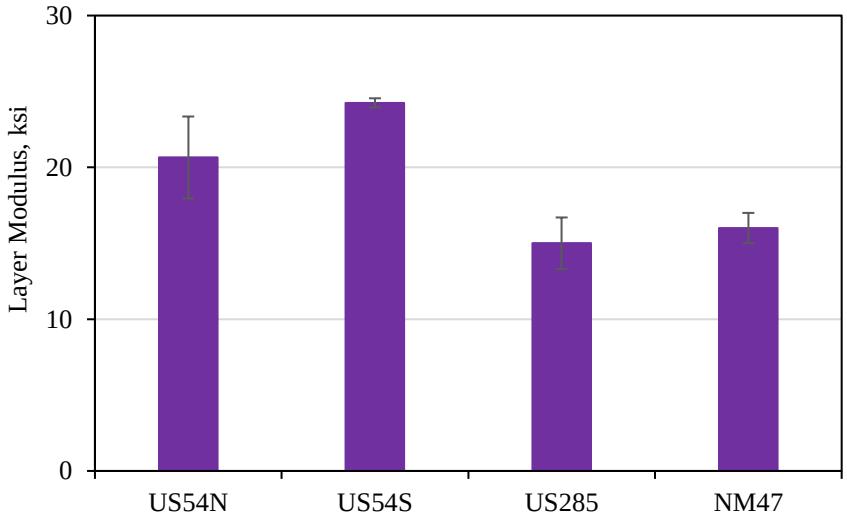


**FIGURE 46 Subgrade modulus from FWD test**

**SUMMARY**

- Three types of field tests such as DCP, CIH and FWD were conducted in this task on the selected pavement sections.
- The resilient modulus of the subgrade soils has been evaluated from the DCP and CIH test results employing empirical relations. The results show that the values vary from 17 to 46 ksi for DCP and 10 ksi to 23 ksi for CIH.
- The CIH obtained base modulus value varies from 10 ksi to 30 ksi.
- The AC modulus of FWD test ranges from 250 ksi to 850 ksi whereas subgrade and base modulus from 13 ksi to 41 ksi and 20 ksi ti 80 ksi.
- These data base can be used for Level 2 and 3 MEPDG analysis.

# MEPDG IMPLEMENTATION

## INTRODUCTION

The primary objective of this task is to implement all the pavement materials properties determined from the laboratory test into MEPDG. The pavement performance in terms of rutting and fatigue cracking is observed based on the MEPDG analysis. The analysis is performed for Level 1, 2 as well as Level 3 and the effect of analysis level on the pavement performance is also observed.

## OVERVIEW

The MEPDG requires laboratory test results to properly characterize the pavement materials for pavement design and analysis. Level 1 requires materials properties determined from the laboratory test and provides highest level of accuracy. Level 2 provides an intermediate level of accuracy where the materials properties are determined through various correlations. Level 3 is the least accurate and uses the default values based on some empirical relations. In this study, all the materials' input parameters required for MEPDG analysis are gathered and analyzed for all level.

## INPUT FOR MEPDG

Pavement performance analysis is performed for seven selected pavement sections: US54N, US54S, US285, I-25 Rio Bravo, US491, NM14 and NM47. The steps of this analysis are described as below:

### Traffic

The major information related to traffic required in MEPDG includes the Annual Average Daily Truck Traffic (AADTT), Growth Rate (GR) of traffic, and distribution of different classes of vehicle. These values are collected and calculated from the detailed traffic information provided by the technical panel members of this project. Some of the processed information is summarized in Table 12. In the first row, CN represents the project Control Number (CN), i.e., project identification number. The Annual Average Daily Traffic (AADT) is the design average as determined by a traffic analyst. The (%) Truck is multiplied with the AADT to determine the design AADTT. The traffic growth rate is determined from the yearly traffic counts. Traffic information for US491 and NM47 pavement site was not available which is why the default traffic information was used in the analysis. However, a value of 2.5 Growth Rate of traffic was used for both US491 and NM47 site.

**TABLE 12 Summary of the traffic input**

| Project | US54N | US54S | US285 | I-25 RB | NM 14 |
|---|---|---|---|---|---|
| CN | 2100250 | G3a12 | 5100411 | 301010 | S100140 |
| AADT | 1398 | 4992 | 5978 | 47258 | 16898 |
| (%) Truck | 57.16 | 40.41 | 17.43 | 10 | 10.12 |
| AADTT | 799 | 2017 | 1042 | 4726 | 1710 |
| GR (%) | 2.7 | 4 | 2.5 | 2.6 | 2.5 |
| DR/Lane | 0.5 | 0.5 | 0.5 | 0.7 | 0.5 |

Vehicle class distribution is another vital traffic input to the MEPDG software. The vehicle class distribution is summarized in Table 13. These are calculated based on the volume of different classes of vehicles during the traffic count. Default vehicle class distribution was used for NM14 and NM47 pavement site as the distribution of vehicle class was not available. The entire analysis is performed for a design period of 20 years.

**TABLE 13 Distribution of vehicle class on pavement sites**

| Project | US54N | US54S | US285 | I-25 RB | US491 |
|---|---|---|---|---|---|
| Class 4 | 13.7 | 17.2 | 14.9 | 12.1 | 31.7 |
| Class 5 | 13.7 | 17.2 | 14.9 | 12.1 | 31.7 |
| Class 6 | 2.3 | 20.7 | 2.7 | 2.2 | 0.8 |
| Class 8 | 34.2 | 9.9 | 15.4 | 18.0 | 17.0 |
| Class 9 | 34.0 | 34.0 | 47.0 | 47.2 | 15.8 |
| Class 10 | 0.2 | 0.7 | 1.8 | 0.8 | 0.4 |
| Class 11 | 0.9 | 0.3 | 3.0 | 5.7 | 1.9 |
| Class 12 | 0.9 | 0.0 | 0.2 | 1.7 | 0.7 |
| Class 13 | 0.0 | 0.0 | 0.2 | 0.1 | 0.1 |

**Layer Thicknesses**

The layer thicknesses of pavement layers were collected from the project manager of each pavement sites during their construction. Table 14 summarized the layer thicknesses of pavement layers of various pavement sites selected for this study. All the pavement sites have a base layer of 6 inches. The thickness of the AC layer is of 6 inches for all of them except for US285 that has a 6.5 inches AC layer. The analysis is performed incorporating these layer thicknesses.

**TABLE 14 Layer thicknesses of the selected pavement sites**

| Construction Site | Base (in) | AC layer (in) |
|---|---|---|
| US54N | 6 | 6 |
| US54S | 6 | 6 |
| US285 | 6 | 6.5 |
| I-25 | 6 | 8 |
| US491 | 6 | 6 |
| NM 47 | 6 | 6 |
| NM 14 | 6 | 6 |

### AC Layer

The Level 1 analyses for an AC layer requires the temperature and frequency varying dynamic modulus and shear modulus as well as phase angle of asphalt binder. The dynamic modulus values of the AC layer are determined from laboratory test as already documented in APPENDIX A. The dynamic shear modulus and phase angle of asphalt binder at different temperatures are summarized in APPENDIX C. This value was determined by conducting dynamic shear rheometer test on the virgin binder at a frequency of 10 rad/sec. Level 2 and 3 require sieve analysis results of the aggregate and the PG binder grade. All this information is also documented.

### Unbound Layers

In the current version of MEPDG, provision of the Level 1 analysis is removed. Therefore, the stress-dependency cannot be assigned to this software. For this reason, the Level 2 and 3 analysis is performed for the unbound layers. This analysis requires the particle gradation and resilient modulus of the unbound layers. The resilient modulus values are determined from the laboratory test. The subgrade resilient modulus value was selected for a confining pressure of 2 psi and a deviator stress of 6 psi. On the other hand, the base materials resilient modulus was selected for a confining stress of 5 psi and a deviator stress of 15 psi as recommended by NCHRP Research Results Digest 285 (*46*). Particle gradation is summarized in Table 5. This table contains the summary of particle gradation, proctor test as well as Atterberg Limit test results for both base and subgrade of the selected pavement sections.

## SUMMARY OF PERFORMANCE

Selected pavement sections are analyzed in the MEPDG which determines the following performance parameters over 20 years:

- Terminal International Roughness Index (IRI), in./mile
- Permanent deformation (rutting)-total pavement, in.
- AC bottom-up fatigue cracking, % lane area
- AC thermal cracking, ft./mile
- AC top-down fatigue cracking, ft./mile

- Permanent deformation-AC only, in.

Table 15 presents pavement performance parameters of the US54N pavement site. These parameters are evaluated for design Level 1, and 2 as well as 3. It is observed that the predicted parameters are smaller than the target parameters for the design Level 1 indicating that this pavement site will serve 20 years before attaining the limiting cracks and rutting. Level 2 and 3 analysis, however, show earlier rutting and top down fatigue cracking on AC.

**TABLE 15 Summary of performance of US54N**

| Distress Type | Level 1 | | Level 2 | | Level 3 | |
|---|---|---|---|---|---|---|
| | Target | Predicted | Target | Predicted | Target | Predicted |
| Terminal IRI (in/mile) | 172 | 132.77 | 172 | 151.59 | 172 | 145.34 |
| Permanent deformation - total pavement (in) | 0.75 | 0.38 | 0.75 | 0.82 | 0.75 | 0.69 |
| AC bottom-up fatigue cracking (% lane area) | 25 | 1.56 | 25 | 2.14 | 25 | 1.73 |
| AC thermal cracking (ft/mile) | 1000 | 27.17 | 1000 | 27.17 | 1000 | 27.17 |
| AC top-down fatigue cracking (ft/mile) | 2000 | 1023.05 | 2000 | 3114.07 | 2000 | 2257.49 |
| Permanent deformation - AC only (in) | 0.40* | 0.22 | 0.40* | 0.61 | 0.40* | 0.53 |

*FHWA report, page 5966 (*47*)

Figure 47 shows rut depth comparison for different design Level obtained from MEPDG analysis for US54N AC mixture. It is seen from the Figure; higher rut depth was observed for design Level 2 compared to Level 1 and Level 3.

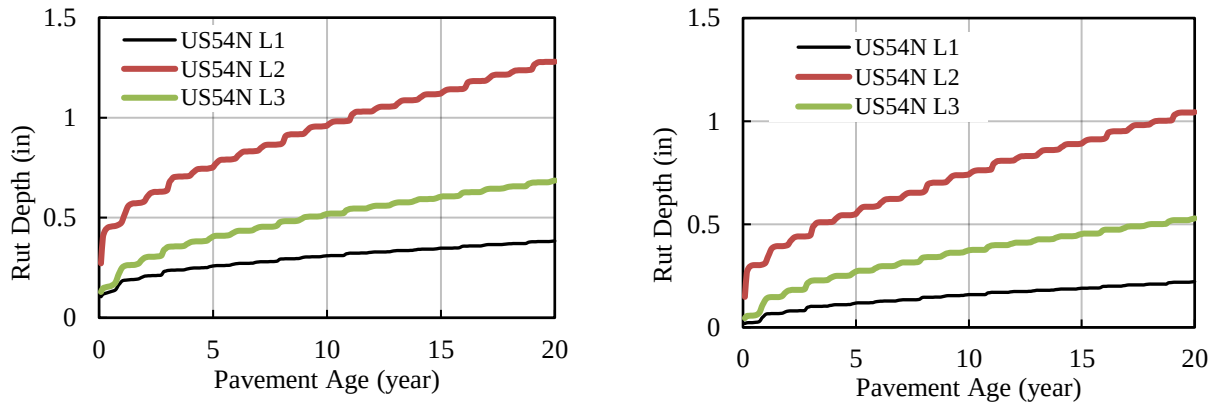


(a) Total rut depth (b) Rut depth in AC only

**FIGURE 47 Rut depth comparison for Level 1, 2 and 3**

Figure 48 illustrates the bottom up cracking comparison for different design Level obtained from MEPDG analysis for US54N AC mixture. Like rut depth, higher bottom up cracking was observed for design Level 2 compared to other Levels.

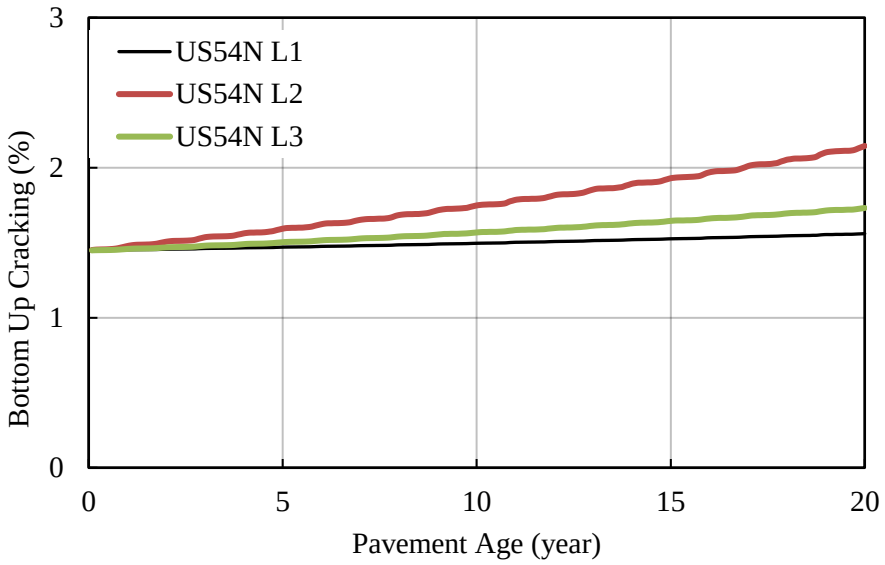


**FIGURE 48 Bottom up cracking for Level 1, 2 and 3**

Table 16 presents pavement performance parameters of the US54S pavement site. These parameters are evaluated for design Level 1, and 2 as well as 3. It is observed that the predicted parameters are smaller than the target parameters for the design Level 1 indicating that this pavement site will serve 20 years before attaining the limiting cracks and rutting. The PG binder grade, RAP content and aggregate source are the same for UN54N and US54S. UN54S, however, shows higher rutting for design Level 1. This is because of the higher AADTT and traffic growth rate factor. Level 2 and 3 analysis also show earlier rutting and top down fatigue cracking on AC. This is also apparent from Figure 49 where a comparison of rut depth has been made among the different design levels.

**TABLE 16 Summary of performance of US54S**

| Distress Type | Level 1 | | Level 2 | | Level 3 | |
|---|---|---|---|---|---|---|
| | Target | Predicted | Target | Predicted | Target | Predicted |
| Terminal IRI (in/mile) | 172 | 139.17 | 172 | 176.15 | 172 | 165.99 |
| Permanent deformation - total pavement (in) | 0.75 | 0.49 | 0.75 | 1.28 | 0.75 | 1.1 |
| AC bottom-up fatigue cracking (% lane area) | 25 | 2.04 | 25 | 20.88 | 25 | 8.66 |
| AC thermal cracking (ft/mile) | 1000 | 27.17 | 1000 | 27.17 | 1000 | 27.17 |
| AC top-down fatigue cracking (ft/mile) | 2000 | 1352.39 | 2000 | 5678.52 | 2000 | 3360.99 |
| Permanent deformation - AC only (in) | 0.40* | 0.30 | 0.40* | 1.04 | 0.40* | 0.88 |

*FHWA report, page 5966 (*47*)

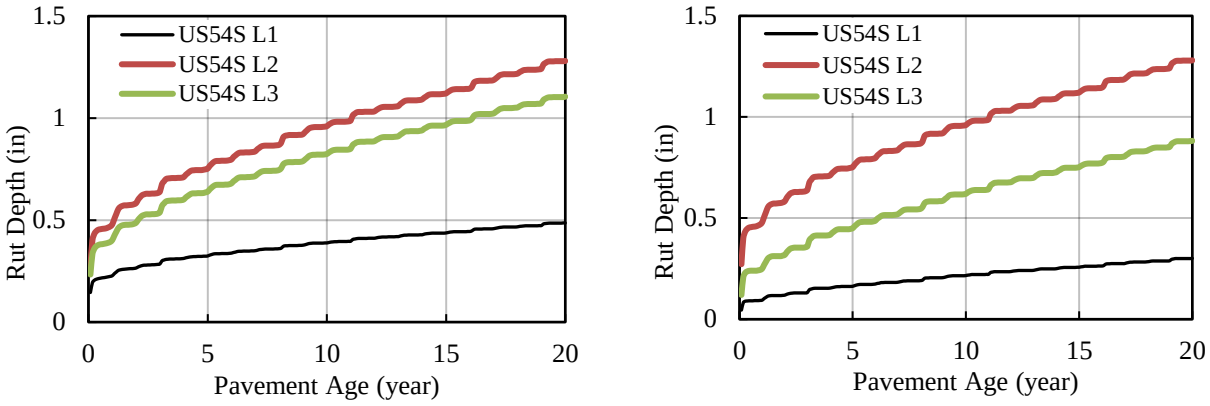


(a) Total rut depth (b) Rut depth in AC only

**FIGURE 49 Rut depth comparison for Level 1, 2 and 3**

Levels 2 and 3 analysis for US54N and US54S show higher rutting in AC layer as well as higher fatigue cracking than Level 1. This is because Levels 2 and 3 under predicts the dynamic modulus value determined from the aggregate gradation and PG binder grade. Figure 50 demonstrates a comparison of mastercurves of design Levels 1, 2 and 3 constructed following the MEPDG software analysis. It is observed from Figure 50 that the lowest dynamic modulus values were evaluated for design Level 2. The Root Mean Square of Error (RMSE, %) was calculated for the dynamic modulus values of design Levels 2 and 3 with respect to Level 1. The RMSE value was found to be 70% for Level 2 and 55% for Level 3. It implies that predicted dynamic modulus values for design Levels 2 and 3 are statistically different than Level 1.

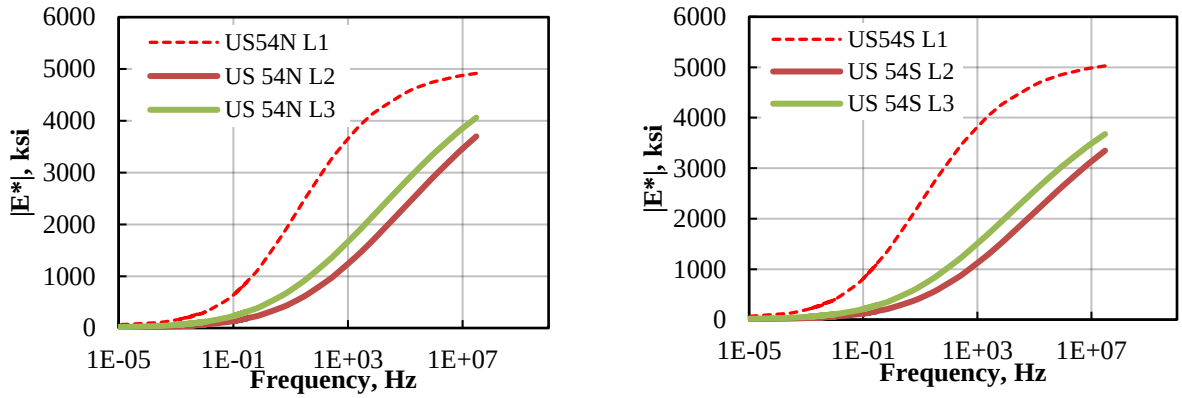


(c) US 54N (d) US 54S

**FIGURE 50 Dynamic modulus comparison for Level 1, 2 and 3**

Table 17 presents pavement performance parameters of the US285 Clines Corners pavement site. These parameters are evaluated for design Levels 1, 2 and 3. It is observed that the predicted parameters are smaller than the target parameters for the design Level 1 indicating that this pavement site will serve 20 years before attaining the limiting cracks and rutting. Levels 2 and 3 analysis, however, show earlier rutting on AC. The dynamic modulus of the AC layer cannot be incorporated in Levelss 2 and 3. US285 AC layer contains 35% RAP and its dynamic modulus value is found to be higher than the US54N and US54S at low and high frequency level. Since

only aggregate gradation was used in Levels 2 and 3, the analysis results show earlier failure of the pavement due to rutting.

**TABLE 17 Summary of performance of US285**

| Distress Type | Level 1 | | Level 2 | | Level 3 | |
|---|---|---|---|---|---|---|
| | Target | Predicted | Target | Predicted | Target | Predicted |
| Terminal IRI (in/mile) | 172 | 153.51 | 172 | 177.2 | 172 | 163.64 |
| Permanent deformation - total pavement (in) | 0.75 | 0.62 | 0.75 | 1.13 | 0.75 | 0.87 |
| AC bottom-up fatigue cracking (% lane area) | 25 | 2.46 | 25 | 21.64 | 25 | 4.54 |
| AC thermal cracking (ft/mile) | 1000 | 27.17 | 1000 | 27.17 | 1000 | 27.17 |
| AC top-down fatigue cracking (ft/mile) | 2000 | 278.51 | 2000 | 1090.92 | 2000 | 1394.47 |
| Permanent deformation - AC only (in) | 0.40* | 0.23 | 0.40* | 0.64 | 0.40* | 0.59 |

*FHWA report, page 5966 (*47*)

Table 18 presents pavement performance parameters of the I-25 Rio Bravo pavement site. These parameters are evaluated for design Levels 1, 2 and 3. It is observed that earlier rutting and top down fatigue cracking on AC occur for all analysis level indicating that this pavement site will not serve 20 years before attaining the limiting cracks and rutting. The reason is that this pavement site has the highest AADTT that causes rutting and fatigue on the pavement.

**TABLE 18 Summary of performance of I-25 Rio Bravo**

| Distress Type | Level 1 | | Level 2 | | Level 3 | |
|---|---|---|---|---|---|---|
| | Target | Predicted | Target | Predicted | Target | Predicted |
| Terminal IRI (in/mile) | 172 | 152.05 | 172 | 184.36 | 172 | 179.76 |
| Permanent deformation - total pavement (in) | 0.75 | 0.98 | 0.75 | 1.72 | 0.75 | 1.49 |
| AC bottom-up fatigue cracking (% lane area) | 25 | 1.89 | 25 | 3.39 | 25 | 2.22 |
| AC thermal cracking (ft/mile) | 1000 | 27.17 | 1000 | 27.17 | 1000 | 27.17 |
| AC top-down fatigue cracking (ft/mile) | 2000 | 1849.7 | 2000 | 4000.78 | 2000 | 2706.39 |
| Permanent deformation - AC only (in) | 0.40* | 0.81 | 0.40* | 1.51 | 0.40* | 1.33 |

*FHWA report, page 5966 (*47*)

Figure 51 shows a comparison of dynamic modulus input values among the design Levels 1, 2 and 3 for AC mixture of US285 and I-25. As mentioned in the preceding sections, Level 1 uses the laboratory determined dynamic modulus values whereas Level 2 uses gradation and binder test results and Level 3 uses aggregate gradation and PG binder grade. It is evident from Figure 51 that Levels 2 and 3 under predicts the dynamic modulus value determined from the aggregate gradation and PG binder grade resulting in higher rutting and cracking.

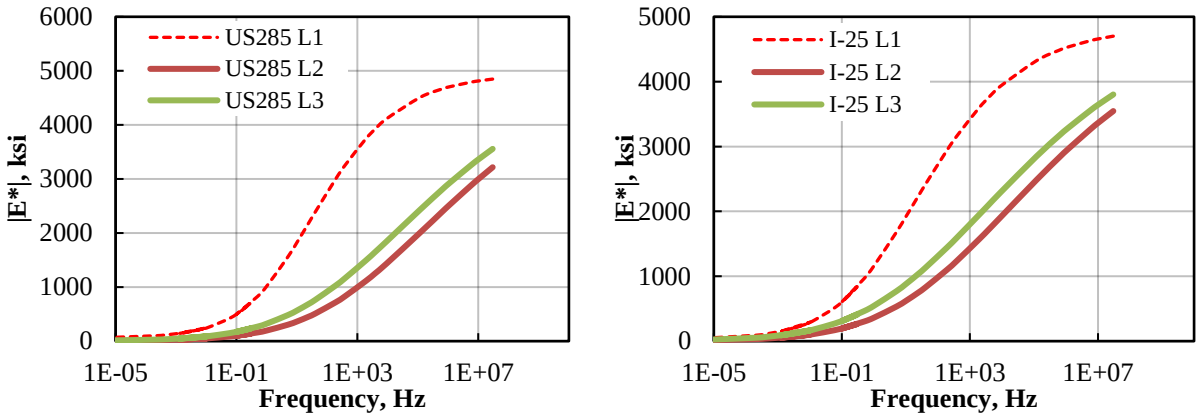


(a) US 285 (b) I-25

**FIGURE 51 Dynamic modulus comparison for Level 1, 2 and 3**

Table 19 summarizes pavement performance parameters of the US491 sites. These parameters are evaluated for design Levels 1, 2 and 3. It is observed that earlier rutting and top down fatigue cracking on AC occur for all analysis level for each of the pavement site indicating that these pavement sites will not serve 20 years before attaining the limiting cracks and rutting. Higher rutting and fatigue cracking were also observed in design Levels 2 and 3 compared to design Level 1. The reason is already explained.

**TABLE 19 Summary of performance of US 491**

| Distress Type | Level 1 | | Level 2 | | Level 3 | |
|---|---|---|---|---|---|---|
| | Target | Predicted | Target | Predicted | Target | Predicted |
| Terminal IRI (in/mile) | 172 | 150.43 | 172 | 177.47 | 172 | 167.44 |
| Permanent deformation - total pavement (in) | 0.75 | 0.82 | 0.75 | 1.4 | 0.75 | 1.23 |
| AC bottom-up fatigue cracking (% lane area) | 25 | 4.33 | 25 | 21.98 | 25 | 4.75 |
| AC thermal cracking (ft/mile) | 1000 | 27.17 | 1000 | 27.17 | 1000 | 26.25 |
| AC top-down fatigue cracking (ft/mile) | 2000 | 2867.66 | 2000 | 4619.23 | 2000 | 3188.42 |
| Permanent deformation - AC only (in) | 0.40* | 0.63 | 0.40* | 1.18 | 0.40* | 1.07 |

*FHWA report, page 5966 (*47*)

Table 20 presents pavement performance parameters of the NM14. These parameters have been evaluated for design Level 1, 2 and 3. It is observed that earlier rutting and top down fatigue cracking on AC occur for all analysis level of the pavement site indicating that these pavement sites will not serve 20 years before attaining the limiting cracks and rutting. Higher rutting and fatigue cracking were also observed in design Level 2 and 3 compared to design Level 1.

**TABLE 20 Summary of performance of NM14**

| Distress Type | Level 1 | | Level 2 | | Level 3 | |
|---|---|---|---|---|---|---|
| | Target | Predicted | Target | Predicted | Target | Predicted |
| Terminal IRI (in/mile) | 172 | 146.39 | 172 | 171.9 | 172 | 161.86 |
| Permanent deformation - total pavement (in) | 0.75 | 0.68 | 0.75 | 1.26 | 0.75 | 1.06 |
| AC bottom-up fatigue cracking (% lane area) | 25 | 2.04 | 25 | 10.93 | 25 | 2.17 |
| AC thermal cracking (ft/mile) | 1000 | 27.17 | 1000 | 27.17 | 1000 | 27.17 |
| AC top-down fatigue cracking (ft/mile) | 2000 | 1958.36 | 2000 | 3779.56 | 2000 | 2742.03 |
| Permanent deformation - AC only (in) | 0.40* | 0.45 | 0.40* | 0.99 | 0.40* | 0.88 |

*FHWA report, page 5966 (*47*)

Table 21 presents pavement performance parameters of the NM47. These parameters have been evaluated for design Levels 1, 2 and 3. It is observed that earlier rutting and top down fatigue cracking on AC occur for all analysis level of the pavement site indicating that these pavement sites will not serve 20 years before attaining the limiting cracks and rutting. Like other analysis results higher rutting and fatigue cracking were also observed in design Levels 2 and 3 compared to design Level 1. It should be noted that the rut depth and fatigue cracking comparison for various design Level for the other AC mixtures have also been plotted and similar trends were observed. Those are not shown here.

**TABLE 21 Summary of performance of NM47**

| Distress Type | Level 1 | | Level 2 | | Level 3 | |
|---|---|---|---|---|---|---|
| | Target | Predicted | Target | Predicted | Target | Predicted |
| Terminal IRI (in/mile) | 172 | 143.3 | 172 | 190.23 | 172 | 179.04 |
| Permanent deformation - total pavement (in) | 0.75 | 0.76 | 0.75 | 1.79 | 0.75 | 1.6 |
| AC bottom-up fatigue cracking (% lane area) | 25 | 2.17 | 25 | 20.69 | 25 | 4.7 |
| AC thermal cracking (ft/mile) | 1000 | 27.17 | 1000 | 27.17 | 1000 | 27.17 |
| AC top-down fatigue cracking (ft/mile) | 2000 | 2692.23 | 2000 | 5995.25 | 2000 | 3977.18 |
| Permanent deformation - AC only (in) | 0.40* | 0.57 | 0.40* | 1.56 | 0.40* | 1.41 |

*FHWA report, page 5966 (*47*)

## SUMMARY

- Incorporation of pavement materials properties into MEPDG software has been described in this section.
- For some of the pavement sites, Level 1 analysis shows the predicted parameters are within the target limit whereas Levels 2 and 3 analysis illustrates earlier failure of the pavement. The lack of proper material characterization in Levels 2 and 3 is attributed to this fact.

THIS PAGE LEFT INTENTIONALLY BLANK

# CONCLUSIONS AND RECOMMENDATIONS

## GENERAL

This report details the activities and results for the advanced calibration project. Subgrade, base, asphalt concrete, binder and aggregate have been collected from a total of seven pavement reconstruction sites selected for this study in the state of New Mexico. Comprehensive laboratory tests have been conducted on these materials for MEPDG implementation. The findings of this study are expected to be useful and helpful for pavement engineer and designer.

## CONCLUSIONS

Based on the test results, analysis and discussion presented in this study, the following conclusions can be drawn:

- Dynamic modulus of AC is sensitive to the RAP content and PG binder grade. It was observed that the AC layers in pavement sections that contain high RAP content and PG grade exhibit higher dynamic modulus.
- The FEL tests were conducted on the selected AC mixtures with varying RAP content and PG binder grade which were collected from seven different pavement sites. Unlike the trend of dynamic modulus, FEL of the AC layers which have higher RAP content show smaller FEL. It indicates that incorporation of RAP leads to a significant reduction in the fatigue performance of the AC mixture.
- Based on the measured FEL values, it was observed that range of the FEL of the AC mixtures collected from the selected pavement sites is 100 ~ 150 micro-strain. Now, it is recommended to incorporate this range during the Mechanistic-Empirical (M-E) analysis of pavement.
- The DSR tests were conducted on the collected virgin binder. From the test results, it was observed that the dynamic shear modulus of asphalt binder increases with loading frequency and decreases with temperature. In addition, the phase angle (δ) value of the asphalt binder decreases with loading frequency and increases with temperature. The test results were later incorporated to the pavement M-E analysis as Levels 1 and 2 inputs.
- The resilient modulus of the unbound layer materials, i.e., fine soil from subgrade and aggregates from base, increase with bulk stress, which is known as ‘stress hardening’. Under this behavior, particles get compacted into a denser state with increase in bulk stress, thus, leads to a higher stiffness. It indicates that the modulus of unbound layers increase with high tire pressure.
- It is known that the deviator stress (octahedral shear stress) also increases with increase in tire pressure imposed by different types of vehicles. There is a possibility that the resilient modulus may decrease with increase in octahedral shear stress, which is known as ‘stress softening’. Under this behavior, particles of the fine grained soils starts sliding over one another resulting in higher shear deformation and less resilient modulus. Resilient modulus tests on fine soil, as collected from seven different pavement sites, shows that the subgrade does not exhibit stress softening except the US285.

- Several field tests, i.e., DCP, CIH and FWD, were conducted on the selected pavement sites to determine the layer modulus. The layers modulus obtained from the field test can be implemented in M-E analysis as Levels 2 and 3 input.
- The MEPDG analysis was performed for all the selected pavement sections employing the generated database for design Levels 1, 2 and 3 to observe the pavement performance in terms of rutting and fatigue cracking. Based on the summary of the MEPDG outcomes, it was observed that the predicted fatigue cracking and rutting performance of the pavement are better for design Level 1 than Levels 2 and 3. The reason is that Levels 2 and 3 underestimate the dynamic modulus of the AC materials than the actual value obtained from the laboratory test results. The RMSE value was found to be 75% for Level 2 and about 55% for Level 3 indicating that the dynamic modulus values obtained from design Level 2 and 3 are significantly different than Level 1 which remarkably affect the pavement performance. Therefore, it can be concluded that the Levels 2 and 3 overdesign a pavement.
- A database of all the materials properties obtained from the laboratory test has been generated that can be directly integrated into MEPDG. This database is expected to be helpful for pavement engineer and designer.

## RECOMMENDATIONS

Recommendations are made to perform further research in the following area:

- A thorough field performance monitoring of the selected pavement throughout its entire design life and compared with MEPDG prediction value to calibrate the output parameters.
- An extensive research study on the stress hardening or softening behavior of unbound materials and the effect of moisture can be accomplished and incorporated in M-E analysis.

## REFERENCES


1. Muthadi, N.R. and Y.R. Kim. "Local Calibration of Mechanistic-Empirical Pavement Design Guide for Flexible Pavement Design." In *Transportation Research Record: Journal of the Transportation Research Boar;* No. 2087, Transportation Research Board of the National Academies, Washington, D.C., 2008, pp. 131–141.
   DOI: 10.3141/2087-14

2. Li, J., L.M. Pierce, J. Uhlmeyer. Calibration of Flexible Pavement in Mechanistic-Empirical Pavement Design Guide for Washington State. In *Transportation Research Record: Journal of the Transportation Research Board., No.2095*, TRB, National Research Council, Washington, D.C., 2009, pp. 73-83.
   DOI: 10.3141/2095-08

3. Hoegh, K., L. Khazanovich, and M. Jensen. Calibration of Mechanistic-Empirical Pavement Design Guide Rutting Model. In Transportation Research Record: Journal of the Transportation Research Board., No.2180, TRB, National Research Council, Washington, D.C., 2010, pp. 130-141.

4. Hall, K.D., D.X. Xiao, and K.C.P. Wang. Calibration of the Mechanistic-Empirical Pavement Design Guide for Flexible Pavement Design in Arkansas. In Transportation Research Record: Journal of the Transportation Research Board., No.2226, TRB, National Research Council, Washington, D.C., 2010, pp. 135-141.

5. Momin, S.A.. Local Calibration of Mechanistic Empirical Pavement Design Guide for North Eastern United States. *University of Texas – Arlington,* 2011.

6. Pierce, L.M., K.A. Zimmerman, and N. Saadatmand Use of Pavement Management Data for Calibration of the Mechanistic-Empirical Pavement Design Guide. Federal Highway Administration funded project, 2011.

7. Wu, Z., X. Yang, and Z. Zhang. Evaluation of MEPDG Flexible Pavement Design Using Pavement Management System Data: Louisiana Experience. In *International Journal of Pavement Engineering Vol.* 14(7), Louisiana Transportation Research Centre, Baton Rouge, LA,2013, pp. 674-685.
   DOI: 10.1080/10298436.2012.723709

8. Quintus, H.L.V., J. Mallela, R. Bonaquist, C.W. Schwartz, and R.L. Carvalho. Calibration of Rutting Models for Structural and Mix Design. *National Cooperative Highway Research Program Transportation Research Board of the National Academies,* Report 719, Transportation Research Board, National Research Council, Washington, D.C., 2012.

9. Waseem, A. and X. Yuan. Longitudinal Local Calibration of MEPDG Permanent Deformation Models for Reconstructed Flexible Pavements Using PMS Data. *Int. J. Pavement Res. Technol.Vol.* 6(4), Chinese Society of Pavement Engineering, 2013, pp. 304-312.

DOI:10.6135/ijprt.org.tw/2013.6(4).304

10. Le A.T., H.J. Lee, H.M. Park, and T.W. Kim. Development of Korean Pavement Design Guide for Asphalt Pavements Based on the Mechanistic-Empirical Design Principle. *Baltic Journal of Road and Bridge Engineering, Vol.* 6(3), 2011, pp. 169-176 doi: 10.3846/bjrbe.2011.22

11. Saleh, M.F. Implications of Using Calibrated and Validated Performance Transfer Functions in the Mechanistic Empirical Pavement Design Procedure. *International Journal of Pavement Research and Technology. Vol.* 4(2), Chinese Society of Pavement Engineering, 2011, pp. 111-117.

12. Suh, Y., N. Cho, and S. Mun. Development of Mechanistic-Empirical Design Method for an Asphalt Pavement Rutting Model Using APT. *Construction and Building Materials, Vol.* 25, 2011, pp. 1685-1690. doi:10.1016/j.conbuildmat.2010.10.014

13. Newcomb, D.E., and H.V. Quintus. Wanted: Transfer Functions-Experience Needed! *Hot Mix Asphalt Technology,* Hot Mix Asphalt Technology, 2002, pp. 22-25.

14. National Corporative Highway Research Program. Changes to the Mechanistic-Empirical Pavement Design Guide Software through Version 0.900. *Research Results Digest.,Vol.* 308, Transportation Research Board of the National Academies, 2006.

15. Golalipour, A. Modification of Multiple Stress Creep and Recovery Test Procedure and Usage in Specification. University of Wisconsin-Madison, 2011.

16. Zhou, C., B. Huang, X. Shu, Q. Dong. (2013). Validating MEPDG with Tennessee Pavement Performance Data. *Journal of Transportation Engineering, Vol.* 139(3), American Society of Civil Engineers, 2013, pp. 306-312. DOI: 10.1061/(ASCE)TE.1943-5436.0000487

17. Wen, H. and S. Bhusal. A Laboratory Study to Predict the Rutting and Fatigue Behavior of Asphalt Concrete Using the Indirect Tensile Test. *Journal of Testing and Evaluation, Vol.* 41(2), ASTM International, West Conshohocken, PA, 2013, pp. 1-6. doi:10.1520/JTE20120004

18. Priest, A.L. Calibration of Fatigue Transfer Functions for Mechanistic-Empirical Flexible Pavement Design. *M.S. Thesis, Auburn University,* 2005.

19. Xiao, D.X., K.C.P. Wang, and K.D. Hall. Matching Distress Definitions in Field and in MEPDG for Local Calibration. Roanoke, Virginia. Oct. 25-27, 2010.

20. Wang, R., Z. Zhou, D. Chen, G. Zheng, T. Scullion, and L.F. Walubita. Characterization of Rutting (Permanent Strain) Development of A-2-4 and A-4 Subgrade Soils Under the

HVS Loading. *Journal of Performance of Constructed Facilities, Vol.* 24(4), American Society of Civil Engineers, 2010, pp. 382-389.
DOI: 10.1061/_ASCE_CF.1943-5509.0000107

21. Zborowski, A. and K.E., Kaloush. A Fracture Energy Approach to Model the Thermal Cracking Performance of Asphalt Rubber Mixtures. *Road Materials and Pavement Design, Vol.* 12(2), Taylor and Francis, 2011, pp. 377-395. DOI: 10.1080/14680629.2011.9695250

22. Huvstig, A. Model for the Prediction of Rutting in Roads, a NordFoU Result. *Procedia-Social and Behavioral Sciences No.* 48, Programme Committee of the Transport Research Arena, 2012, pp. 2816-2826. doi: 10.1016/j.sbspro.2012.06.1250

23. Li, J., L.M. Pierce, M.E. Hallenbeck, and J. Uhlmeyer. Sensitivity of Axle Load Spectra in the Mechanistic-Empirical Pavement Design Guide for the Washington State Department of Transportation. *Journal of the Transportation Research Board., No.* 2093, Transportation Research Board of the National Academies, Washington, D.C., 2009, pp. 50-56.

24. Sumee, N. Sensitivity of MEPDG Using Advanced Statistical Analyses. University of New Mexico, Albuquerque, New Mexico, 2010.

25. Diefenderfer, S.D. Analysis of the Mechanistic-Empirical Pavement Design Guide Performance Predictions: Influence of Asphalt Material Input Properties. *Virginia Transportation Research Council. Final Report for* FHWA/VTRC 11-R3, Virginia Transportation Research Council, 2010, pp. 1-47.

26. El-Badawy, S.M. Recommended Changes to Designs Not Meeting Criteria Using the Mechanistic-Empirical Pavement Design Guide. *Int. J. Pavement Res. Technol.Vol.* 5(1), Chinese Society of Pavement Engineering, 2012, pp. 54-61.

27. Orobio, A. and J.P. Zaniewski. Sampling-Based Sensitivity Analysis of the Mechanistic-Empirical Pavement Design Guide Applied to Material Inputs. *Journal of the Transportation Research Board, No.* 2226, Transportation Research Board of the National Academies, Washington, D.C., 2011, pp. 85-93.

28. Schwartz, C.W., R. Li, S.H. Kim, H. Ceylan, K. Gopalakrishnan. (2011). Sensitivity Evaluation of MEPDG Performance Prediction. *National Cooperative Highway Research Program Transportation Research Board of the National Academies.* Final Report Project 1-47, 2011

29. Cooper, S.B., M.A. Elseifi, and L.N. Mohammad. Parametric Evaluation of Design Input Parameters on the Mechanistic-Empirical Pavement Design Guide Predicted Performance. *Int. J. Pavement Res. Technol.* 5(4), Chinese Society of Pavement Engineers, 2012, pp. 218-224.

30. AASHTO T 312-07. Standard Method of Test for Preparing and Determining the Density of Asphalt Mixture Specimens by Means of the Superpave Gyratory Compactor. *Standard Specifications for Transportation Materials and Methods of Sampling and Testing*, 31st Edition. AASHTO, Washington, D.C., 2011.

31. AASHTO T 342-11. Standard Method of Test for Determining Dynamic Modulus of Hot-Mix Asphalt Concrete Mixtures. *Standard Specifications for Transportation Materials and Methods of Sampling and Testing*, 31st Edition. AASHTO, Washington, D.C., 2011.

32. Kim, R. Y., (2009). "Modeling of Asphalt Concrete", American society of Civil Engineers, 1801 Alexander bell Drive, Reston, VA, USA.

33. Tarefder, R.A., and G. Barlas. Determining Fatigue Endurance Limits of New Mexico Asphalt Mixes for Designing Perpetual Pavements and Implementation of MEPDG to its Full Capacity. Final Report, Report No. NM11MSC-02, New Mexico Department of Transportation (NMDOT), Albuquerque, NM, 2013.

34. AASHTO T 209. Standard Method of Test for Determining Maximum Specific Gravity and Density of Hot Mix Asphalt. Standard Specifications for Transportation Materials and Methods of Sampling and Testing, 27th Edition. American Association of State.

35. AASHTO T 166-07. Bulk Specific Gravity of Compacted Hot Mix Asphalt using Saturated Surface-Dry Specimens. Standard Specifications for Transportation Materials and Methods of Sampling and Testing, 27th Edition. American Association of State.

36. AASHTO T 269-07. Standard Method of Test for Percent Air Voids in Compacted Dense And Open Asphalt Mixtures. Standard Specifications for Transportation Materials and Methods of Sampling and Testing, 27th Edition. American Association of State.

37. AASHTO T 321-07. Determining the Fatigue Life of Compacted Hot-Mix Asphalt (HMA) Subjected to Repeated Flexural Bending. Standard Specifications for Transportation Materials and Methods of Sampling and Testing, 31st Edition. AASHTO, Washington, D.C., 2011.

38. AASHTO T 315-09. Standard Method of Test for Determining the Rheological Properties of Asphalt Binder Using Dynamic Shear Rheometer (DSR). Standard Specifications for Transportation Materials and Methods of Sampling and Testing, 31st Edition. AASHTO, Washington, D.C., 2011.

39. ASTM D2216-10. Standard Test Methods for Laboratory Determination of Water (Moisture) Content of Soil and Rock by Mass. ASTM International, West Conshohocken, PA, 2008.

40. ASTM D 698. Standard Test Methods for Laboratory Compaction Characteristics of Soil Using Standard Effort. ASTM International, West Conshohocken, PA, 2008.

41. AASHTO T 307-99 Determining the Resilient Modulus of Soils and Aggregate Materials. *Standard Specifications for Transportation Materials and Methods of Sampling and Testing,* 27th Edition. AASHTO, Washington, D.C., 2012.

42. Uzan, J. Characterization of Granular Materials. In *Transportation Research Record: Journal of Transportation Research Board, No. 1022*, Transportation Research Board of the National Academies, Washington, D.C., 1985, pp. 52–59.

43. ASTM D 6951-M09. *Standard Test Methods for* Use of the Dynamic Cone Penetrometer in Shallow Pavement Applications. ASTM International, West Conshohocken, PA, 2007.

44. ASTM D 5878-02. *Standard Test Methods for Determination of Impact Value of a Soil*. ASTM International, West Conshohocken, PA, 2007.

45. Clegg, B. (1994). "Calculation of penetration and elastic modulus from CIV." Technical Note No. 1. Dr Baden Clegg Pty Ltd, Dalkeith, Western Australia.

46. Transportation Research Board. Laboratory Determination of Resilient Modulus for Flexible Pavement Design, NCHRP Research Results Digest 285, Transportation Research Board, Washington, D.C., January 2004.

47. Department of Transformation, Federal Highway Administration. National Highway Performance Program, 23, CFR Part 490, page 5966, 2017.

# APPENDIX A

**TABLE A-1 Dynamic modulus summary sheet for US 54N mix**

| Conditions | | Specimen 1 | | Specimen 2 | | Specimen 3 | | Modulus | | Phase Angle (Degrees) | |
|---|---|---|---|---|---|---|---|---|---|---|---|
| Temperature, °F | Frequency, Hz | Modulus, ksi | Phage Angle, degree | Modulus, ksi | Phage Angle, degree | Modulus, ksi | Phage Angle, degree | Avg. Modulus, ksi | CV, % | Avg. P. Angle, degree | Standard Dev, degree |
| 14 | 25 | 7684.87 | 5.1 | 4843.30 | 0.3 | 6130.56 | 13.9 | 6219.58 | 22.88 | 6.4 | 6.90 |
| 14 | 10 | 6446.18 | 7.1 | 5217.38 | 6.2 | 6981.18 | 5.2 | 6214.91 | 14.55 | 6.2 | 0.95 |
| 14 | 5 | 6249.41 | 6.8 | 5050.66 | 5.8 | 6756.72 | 5.4 | 6018.93 | 14.56 | 6.0 | 0.72 |
| 14 | 1 | 5780.53 | 6.7 | 4527.52 | 6.5 | 6317.67 | 6.7 | 5541.91 | 16.58 | 6.6 | 0.12 |
| 14 | 0.5 | 5292.93 | 9.1 | 4497.33 | 4.5 | 5800.36 | 4.8 | 5196.87 | 12.64 | 6.1 | 2.57 |
| 14 | 0.1 | 4978.54 | 9.3 | 4007.97 | 8.1 | 5360.73 | 9.3 | 4782.41 | 14.58 | 8.9 | 0.69 |
| 40 | 25 | 4673.13 | 1.8 | 3656.17 | 7.1 | 4710.44 | 18.7 | 4346.58 | 13.76 | 9.2 | 8.64 |
| 40 | 10 | 4393.64 | 11.0 | 3750.85 | 10.0 | 4948.14 | 10.6 | 4364.21 | 13.73 | 10.5 | 0.50 |
| 40 | 5 | 4002.31 | 11.5 | 3478.18 | 10.8 | 4786.73 | 9.8 | 4089.08 | 16.11 | 10.7 | 0.85 |
| 40 | 1 | 3330.36 | 15.1 | 2935.73 | 12.7 | 3848.61 | 13.6 | 3371.57 | 13.58 | 13.8 | 1.21 |
| 40 | 0.5 | 3202.25 | 15.8 | 2709.05 | 11.3 | 3701.41 | 18.0 | 3204.24 | 15.49 | 15.0 | 3.42 |
| 40 | 0.1 | 2453.09 | 19.2 | 2131.99 | 16.4 | 2744.59 | 18.1 | 2443.22 | 12.54 | 17.9 | 1.41 |
| 70 | 25 | 2055.14 | 24.1 | 2000.74 | 18.7 | 2594.70 | 20.4 | 2216.86 | 14.81 | 21.1 | 2.76 |
| 70 | 10 | 1809.21 | 24.6 | 1720.07 | 20.1 | 2309.30 | 20.2 | 1946.19 | 16.32 | 21.6 | 2.57 |
| 70 | 5 | 1678.22 | 26.0 | 1513.29 | 21.7 | 1995.38 | 21.8 | 1728.96 | 14.17 | 23.2 | 2.45 |
| 70 | 1 | 1224.83 | 30.9 | 1063.09 | 25.3 | 1324.19 | 26.8 | 1204.04 | 10.95 | 27.7 | 2.90 |
| 70 | 0.5 | 1101.93 | 29.4 | 908.92 | 28.6 | 1071.59 | 28.8 | 1027.48 | 10.10 | 28.9 | 0.42 |
| 70 | 0.1 | 632.53 | 33.8 | 586.07 | 29.4 | 688.59 | 29.4 | 635.73 | 8.07 | 30.9 | 2.54 |
| 100 | 25 | 1095.90 | 31.3 | 899.95 | 29.7 | 855.63 | 35.1 | 950.49 | 13.45 | 32.0 | 2.77 |
| 100 | 10 | 760.76 | 32.6 | 676.79 | 29.9 | 611.49 | 33.5 | 683.01 | 10.96 | 32.0 | 1.87 |
| 100 | 5 | 584.33 | 33.0 | 518.44 | 30.2 | 470.08 | 33.7 | 524.28 | 10.94 | 32.3 | 1.85 |
| 100 | 1 | 366.26 | 30.8 | 285.71 | 34.3 | 249.90 | 33.6 | 300.62 | 19.83 | 32.9 | 1.85 |
| 100 | 0.5 | 305.95 | 29.2 | 226.78 | 33.1 | 196.39 | 32.0 | 243.04 | 23.27 | 31.4 | 2.01 |
| 100 | 0.1 | 218.36 | 23.6 | 155.45 | 24.5 | 124.31 | 27.3 | 166.04 | 28.85 | 25.1 | 1.93 |
| 130 | 25 | 330.36 | 34.7 | 217.68 | 38.7 | 248.23 | 34.5 | 265.42 | 21.95 | 36.0 | 2.37 |
| 130 | 10 | 243.13 | 32.2 | 152.88 | 34.5 | 183.14 | 29.2 | 193.05 | 23.80 | 32.0 | 2.66 |
| 130 | 5 | 209.44 | 30.5 | 105.16 | 32.1 | 146.16 | 26.9 | 153.59 | 34.21 | 29.8 | 2.66 |
| 130 | 1 | 168.56 | 23.7 | 68.46 | 26.9 | 94.29 | 22.5 | 110.44 | 47.06 | 24.4 | 2.27 |
| 130 | 0.5 | 142.86 | 21.8 | 61.99 | 23.0 | 76.15 | 21.5 | 93.67 | 46.11 | 22.1 | 0.79 |
| 130 | 0.1 | 106.93 | 18.1 | 42.13 | 18.0 | 58.81 | 17.2 | 69.29 | 48.56 | 17.8 | 0.49 |

**TABLE A-2 Dynamic modulus summary sheet for US 54S mix**

| Conditions | | Specimen 1 | | Specimen 2 | | Specimen 3 | | Modulus | | Phase Angle (Degrees) | |
|---|---|---|---|---|---|---|---|---|---|---|---|
| Temperature, °F | Frequency, Hz | Modulus, ksi | Phage Angle, degree | Modulus, ksi | Phage Angle, degree | Modulus, ksi | Phage Angle, degree | Avg. Modulus, ksi | CV, % | Avg. P. Angle, degree | Standard Dev, degree |
| 14 | 25 | 4238.15 | 22.2 | 7286.97 | 2.5 | 6621.15 | 6.3 | 6048.76 | 26.50 | 10.3 | 10.45 |
| 14 | 10 | 4117.25 | 6.2 | 7170.46 | 5.8 | 7199.43 | 5.8 | 6162.38 | 28.74 | 5.9 | 0.23 |
| 14 | 5 | 3970.45 | 6.0 | 6931.17 | 5.7 | 6990.86 | 5.0 | 5964.16 | 28.95 | 5.6 | 0.51 |
| 14 | 1 | 3540.41 | 8.3 | 6107.30 | 7.2 | 6375.34 | 6.8 | 5341.01 | 29.30 | 7.4 | 0.78 |
| 14 | 0.5 | 3488.47 | 5.0 | 6205.63 | 3.2 | 6394.26 | 8.8 | 5362.78 | 30.32 | 5.7 | 2.86 |
| 14 | 0.1 | 3196.53 | 9.0 | 5558.02 | 8.3 | 5659.55 | 5.7 | 4804.70 | 29.01 | 7.7 | 1.74 |
| 40 | 25 | 3659.23 | 3.6 | 5426.27 | 0.6 | 5225.18 | 7.9 | 4770.23 | 20.28 | 4.0 | 3.67 |
| 40 | 10 | 3128.01 | 9.3 | 5447.51 | 8.4 | 5280.71 | 8.1 | 4618.74 | 28.01 | 8.6 | 0.62 |
| 40 | 5 | 2990.77 | 9.6 | 5105.55 | 9.2 | 4952.27 | 8.0 | 4349.53 | 27.11 | 8.9 | 0.83 |
| 40 | 1 | 2608.99 | 9.9 | 4481.05 | 10.9 | 4163.58 | 11.4 | 3751.20 | 26.71 | 10.7 | 0.76 |
| 40 | 0.5 | 2326.09 | 12.5 | 4192.25 | 14.8 | 3767.14 | 10.1 | 3428.49 | 28.53 | 12.5 | 2.35 |
| 40 | 0.1 | 1989.94 | 14.5 | 3323.35 | 15.1 | 3205.33 | 14.6 | 2839.54 | 25.99 | 14.7 | 0.32 |
| 70 | 25 | 1991.75 | 7.8 | 2609.81 | 16.3 | 3067.83 | 15.4 | 2556.47 | 21.12 | 13.2 | 4.67 |
| 70 | 10 | 1828.81 | 15.9 | 2176.11 | 20.7 | 2689.16 | 17.1 | 2231.36 | 19.40 | 17.9 | 2.50 |
| 70 | 5 | 1685.51 | 16.6 | 1953.47 | 21.5 | 2383.77 | 18.1 | 2007.58 | 17.55 | 18.7 | 2.51 |
| 70 | 1 | 1220.46 | 19.4 | 1367.33 | 26.5 | 1680.80 | 21.4 | 1422.87 | 16.53 | 22.4 | 3.66 |
| 70 | 0.5 | 1065.66 | 23.2 | 1217.86 | 27.4 | 1437.24 | 22.6 | 1240.25 | 15.06 | 24.4 | 2.62 |
| 70 | 0.1 | 743.40 | 25.6 | 882.81 | 30.2 | 979.09 | 27.1 | 868.43 | 13.65 | 27.6 | 2.35 |
| 100 | 25 | 801.61 | 23.6 | 1243.11 | 33.6 | 1503.43 | 12.3 | 1182.72 | 30.00 | 23.2 | 10.66 |
| 100 | 10 | 640.31 | 26.3 | 1007.70 | 27.1 | 1189.37 | 24.6 | 945.79 | 29.58 | 26.0 | 1.28 |
| 100 | 5 | 506.75 | 27.4 | 786.42 | 28.2 | 865.20 | 27.6 | 719.46 | 26.18 | 27.7 | 0.42 |
| 100 | 1 | 310.86 | 29.0 | 457.61 | 33.9 | 524.90 | 29.7 | 431.13 | 25.39 | 30.9 | 2.65 |
| 100 | 0.5 | 251.82 | 29.6 | 363.84 | 34.3 | 430.04 | 29.4 | 348.56 | 25.84 | 31.1 | 2.77 |
| 100 | 0.1 | 163.94 | 27.5 | 231.65 | 30.8 | 308.34 | 24.4 | 234.64 | 30.79 | 27.6 | 3.20 |
| 130 | 25 | 372.98 | 30.5 | 378.02 | 34.3 | 457.24 | 37.9 | 402.75 | 11.73 | 34.2 | 3.70 |
| 130 | 10 | 268.84 | 32.5 | 270.04 | 30.9 | 340.02 | 32.6 | 292.97 | 13.91 | 32.0 | 0.95 |
| 130 | 5 | 217.38 | 31.8 | 215.18 | 28.6 | 277.48 | 31.1 | 236.68 | 14.94 | 30.5 | 1.68 |
| 130 | 1 | 133.63 | 30.4 | 138.15 | 25.6 | 168.27 | 29.1 | 146.68 | 12.84 | 28.4 | 2.48 |
| 130 | 0.5 | 104.17 | 29.4 | 113.20 | 24.3 | 140.34 | 27.4 | 119.24 | 15.79 | 27.0 | 2.57 |
| 130 | 0.1 | 87.94 | 23.4 | 84.99 | 20.2 | 100.81 | 23.7 | 91.24 | 9.22 | 22.4 | 1.94 |

**TABLE A-3 Dynamic modulus summary sheet for US285 mix**

| Conditions | | Specimen 1 | | Specimen 2 | | Specimen 3 | | Modulus | | Phase Angle (Degrees) | |
|---|---|---|---|---|---|---|---|---|---|---|---|
| Temperature, °F | Frequency, Hz | Modulus, ksi | Phage Angle, degree | Modulus, ksi | Phage Angle, degree | Modulus, ksi | Phage Angle, degree | Avg. Modulus, ksi | CV, % | Avg. P. Angle, degree | Standard Dev, degree |
| 14 | 25 | 7833.18 | 11.6 | 5565.87 | 11.0 | 7069.40 | 9.8 | 6822.82 | 16.91 | 10.8 | 0.92 |
| 14 | 10 | 6794.38 | 5.9 | 7097.99 | 6.9 | 6138.71 | 8.0 | 6677.03 | 7.34 | 6.9 | 1.05 |
| 14 | 5 | 6814.31 | 5.2 | 6947.60 | 6.9 | 5871.98 | 8.5 | 6544.63 | 8.96 | 6.9 | 1.65 |
| 14 | 1 | 6109.85 | 4.1 | 6013.29 | 11.8 | 5112.58 | 9.0 | 5745.24 | 9.57 | 8.3 | 3.90 |
| 14 | 0.5 | 5640.63 | 8.8 | 5537.35 | 7.7 | 5134.22 | 8.0 | 5437.40 | 4.92 | 8.2 | 0.57 |
| 14 | 0.1 | 5252.03 | 7.8 | 5002.51 | 12.2 | 4298.13 | 12.5 | 4850.89 | 10.20 | 10.8 | 2.63 |
| 40 | 25 | 4129.35 | 17.1 | 3634.62 | 17.5 | 4793.39 | 14.0 | 4185.79 | 13.89 | 16.2 | 1.92 |
| 40 | 10 | 3716.22 | 11.4 | 3805.90 | 16.1 | 3907.74 | 13.2 | 3809.96 | 2.52 | 13.6 | 2.37 |
| 40 | 5 | 3463.97 | 12.0 | 3481.87 | 16.6 | 3617.34 | 13.8 | 3521.06 | 2.38 | 14.1 | 2.32 |
| 40 | 1 | 2785.63 | 15.5 | 2770.82 | 18.5 | 2868.83 | 16.2 | 2808.42 | 1.88 | 16.7 | 1.57 |
| 40 | 0.5 | 2627.79 | 16.2 | 2442.37 | 21.1 | 2697.71 | 17.6 | 2589.29 | 5.10 | 18.3 | 2.52 |
| 40 | 0.1 | 1947.60 | 19.6 | 1804.92 | 23.1 | 1928.93 | 20.9 | 1893.82 | 4.09 | 21.2 | 1.77 |
| 70 | 25 | 2448.71 | 21.5 | 1700.65 | 23.2 | 2310.10 | 14.2 | 2153.15 | 18.48 | 19.6 | 4.78 |
| 70 | 10 | 1917.93 | 21.2 | 1829.61 | 24.0 | 1730.16 | 22.5 | 1825.90 | 5.14 | 22.6 | 1.40 |
| 70 | 5 | 1670.36 | 22.5 | 1598.16 | 25.4 | 1478.45 | 23.7 | 1582.32 | 6.13 | 23.9 | 1.46 |
| 70 | 1 | 1124.92 | 27.6 | 1069.73 | 30.8 | 952.95 | 26.6 | 1049.20 | 8.37 | 28.3 | 2.19 |
| 70 | 0.5 | 908.00 | 30.1 | 916.31 | 29.7 | 743.61 | 29.2 | 855.98 | 11.38 | 29.7 | 0.45 |
| 70 | 0.1 | 562.18 | 30.8 | 546.18 | 32.9 | 470.73 | 30.5 | 526.37 | 9.28 | 31.4 | 1.31 |
| 100 | 25 | 985.80 | 21.2 | 901.22 | 31.8 | 726.65 | 31.3 | 871.22 | 15.17 | 28.1 | 5.98 |
| 100 | 10 | 661.93 | 28.5 | 704.51 | 31.2 | 535.05 | 30.0 | 633.83 | 13.91 | 29.9 | 1.35 |
| 100 | 5 | 529.28 | 28.8 | 564.53 | 31.5 | 424.94 | 30.2 | 506.25 | 14.34 | 30.2 | 1.35 |
| 100 | 1 | 311.07 | 27.9 | 334.60 | 31.8 | 249.24 | 30.2 | 298.30 | 14.78 | 30.0 | 1.96 |
| 100 | 0.5 | 249.91 | 27.6 | 270.30 | 30.2 | 197.53 | 29.3 | 239.25 | 15.69 | 29.0 | 1.32 |
| 100 | 0.1 | 161.93 | 23.6 | 176.85 | 27.8 | 130.51 | 25.3 | 156.43 | 15.12 | 25.6 | 2.11 |
| 130 | 25 | 305.45 | 28.3 | 387.15 | 33.2 | 241.17 | 35.1 | 311.26 | 23.51 | 32.2 | 3.51 |
| 130 | 10 | 211.13 | 29.5 | 278.76 | 29.5 | 195.00 | 29.9 | 228.29 | 19.46 | 29.6 | 0.23 |
| 130 | 5 | 167.25 | 26.8 | 220.03 | 29.1 | 165.04 | 27.3 | 184.11 | 16.91 | 27.7 | 1.21 |
| 130 | 1 | 119.26 | 21.8 | 159.29 | 24.6 | 120.48 | 22.9 | 133.01 | 17.12 | 23.1 | 1.41 |
| 130 | 0.5 | 97.25 | 20.9 | 135.26 | 22.5 | 108.93 | 19.7 | 113.81 | 17.11 | 21.0 | 1.40 |
| 130 | 0.1 | 74.59 | 17.9 | 105.18 | 16.2 | 100.33 | 15.0 | 93.37 | 17.61 | 16.4 | 1.46 |

**TABLE A-4 Dynamic modulus summary sheet for US491 (top layer) mix**

| Conditions | | Specimen 1 | | Specimen 2 | | Specimen 3 | | Modulus | | Phase Angle (Degrees) | |
|---|---|---|---|---|---|---|---|---|---|---|---|
| Temperature, °F | Frequency, Hz | Modulus, ksi | Phage Angle, degree | Modulus, ksi | Phage Angle, degree | Modulus, ksi | Phage Angle, degree | Avg. Modulus, ksi | CV, % | Avg. P. Angle, degree | Standard Dev, degree |
| 14 | 25 | 5703.46 | 8.7 | 6291.33 | 14.5 | 6422.47 | 22.6 | 6139.09 | 6.24 | 15.3 | 6.98 |
| 14 | 10 | 5945.71 | 9.3 | 6703.58 | 6.2 | 7115.04 | 7.2 | 6588.11 | 9.00 | 7.6 | 1.58 |
| 14 | 5 | 5778.72 | 9.6 | 6583.39 | 5.5 | 6723.93 | 7.8 | 6362.02 | 8.02 | 7.6 | 2.06 |
| 14 | 1 | 5288.81 | 10.1 | 5850.80 | 7.7 | 5965.53 | 13.8 | 5701.71 | 6.35 | 10.5 | 3.07 |
| 14 | 0.5 | 5226.22 | 12.3 | 5777.87 | 10.0 | 6039.41 | 8.6 | 5681.17 | 7.31 | 10.3 | 1.87 |
| 14 | 0.1 | 4288.61 | 13.7 | 5111.87 | 8.8 | 5004.04 | 12.5 | 4801.51 | 9.32 | 11.7 | 2.55 |
| 40 | 25 | 4135.85 | 12.8 | 3039.77 | 20.9 | 2246.54 | 4.1 | 3140.72 | 30.21 | 12.6 | 8.40 |
| 40 | 10 | 3749.64 | 14.0 | 3073.34 | 14.2 | 4346.80 | 13.8 | 3723.26 | 17.11 | 14.0 | 0.20 |
| 40 | 5 | 3438.81 | 15.0 | 2857.25 | 14.8 | 3998.89 | 14.1 | 3431.65 | 16.63 | 14.6 | 0.47 |
| 40 | 1 | 2788.49 | 17.9 | 2295.83 | 17.4 | 3203.87 | 16.9 | 2762.73 | 16.45 | 17.4 | 0.50 |
| 40 | 0.5 | 2437.06 | 20.6 | 2146.99 | 18.2 | 2797.30 | 18.3 | 2460.45 | 13.24 | 19.0 | 1.36 |
| 40 | 0.1 | 1800.18 | 22.6 | 1579.56 | 21.7 | 2200.36 | 20.5 | 1860.03 | 16.92 | 21.6 | 1.05 |
| 70 | 25 | 2019.41 | 23.4 | 1591.09 | 21.2 | 933.93 | 13.2 | 1514.81 | 36.09 | 19.3 | 5.37 |
| 70 | 10 | 1605.99 | 23.1 | 1320.11 | 22.4 | 1900.05 | 22.5 | 1608.71 | 18.03 | 22.7 | 0.38 |
| 70 | 5 | 1382.47 | 24.5 | 1148.75 | 23.2 | 1609.51 | 23.6 | 1380.25 | 16.69 | 23.8 | 0.67 |
| 70 | 1 | 934.50 | 28.0 | 773.17 | 26.9 | 1075.47 | 26.8 | 927.71 | 16.31 | 27.2 | 0.67 |
| 70 | 0.5 | 787.21 | 28.9 | 641.99 | 28.4 | 903.24 | 28.0 | 777.48 | 16.84 | 28.4 | 0.45 |
| 70 | 0.1 | 499.87 | 29.9 | 411.79 | 29.0 | 580.14 | 29.6 | 497.27 | 16.93 | 29.5 | 0.46 |
| 100 | 25 | 608.91 | 31.7 | 621.21 | 26.3 | 766.22 | 22.2 | 665.45 | 13.15 | 26.7 | 4.76 |
| 100 | 10 | 480.59 | 29.6 | 438.57 | 29.7 | 707.48 | 27.6 | 542.21 | 26.68 | 29.0 | 1.18 |
| 100 | 5 | 384.83 | 29.1 | 344.08 | 30.1 | 565.20 | 27.7 | 431.37 | 27.28 | 29.0 | 1.21 |
| 100 | 1 | 240.19 | 27.9 | 207.53 | 29.0 | 359.69 | 26.7 | 269.13 | 29.76 | 27.9 | 1.15 |
| 100 | 0.5 | 201.82 | 27.1 | 166.52 | 27.2 | 296.41 | 25.2 | 221.58 | 30.31 | 26.5 | 1.13 |
| 100 | 0.1 | 146.34 | 23.2 | 111.03 | 23.3 | 205.40 | 20.7 | 154.26 | 30.91 | 22.4 | 1.47 |
| 130 | 25 | 274.36 | 30.5 | 212.80 | 35.2 | 306.50 | 30.8 | 264.55 | 18.00 | 32.2 | 2.63 |
| 130 | 10 | 205.92 | 27.2 | 161.23 | 29.2 | 230.75 | 25.6 | 199.30 | 17.68 | 27.3 | 1.80 |
| 130 | 5 | 169.49 | 25.8 | 126.36 | 27.5 | 188.33 | 23.2 | 161.39 | 19.69 | 25.5 | 2.17 |
| 130 | 1 | 120.42 | 18.0 | 84.23 | 22.5 | 137.47 | 18.6 | 114.04 | 23.84 | 19.7 | 2.44 |
| 130 | 0.5 | 100.80 | 17.8 | 72.60 | 20.1 | 127.15 | 15.9 | 100.18 | 27.23 | 17.9 | 2.10 |
| 130 | 0.1 | 84.72 | 13.0 | 54.78 | 16.8 | 106.20 | 9.8 | 81.90 | 31.53 | 13.2 | 3.50 |

**TABLE A-5 Dynamic modulus summary sheet for US491 (bottom layer) mix**

| Conditions | | Specimen 1 | | Specimen 2 | | Specimen 3 | | Modulus | | Phase Angle (Degrees) | |
|---|---|---|---|---|---|---|---|---|---|---|---|
| Temperature, °F | Frequency, Hz | Modulus, ksi | Phage Angle, degree | Modulus, ksi | Phage Angle, degree | Modulus, ksi | Phage Angle, degree | Avg. Modulus, ksi | CV, % | Avg. P. Angle, degree | Standard Dev, degree |
| 14 | 25 | 5121.23 | 7.4 | 7188.42 | 4.1 | 6223.30 | 6.6 | 6177.65 | 16.74 | 6.0 | 1.72 |
| 14 | 10 | 4981.90 | 8.7 | 6863.88 | 6.0 | 6062.46 | 6.4 | 5969.41 | 15.82 | 7.0 | 1.46 |
| 14 | 5 | 4805.15 | 8.8 | 6717.15 | 6.4 | 5738.70 | 6.8 | 5753.67 | 16.62 | 7.3 | 1.29 |
| 14 | 1 | 4201.84 | 9.2 | 6442.28 | 6.1 | 5495.01 | 6.4 | 5379.71 | 20.91 | 7.2 | 1.71 |
| 14 | 0.5 | 4182.57 | 9.6 | 5746.33 | 6.6 | 4954.61 | 6.5 | 4961.17 | 15.76 | 7.6 | 1.76 |
| 14 | 0.1 | 3568.75 | 11.4 | 5231.81 | 9.1 | 4538.29 | 8.4 | 4446.28 | 18.79 | 9.6 | 1.57 |
| 40 | 25 | 3767.65 | 12.4 | 5060.87 | 7.8 | 4195.22 | 9.9 | 4341.25 | 15.18 | 10.0 | 2.30 |
| 40 | 10 | 3442.07 | 13.6 | 4505.64 | 10.7 | 3930.55 | 11.4 | 3959.42 | 13.45 | 11.9 | 1.51 |
| 40 | 5 | 3145.91 | 15.0 | 4184.16 | 11.0 | 3637.93 | 12.2 | 3656.00 | 14.21 | 12.7 | 2.05 |
| 40 | 1 | 2542.83 | 16.0 | 3479.17 | 12.2 | 2969.67 | 14.7 | 2997.22 | 15.64 | 14.3 | 1.93 |
| 40 | 0.5 | 2270.15 | 21.6 | 2978.03 | 18.0 | 2674.14 | 13.8 | 2640.77 | 13.45 | 17.8 | 3.90 |
| 40 | 0.1 | 1715.46 | 22.2 | 2404.83 | 19.5 | 2032.58 | 20.3 | 2050.96 | 16.82 | 20.7 | 1.39 |
| 70 | 25 | 1681.45 | 24.5 | 2483.87 | 16.2 | 2197.97 | 21.5 | 2121.10 | 19.17 | 20.7 | 4.20 |
| 70 | 10 | 1239.90 | 24.9 | 2047.02 | 19.6 | 1784.97 | 20.6 | 1690.63 | 24.35 | 21.7 | 2.82 |
| 70 | 5 | 1057.61 | 26.6 | 1788.54 | 20.9 | 1540.38 | 21.4 | 1462.17 | 25.42 | 23.0 | 3.16 |
| 70 | 1 | 695.30 | 29.4 | 1254.24 | 26.6 | 1010.93 | 28.4 | 986.82 | 28.40 | 28.1 | 1.42 |
| 70 | 0.5 | 576.72 | 30.6 | 1012.37 | 29.5 | 825.18 | 29.8 | 804.76 | 27.16 | 30.0 | 0.57 |
| 70 | 0.1 | 370.79 | 30.2 | 639.49 | 31.1 | 542.05 | 28.2 | 517.44 | 26.29 | 29.8 | 1.48 |
| 100 | 25 | 517.18 | 28.9 | 715.27 | 29.4 | 609.38 | 29.2 | 613.94 | 16.15 | 29.2 | 0.25 |
| 100 | 10 | 385.91 | 29.2 | 514.79 | 31.8 | 461.37 | 28.4 | 454.02 | 14.26 | 29.8 | 1.78 |
| 100 | 5 | 300.04 | 30.2 | 454.34 | 31.3 | 364.18 | 28.9 | 372.85 | 20.79 | 30.1 | 1.20 |
| 100 | 1 | 178.71 | 29.1 | 310.72 | 28.8 | 221.10 | 27.9 | 236.84 | 28.46 | 28.6 | 0.62 |
| 100 | 0.5 | 143.03 | 27.5 | 269.13 | 25.7 | 178.80 | 27.4 | 196.99 | 32.99 | 26.9 | 1.01 |
| 100 | 0.1 | 96.63 | 23.2 | 187.39 | 22.1 | 118.69 | 23.3 | 134.24 | 35.26 | 22.9 | 0.67 |
| 130 | 25 | 138.27 | 31.3 | 231.84 | 34.1 | 211.91 | 31.0 | 194.01 | 25.40 | 32.1 | 1.71 |
| 130 | 10 | 107.25 | 26.7 | 183.67 | 28.3 | 162.99 | 30.5 | 151.30 | 26.12 | 28.5 | 1.91 |
| 130 | 5 | 84.66 | 25.9 | 175.73 | 23.6 | 134.96 | 29.5 | 131.79 | 34.61 | 26.3 | 2.97 |
| 130 | 1 | 61.77 | 21.8 | 132.03 | 19.4 | 88.53 | 23.1 | 94.11 | 37.68 | 21.4 | 1.88 |
| 130 | 0.5 | 56.61 | 18.7 | 116.82 | 13.7 | 75.58 | 22.9 | 83.00 | 37.08 | 18.4 | 4.61 |
| 130 | 0.1 | 47.96 | 15.8 | 100.93 | 11.1 | 60.64 | 16.8 | 69.84 | 39.60 | 14.6 | 3.04 |

**TABLE A-6 Dynamic modulus summary sheet for NM 14 mix**

| Conditions | | Specimen 1 | | Specimen 2 | | Specimen 3 | | Modulus | | Phase Angle (Degrees) | |
|---|---|---|---|---|---|---|---|---|---|---|---|
| Temperature, °F | Frequency, Hz | Modulus, ksi | Phage Angle, degree | Modulus, ksi | Phage Angle, degree | Modulus, ksi | Phage Angle, degree | Avg. Modulus, ksi | CV, % | Avg. P. Angle, degree | Standard Dev, degree |
| 14 | 25 | 7752.48 | 1.3 | 10090.62 | 1.2 | 7905.32 | 8.7 | 8582.81 | 15.24 | 3.73 | 4.30 |
| 14 | 10 | 7621.35 | 6.4 | 8557.16 | 6.8 | 8180.88 | 6.3 | 8119.80 | 5.80 | 6.50 | 0.26 |
| 14 | 5 | 7446.09 | 6.2 | 8099.12 | 6.7 | 7906.76 | 6.7 | 7817.32 | 4.29 | 6.53 | 0.29 |
| 14 | 1 | 6659.83 | 8.1 | 7384.27 | 4.8 | 7019.84 | 9.4 | 7021.31 | 5.16 | 7.43 | 2.37 |
| 14 | 0.5 | 6096.70 | 6.8 | 6650.66 | 11.3 | 6542.89 | 5.6 | 6430.08 | 4.57 | 7.90 | 3.00 |
| 14 | 0.1 | 5409.11 | 10.4 | 6037.66 | 9.6 | 5780.38 | 10 | 5742.38 | 5.50 | 10.00 | 0.40 |
| 40 | 25 | 4987.42 | 9.1 | 5172.81 | 61.9 | 5581.34 | 11.6 | 5247.19 | 5.79 | 27.53 | 29.79 |
| 40 | 10 | 4577.06 | 12.2 | 7835.00 | 9.1 | 5456.09 | 12.2 | 5956.05 | 28.30 | 11.17 | 1.79 |
| 40 | 5 | 4161.33 | 13 | 5267.39 | 14.3 | 4991.47 | 13.3 | 4806.73 | 11.98 | 13.53 | 0.68 |
| 40 | 1 | 3217.11 | 17.7 | 4118.64 | 17.4 | 3609.21 | 18 | 3648.32 | 12.39 | 17.70 | 0.30 |
| 40 | 0.5 | 2927.83 | 19.9 | 3705.15 | 21.6 | 3232.53 | 18.2 | 3288.50 | 11.91 | 19.90 | 1.70 |
| 40 | 0.1 | 2029.05 | 23.9 | 2707.46 | 25.4 | 2205.56 | 23.7 | 2314.02 | 15.21 | 24.33 | 0.93 |
| 70 | 25 | 2060.73 | 20.7 | 1247.86 | 70.9 | 1849.95 | 21.5 | 1719.51 | 24.53 | 37.70 | 28.75 |
| 70 | 10 | 1610.85 | 24.2 | 2915.78 | 12.1 | 1571.10 | 28 | 2032.58 | 37.64 | 21.43 | 8.30 |
| 70 | 5 | 1337.66 | 25.8 | 2298.03 | 17.2 | 1410.41 | 29.9 | 1682.04 | 31.79 | 24.30 | 6.48 |
| 70 | 1 | 821.79 | 29 | 1439.20 | 18.3 | 775.90 | 30.6 | 1012.30 | 36.59 | 25.97 | 6.69 |
| 70 | 0.5 | 623.50 | 30.9 | 1168.09 | 19.4 | 596.45 | 31.5 | 796.01 | 40.52 | 27.27 | 6.82 |
| 70 | 0.1 | 371.43 | 28.5 | 711.69 | 131.3 | 366.82 | 25.1 | 483.31 | 40.92 | 61.63 | 60.36 |
| 100 | 25 | 523.78 | 31.4 | 795.53 | 12.7 | 405.61 | 31.3 | 574.98 | 34.77 | 25.13 | 10.77 |
| 100 | 10 | 363.19 | 30.9 | 596.83 | 27.4 | 263.18 | 36.3 | 407.73 | 41.99 | 31.53 | 4.48 |
| 100 | 5 | 267.27 | 30.4 | 435.77 | 24.5 | 211.73 | 31.2 | 304.92 | 38.26 | 28.70 | 3.66 |
| 100 | 1 | 166.86 | 26.1 | 264.39 | 22 | 129.44 | 25.8 | 186.89 | 37.28 | 24.63 | 2.28 |
| 100 | 0.5 | 133.49 | 24.7 | 207.33 | 20 | 105.17 | 23.4 | 148.66 | 35.48 | 22.70 | 2.42 |
| 100 | 0.1 | 97.20 | 19.7 | 149.39 | 13.8 | 76.74 | 17.4 | 107.78 | 34.76 | 16.97 | 2.97 |
| 130 | 25 | 109.68 | 28.8 | 181.90 | 21.8 | 85.38 | 33.9 | 125.65 | 39.95 | 28.17 | 6.07 |
| 130 | 10 | 89.67 | 27.3 | 152.21 | 23.5 | 102.83 | 26.4 | 114.90 | 28.70 | 25.73 | 1.98 |
| 130 | 5 | 72.17 | 25.2 | 119.65 | 21 | 89.61 | 20.9 | 93.81 | 25.60 | 22.37 | 2.45 |
| 130 | 1 | 54.87 | 19.5 | 95.03 | 14.1 | 72.07 | 14.4 | 73.99 | 27.23 | 16.00 | 3.03 |
| 130 | 0.5 | 48.31 | 18.3 | 86.96 | 11.9 | 65.85 | 12.6 | 67.04 | 28.86 | 14.27 | 3.51 |
| 130 | 0.1 | 41.57 | 14.8 | 78.03 | 8.4 | 54.60 | 12.6 | 58.07 | 31.82 | 11.93 | 3.25 |

**TABLE A-7 Dynamic modulus summary sheet for NM 47 mix**

| Conditions | | Specimen 1 | | Specimen 2 | | Specimen 3 | | Modulus | | Phase Angle (Degrees) | |
|---|---|---|---|---|---|---|---|---|---|---|---|
| Temperature, °F | Frequency, Hz | Modulus, ksi | Phage Angle, degree | Modulus, ksi | Phage Angle, degree | Modulus, ksi | Phage Angle, degree | Avg. Modulus, ksi | CV, % | Avg. P. Angle, degree | Standard Dev, degree |
| 14 | 25 | 10217.35 | 8.6 | 10158.34 | 9.1 | 10080.17 | 8.8 | 10151.95 | 0.68 | 8.8 | 0.25 |
| 14 | 10 | 10826.92 | 4.9 | 10806.28 | 5.2 | 10679.04 | 6.0 | 10770.75 | 0.74 | 5.4 | 0.57 |
| 14 | 5 | 10579.59 | 4.8 | 10609.70 | 4.8 | 10575.24 | 5.5 | 10588.18 | 0.18 | 5.0 | 0.40 |
| 14 | 1 | 9751.84 | 3.8 | 9916.98 | 7.5 | 9448.73 | 7.9 | 9705.85 | 2.45 | 6.4 | 2.26 |
| 14 | 0.5 | 9653.52 | 3.9 | 9695.09 | 6.2 | 9488.42 | 7.0 | 9612.34 | 1.14 | 5.7 | 1.61 |
| 14 | 0.1 | 8338.66 | 7.7 | 8455.16 | 6.1 | 8420.89 | 5.9 | 8404.90 | 0.71 | 6.6 | 0.99 |
| 40 | 25 | 7141.06 | 13.7 | 7018.64 | 13.6 | 7065.77 | 13.3 | 7075.16 | 0.87 | 13.5 | 0.21 |
| 40 | 10 | 7254.77 | 11.4 | 7051.85 | 11.6 | 6917.11 | 11.7 | 7074.58 | 2.40 | 11.6 | 0.15 |
| 40 | 5 | 6717.58 | 11.9 | 6328.59 | 13.5 | 6406.31 | 12.2 | 6484.16 | 3.17 | 12.5 | 0.85 |
| 40 | 1 | 5419.91 | 15.6 | 5271.51 | 15.4 | 5281.23 | 13.6 | 5324.22 | 1.56 | 14.9 | 1.10 |
| 40 | 0.5 | 5145.54 | 18.8 | 4707.45 | 12.6 | 4770.47 | 20.9 | 4874.49 | 4.86 | 17.4 | 4.32 |
| 40 | 0.1 | 3704.90 | 21.3 | 3606.92 | 21.0 | 3488.79 | 21.5 | 3600.20 | 3.01 | 21.3 | 0.25 |
| 70 | 25 | 3505.37 | 20.8 | 2795.59 | 23.6 | 3317.05 | 22.6 | 3206.00 | 11.47 | 22.3 | 1.42 |
| 70 | 10 | 3191.96 | 21.1 | 2460.10 | 23.1 | 2762.17 | 23.1 | 2804.74 | 13.11 | 22.4 | 1.15 |
| 70 | 5 | 2779.13 | 22.6 | 2297.93 | 24.9 | 2364.73 | 24.6 | 2480.60 | 10.51 | 24.0 | 1.25 |
| 70 | 1 | 1913.27 | 23.8 | 1533.04 | 29.9 | 1561.48 | 28.5 | 1669.26 | 12.69 | 27.4 | 3.20 |
| 70 | 0.5 | 1513.63 | 25.4 | 1395.50 | 30.3 | 1313.79 | 28.8 | 1407.64 | 7.14 | 28.2 | 2.51 |
| 70 | 0.1 | 987.77 | 27.8 | 833.88 | 31.6 | 805.47 | 29.3 | 875.71 | 11.20 | 29.6 | 1.91 |
| 100 | 25 | 1062.20 | 34.6 | 1031.94 | 34.9 | 1010.77 | 35.5 | 1034.97 | 2.50 | 35.0 | 0.46 |
| 100 | 10 | 761.37 | 33.5 | 734.62 | 33.3 | 711.15 | 34.4 | 735.72 | 3.41 | 33.7 | 0.59 |
| 100 | 5 | 588.69 | 33.0 | 570.76 | 32.8 | 549.30 | 33.7 | 569.58 | 3.46 | 33.2 | 0.47 |
| 100 | 1 | 337.71 | 31.2 | 334.60 | 29.9 | 324.76 | 30.0 | 332.36 | 2.03 | 30.4 | 0.72 |
| 100 | 0.5 | 271.72 | 28.4 | 268.17 | 27.6 | 258.29 | 27.9 | 266.06 | 2.62 | 28.0 | 0.40 |
| 100 | 0.1 | 178.59 | 22.7 | 177.35 | 21.4 | 174.76 | 20.9 | 176.90 | 1.11 | 21.7 | 0.93 |
| 130 | 25 | 195.12 | 38.9 | 186.27 | 40.1 | 158.18 | 39.4 | 179.86 | 10.72 | 39.5 | 0.60 |
| 130 | 10 | 144.78 | 33.1 | 131.47 | 34.0 | 108.15 | 33.9 | 128.14 | 14.47 | 33.7 | 0.49 |
| 130 | 5 | 117.14 | 30.6 | 110.23 | 29.9 | 83.76 | 31.3 | 103.71 | 16.99 | 30.6 | 0.70 |
| 130 | 1 | 85.04 | 23.7 | 75.95 | 23.3 | 53.18 | 24.8 | 71.39 | 22.99 | 23.9 | 0.78 |
| 130 | 0.5 | 79.28 | 21.1 | 68.91 | 20.4 | 47.35 | 21.9 | 65.18 | 24.98 | 21.1 | 0.75 |
| 130 | 0.1 | 74.41 | 11.9 | 63.08 | 16.0 | 40.70 | 16.1 | 59.39 | 28.88 | 14.7 | 2.40 |

# APPENDIX B

**TABLE B-1 Beam fatigue test results for AC of I-25**

| Construction Site | Applied strain (με) | E (MPa) | $N_f$ |
|---|---|---|---|
| I-25 | 800 | 4182 | 7150 |
| | 800 | 4500 | 4450 |
| | 600 | 4886 | 8760 |
| | 600 | 4947 | 19640 |
| | 400 | 4875 | 17920 |
| | 400 | 5000 | 98551 |
| | 200 | 4916 | 114301 |
| | 200 | 5230 | 4621566 |

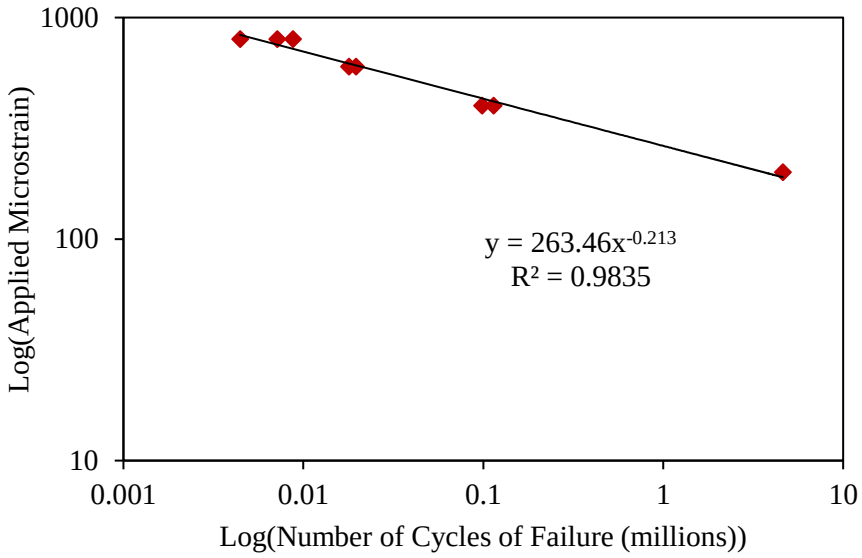


**FIGURE B-1 Log-log $\varepsilon$-$N_f$ curve of I-25 AC mixture**

**TABLE B-2 Beam fatigue test results for AC of US491 bottom layer**

| Construction Site | Applied strain (με) | E (MPa) | $N_f$ |
|---|---|---|---|
| US491 Bottom Layer | 800 | 5058 | 8250 |
| | 800 | 4125 | 9560 |
| | 600 | 5510 | 28504 |
| | 600 | 5236 | 38158 |
| | 400 | 4922 | 252451 |
| | 400 | 4922 | 320451 |
| | 200 | 5600 | 6986253 |
| | 200 | 4836 | 7889563 |

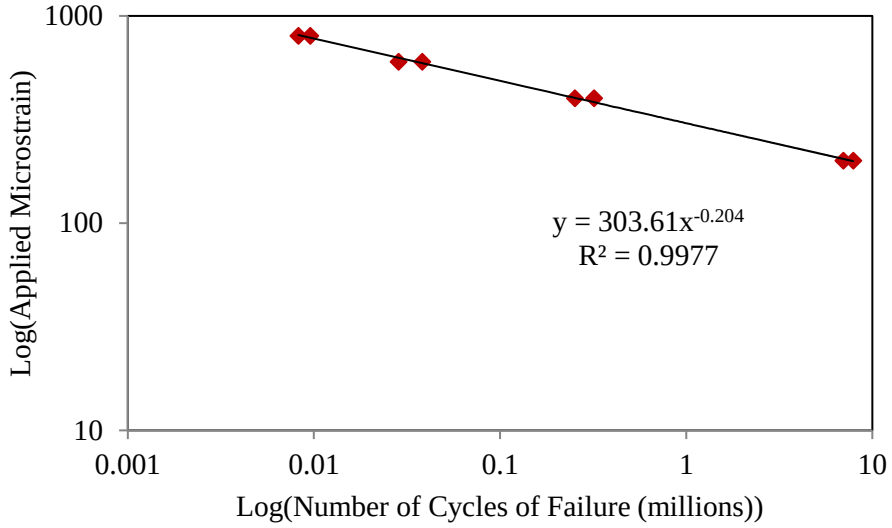


**FIGURE B-2 Log-log $\varepsilon$-$N_f$ curve of US491 bottom layer AC mixture**

**TABLE B-3 Beam fatigue test results for AC of US491 top layer**

| Construction Site | Applied strain (με) | E (Mpa) | $N_f$ |
|---|---|---|---|
| US491 Top Layer | 800 | 4563 | 8656 |
| | 800 | 4325 | 9060 |
| | 600 | 4824 | 29180 |
| | 600 | 4847 | 19012 |
| | 400 | 4568 | 361701 |
| | 400 | 4308 | 338750 |
| | 200 | 4565 | 7742450 |
| | 200 | 4582 | 6933751 |

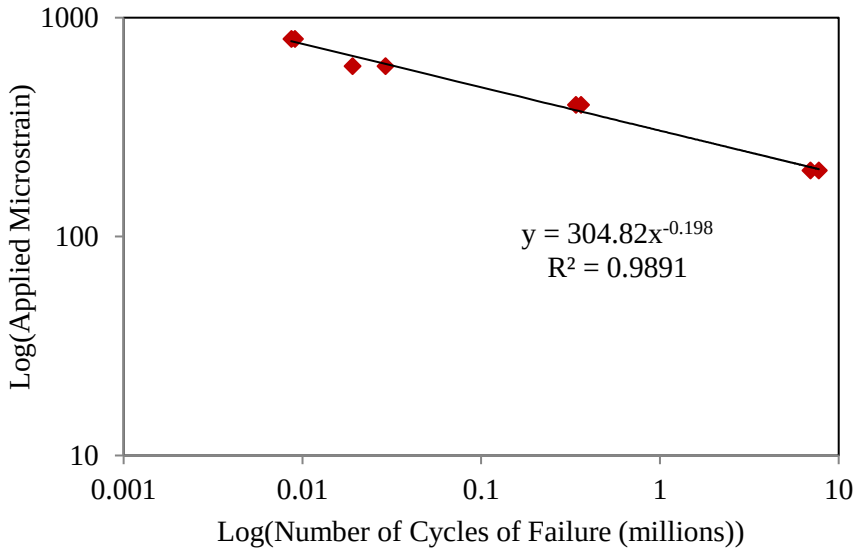


**FIGURE B-3 Log-log $\varepsilon$-$N_f$ curve of US491 top layer AC mixture**

**TABLE B-4 Beam fatigue test results for AC of NM47**

| Construction Site | Applied strain (με) | E (Mpa) | $N_f$ |
|---|---|---|---|
| NM47 | 800 | 1974 | 1795 |
| | 600 | 3307 | 5470 |
| | 600 | 6267 | 7525 |
| | 600 | 5647 | 13981 |
| | 400 | 5171 | 53251 |
| | 400 | 5500 | 103055 |
| | 400 | 6130 | 80604 |
| | 200 | 5054 | 4925651 |

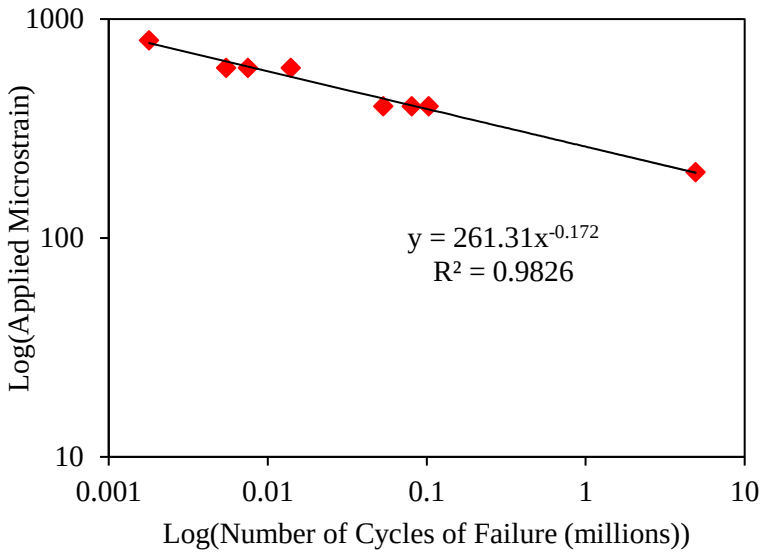


**FIGURE B-4 Log-log $\varepsilon$-$N_f$ curve of NM47 AC mixture**

# APPENDIX C

**TABLE C-1 Dynamic shear modulus test results for virgin PG 64-28 binder**

| Temperature | Angular Frequency | Complex Modulus | Phase Angle | Storage Modulus | Loss Modulus | Complex Viscosity |
|---|---|---|---|---|---|---|
| [°C] | [1/s] | [Pa] | [°] | [Pa] | [Pa] | [Pa·s] |
| 4.4 | 100 | 4.27E+07 | 4.08E+01 | 3.23E+07 | 2.79E+07 | 4.27E+05 |
| | 63.1 | 3.47E+07 | 4.26E+01 | 2.55E+07 | 2.35E+07 | 5.49E+05 |
| | 39.8 | 2.80E+07 | 4.43E+01 | 2.00E+07 | 1.96E+07 | 7.04E+05 |
| | 25.1 | 2.24E+07 | 4.61E+01 | 1.55E+07 | 1.61E+07 | 8.90E+05 |
| | 15.8 | 1.76E+07 | 4.79E+01 | 1.18E+07 | 1.31E+07 | 1.11E+06 |
| | 10 | 1.38E+07 | 4.96E+01 | 8.95E+06 | 1.05E+07 | 1.38E+06 |
| | 6.31 | 1.08E+07 | 5.13E+01 | 6.74E+06 | 8.40E+06 | 1.71E+06 |
| | 3.98 | 8.34E+06 | 5.29E+01 | 5.03E+06 | 6.65E+06 | 2.10E+06 |
| | 2.51 | 6.41E+06 | 5.44E+01 | 3.73E+06 | 5.22E+06 | 2.55E+06 |
| | 1.58 | 4.90E+06 | 5.60E+01 | 2.74E+06 | 4.06E+06 | 3.09E+06 |
| | 1 | 3.71E+06 | 5.75E+01 | 2.00E+06 | 3.13E+06 | 3.71E+06 |
| 13 | 100 | 1.41E+07 | 5.03E+01 | 9.02E+06 | 1.09E+07 | 1.41E+05 |
| | 63.1 | 1.09E+07 | 5.21E+01 | 6.68E+06 | 8.58E+06 | 1.72E+05 |
| | 39.8 | 8.30E+06 | 5.37E+01 | 4.91E+06 | 6.69E+06 | 2.09E+05 |
| | 25.1 | 6.34E+06 | 5.53E+01 | 3.61E+06 | 5.21E+06 | 2.52E+05 |
| | 15.8 | 4.76E+06 | 5.68E+01 | 2.61E+06 | 3.98E+06 | 3.00E+05 |
| | 10 | 3.55E+06 | 5.82E+01 | 1.87E+06 | 3.02E+06 | 3.55E+05 |
| | 6.31 | 2.63E+06 | 5.96E+01 | 1.33E+06 | 2.27E+06 | 4.17E+05 |
| | 3.98 | 1.94E+06 | 6.09E+01 | 9.41E+05 | 1.69E+06 | 4.86E+05 |
| | 2.51 | 1.43E+06 | 6.21E+01 | 6.66E+05 | 1.26E+06 | 5.67E+05 |
| | 1.58 | 1.04E+06 | 6.32E+01 | 4.67E+05 | 9.25E+05 | 6.54E+05 |
| | 1 | 7.52E+05 | 6.43E+01 | 3.27E+05 | 6.78E+05 | 7.52E+05 |
| 21.1 | 100 | 4.03E+06 | 5.90E+01 | 2.08E+06 | 3.45E+06 | 4.03E+04 |
| | 63.1 | 2.97E+06 | 6.04E+01 | 1.47E+06 | 2.58E+06 | 4.71E+04 |
| | 39.8 | 2.18E+06 | 6.16E+01 | 1.03E+06 | 1.91E+06 | 5.46E+04 |
| | 25.1 | 1.58E+06 | 6.28E+01 | 7.24E+05 | 1.41E+06 | 6.31E+04 |
| | 15.8 | 1.14E+06 | 6.39E+01 | 5.03E+05 | 1.03E+06 | 7.22E+04 |
| | 10 | 8.23E+05 | 6.50E+01 | 3.48E+05 | 7.46E+05 | 8.23E+04 |
| | 6.31 | 5.88E+05 | 6.59E+01 | 2.40E+05 | 5.37E+05 | 9.33E+04 |
| | 3.98 | 4.18E+05 | 6.68E+01 | 1.65E+05 | 3.85E+05 | 1.05E+05 |
| | 2.51 | 2.97E+05 | 6.77E+01 | 1.13E+05 | 2.75E+05 | 1.18E+05 |
| | 1.58 | 2.10E+05 | 6.84E+01 | 7.74E+04 | 1.95E+05 | 1.33E+05 |
| | 1 | 1.48E+05 | 6.91E+01 | 5.28E+04 | 1.38E+05 | 1.48E+05 |
| 29.5 | 100 | 1.07E+06 | 6.56E+01 | 4.42E+05 | 9.72E+05 | 1.07E+04 |
| | 63.1 | 7.59E+05 | 6.66E+01 | 3.01E+05 | 6.97E+05 | 1.20E+04 |
| | 39.8 | 5.41E+05 | 6.75E+01 | 2.07E+05 | 4.99E+05 | 1.36E+04 |

| | | | | | | |
|---|---|---|---|---|---|---|
| | 25.1 | 3.83E+05 | 6.83E+01 | 1.42E+05 | 3.56E+05 | 1.53E+04 |
| | 15.8 | 2.71E+05 | 6.91E+01 | 9.67E+04 | 2.53E+05 | 1.71E+04 |
| | 10 | 1.90E+05 | 6.98E+01 | 6.57E+04 | 1.78E+05 | 1.90E+04 |
| | 6.31 | 1.33E+05 | 7.05E+01 | 4.44E+04 | 1.25E+05 | 2.11E+04 |
| | 3.98 | 9.28E+04 | 7.12E+01 | 2.99E+04 | 8.79E+04 | 2.33E+04 |
| | 2.51 | 6.45E+04 | 7.19E+01 | 2.00E+04 | 6.13E+04 | 2.57E+04 |
| | 1.58 | 4.47E+04 | 7.27E+01 | 1.33E+04 | 4.27E+04 | 2.82E+04 |
| | 1 | 3.07E+04 | 7.36E+01 | 8.69E+03 | 2.95E+04 | 3.07E+04 |
| 37.8 | 100 | 3.02E+05 | 7.03E+01 | 1.02E+05 | 2.84E+05 | 3.02E+03 |
| | 63.1 | 2.10E+05 | 7.10E+01 | 6.84E+04 | 1.99E+05 | 3.33E+03 |
| | 39.8 | 1.46E+05 | 7.17E+01 | 4.59E+04 | 1.39E+05 | 3.67E+03 |
| | 25.1 | 1.02E+05 | 7.23E+01 | 3.09E+04 | 9.67E+04 | 4.04E+03 |
| | 15.8 | 7.02E+04 | 7.29E+01 | 2.06E+04 | 6.71E+04 | 4.43E+03 |
| | 10 | 4.83E+04 | 7.37E+01 | 1.36E+04 | 4.63E+04 | 4.83E+03 |
| | 6.31 | 3.30E+04 | 7.45E+01 | 8.84E+03 | 3.18E+04 | 5.23E+03 |
| | 3.98 | 2.26E+04 | 7.53E+01 | 5.75E+03 | 2.19E+04 | 5.68E+03 |
| | 2.51 | 1.54E+04 | 7.62E+01 | 3.66E+03 | 1.49E+04 | 6.12E+03 |
| | 1.58 | 1.04E+04 | 7.72E+01 | 2.30E+03 | 1.01E+04 | 6.54E+03 |
| | 1 | 7.05E+03 | 7.82E+01 | 1.44E+03 | 6.90E+03 | 7.05E+03 |
| 46.2 | 100 | 9.55E+04 | 7.43E+01 | 2.59E+04 | 9.19E+04 | 9.55E+02 |
| | 63.1 | 6.48E+04 | 7.40E+01 | 1.78E+04 | 6.23E+04 | 1.03E+03 |
| | 39.8 | 4.44E+04 | 7.47E+01 | 1.17E+04 | 4.28E+04 | 1.11E+03 |
| | 25.1 | 3.03E+04 | 7.55E+01 | 7.57E+03 | 2.93E+04 | 1.21E+03 |
| | 15.8 | 2.07E+04 | 7.64E+01 | 4.86E+03 | 2.01E+04 | 1.31E+03 |
| | 10 | 1.40E+04 | 7.73E+01 | 3.08E+03 | 1.37E+04 | 1.40E+03 |
| | 6.31 | 9.47E+03 | 7.82E+01 | 1.93E+03 | 9.27E+03 | 1.50E+03 |
| | 3.98 | 6.35E+03 | 7.94E+01 | 1.17E+03 | 6.24E+03 | 1.59E+03 |
| | 2.51 | 4.23E+03 | 8.06E+01 | 6.93E+02 | 4.17E+03 | 1.68E+03 |
| | 1.58 | 2.81E+03 | 8.14E+01 | 4.18E+02 | 2.78E+03 | 1.77E+03 |
| | 1 | 1.85E+03 | 8.25E+01 | 2.42E+02 | 1.83E+03 | 1.85E+03 |
| 54.5 | 100 | 3.46E+04 | 7.68E+01 | 7.92E+03 | 3.37E+04 | 3.46E+02 |
| | 63.1 | 2.25E+04 | 7.69E+01 | 5.11E+03 | 2.19E+04 | 3.57E+02 |
| | 39.8 | 1.51E+04 | 7.75E+01 | 3.28E+03 | 1.48E+04 | 3.80E+02 |
| | 25.1 | 1.01E+04 | 7.85E+01 | 2.02E+03 | 9.95E+03 | 4.04E+02 |
| | 15.8 | 6.77E+03 | 7.94E+01 | 1.24E+03 | 6.66E+03 | 4.27E+02 |
| | 10 | 4.49E+03 | 8.10E+01 | 7.05E+02 | 4.44E+03 | 4.49E+02 |
| | 6.31 | 2.98E+03 | 8.21E+01 | 4.10E+02 | 2.95E+03 | 4.72E+02 |
| | 3.98 | 1.96E+03 | 8.31E+01 | 2.36E+02 | 1.94E+03 | 4.92E+02 |
| | 2.51 | 1.29E+03 | 8.52E+01 | 1.07E+02 | 1.28E+03 | 5.12E+02 |
| | 1.58 | 8.42E+02 | 8.56E+01 | 6.46E+01 | 8.40E+02 | 5.31E+02 |
| | 1 | 5.42E+02 | 8.84E+01 | 1.50E+01 | 5.42E+02 | 5.42E+02 |

**TABLE C-2 Dynamic shear modulus test results for virgin PG 58-28 binder**

| Temperature | Angular Frequency | Complex Modulus | Phase Angle | Storage Modulus | Loss Modulus | Complex Viscosity |
|---|---|---|---|---|---|---|
| [°C] | [1/s] | [Pa] | [°] | [Pa] | [Pa] | [Pa·s] |
| 4.4 | 100 | 3.42E+07 | 4.14E+01 | 2.57E+07 | 2.26E+07 | 3.42E+05 |
| | 63.1 | 2.77E+07 | 4.33E+01 | 2.02E+07 | 1.90E+07 | 4.39E+05 |
| | 39.8 | 2.23E+07 | 4.51E+01 | 1.57E+07 | 1.58E+07 | 5.60E+05 |
| | 25.1 | 1.77E+07 | 4.69E+01 | 1.21E+07 | 1.29E+07 | 7.03E+05 |
| | 15.8 | 1.38E+07 | 4.88E+01 | 9.12E+06 | 1.04E+07 | 8.73E+05 |
| | 10 | 1.08E+07 | 5.06E+01 | 6.83E+06 | 8.32E+06 | 1.08E+06 |
| | 6.31 | 8.28E+06 | 5.25E+01 | 5.04E+06 | 6.57E+06 | 1.31E+06 |
| | 3.98 | 6.40E+06 | 5.43E+01 | 3.73E+06 | 5.19E+06 | 1.61E+06 |
| | 2.51 | 4.89E+06 | 5.60E+01 | 2.73E+06 | 4.05E+06 | 1.95E+06 |
| | 1.58 | 3.71E+06 | 5.78E+01 | 1.98E+06 | 3.14E+06 | 2.34E+06 |
| | 1 | 2.78E+06 | 5.95E+01 | 1.41E+06 | 2.40E+06 | 2.78E+06 |
| 13 | 100 | 1.07E+07 | 5.19E+01 | 6.58E+06 | 8.38E+06 | 1.07E+05 |
| | 63.1 | 8.23E+06 | 5.44E+01 | 4.80E+06 | 6.69E+06 | 1.31E+05 |
| | 39.8 | 6.23E+06 | 5.57E+01 | 3.50E+06 | 5.15E+06 | 1.56E+05 |
| | 25.1 | 4.69E+06 | 5.73E+01 | 2.54E+06 | 3.95E+06 | 1.87E+05 |
| | 15.8 | 3.46E+06 | 5.90E+01 | 1.79E+06 | 2.97E+06 | 2.19E+05 |
| | 10 | 2.58E+06 | 6.06E+01 | 1.27E+06 | 2.25E+06 | 2.58E+05 |
| | 6.31 | 1.89E+06 | 6.22E+01 | 8.81E+05 | 1.67E+06 | 2.99E+05 |
| | 3.98 | 1.37E+06 | 6.37E+01 | 6.08E+05 | 1.23E+06 | 3.44E+05 |
| | 2.51 | 9.90E+05 | 6.51E+01 | 4.16E+05 | 8.98E+05 | 3.94E+05 |
| | 1.58 | 7.14E+05 | 6.64E+01 | 2.86E+05 | 6.54E+05 | 4.50E+05 |
| | 1 | 5.14E+05 | 6.77E+01 | 1.95E+05 | 4.76E+05 | 5.14E+05 |
| 21.1 | 100 | 2.86E+06 | 6.15E+01 | 1.37E+06 | 2.52E+06 | 2.86E+04 |
| | 63.1 | 2.07E+06 | 6.31E+01 | 9.38E+05 | 1.85E+06 | 3.29E+04 |
| | 39.8 | 1.48E+06 | 6.46E+01 | 6.34E+05 | 1.34E+06 | 3.72E+04 |
| | 25.1 | 1.07E+06 | 6.60E+01 | 4.36E+05 | 9.78E+05 | 4.26E+04 |
| | 15.8 | 7.71E+05 | 6.72E+01 | 2.98E+05 | 7.11E+05 | 4.87E+04 |
| | 10 | 5.48E+05 | 6.85E+01 | 2.01E+05 | 5.10E+05 | 5.48E+04 |
| | 6.31 | 3.89E+05 | 6.96E+01 | 1.36E+05 | 3.64E+05 | 6.16E+04 |
| | 3.98 | 2.74E+05 | 7.06E+01 | 9.08E+04 | 2.59E+05 | 6.88E+04 |
| | 2.51 | 1.91E+05 | 7.17E+01 | 6.00E+04 | 1.81E+05 | 7.60E+04 |
| | 1.58 | 1.30E+05 | 7.27E+01 | 3.87E+04 | 1.24E+05 | 8.22E+04 |
| | 1 | 8.77E+04 | 7.37E+01 | 2.46E+04 | 8.42E+04 | 8.77E+04 |
| 29.5 | 100 | 6.99E+05 | 6.93E+01 | 2.47E+05 | 6.54E+05 | 6.99E+03 |
| | 63.1 | 4.93E+05 | 7.04E+01 | 1.66E+05 | 4.64E+05 | 7.81E+03 |
| | 39.8 | 3.46E+05 | 7.14E+01 | 1.10E+05 | 3.28E+05 | 8.69E+03 |
| | 25.1 | 2.38E+05 | 7.24E+01 | 7.18E+04 | 2.27E+05 | 9.47E+03 |
| | 15.8 | 1.64E+05 | 7.34E+01 | 4.68E+04 | 1.57E+05 | 1.03E+04 |

| | | | | | | |
|---|---|---|---|---|---|---|
| | 10 | 1.12E+05 | 7.43E+01 | 3.04E+04 | 1.08E+05 | 1.12E+04 |
| | 6.31 | 7.67E+04 | 7.52E+01 | 1.96E+04 | 7.41E+04 | 1.22E+04 |
| | 3.98 | 5.21E+04 | 7.61E+01 | 1.25E+04 | 5.06E+04 | 1.31E+04 |
| | 2.51 | 3.53E+04 | 7.70E+01 | 7.93E+03 | 3.44E+04 | 1.40E+04 |
| | 1.58 | 2.38E+04 | 7.80E+01 | 4.96E+03 | 2.33E+04 | 1.50E+04 |
| | 1 | 1.61E+04 | 7.89E+01 | 3.11E+03 | 1.58E+04 | 1.61E+04 |
| 37.8 | 100 | 1.85E+05 | 7.48E+01 | 4.85E+04 | 1.78E+05 | 1.85E+03 |
| | 63.1 | 1.24E+05 | 7.54E+01 | 3.13E+04 | 1.20E+05 | 1.97E+03 |
| | 39.8 | 8.36E+04 | 7.63E+01 | 1.98E+04 | 8.13E+04 | 2.10E+03 |
| | 25.1 | 5.63E+04 | 7.71E+01 | 1.25E+04 | 5.49E+04 | 2.24E+03 |
| | 15.8 | 3.81E+04 | 7.79E+01 | 7.96E+03 | 3.73E+04 | 2.40E+03 |
| | 10 | 2.57E+04 | 7.88E+01 | 4.98E+03 | 2.52E+04 | 2.57E+03 |
| | 6.31 | 1.72E+04 | 7.96E+01 | 3.09E+03 | 1.69E+04 | 2.72E+03 |
| | 3.98 | 1.14E+04 | 8.06E+01 | 1.86E+03 | 1.12E+04 | 2.86E+03 |
| | 2.51 | 7.47E+03 | 8.14E+01 | 1.12E+03 | 7.39E+03 | 2.97E+03 |
| | 1.58 | 4.93E+03 | 8.21E+01 | 6.77E+02 | 4.89E+03 | 3.11E+03 |
| | 1 | 3.22E+03 | 8.26E+01 | 4.12E+02 | 3.19E+03 | 3.22E+03 |
| 46.2 | 100 | 5.44E+04 | 7.81E+01 | 1.12E+04 | 5.33E+04 | 5.44E+02 |
| | 63.1 | 3.52E+04 | 7.86E+01 | 6.98E+03 | 3.45E+04 | 5.59E+02 |
| | 39.8 | 2.33E+04 | 7.96E+01 | 4.20E+03 | 2.29E+04 | 5.85E+02 |
| | 25.1 | 1.54E+04 | 8.06E+01 | 2.52E+03 | 1.52E+04 | 6.13E+02 |
| | 15.8 | 1.03E+04 | 8.13E+01 | 1.54E+03 | 1.01E+04 | 6.47E+02 |
| | 10 | 6.77E+03 | 8.24E+01 | 8.97E+02 | 6.71E+03 | 6.77E+02 |
| | 6.31 | 4.41E+03 | 8.32E+01 | 5.22E+02 | 4.37E+03 | 6.98E+02 |
| | 3.98 | 2.84E+03 | 8.40E+01 | 2.97E+02 | 2.82E+03 | 7.13E+02 |
| | 2.51 | 1.86E+03 | 8.50E+01 | 1.61E+02 | 1.85E+03 | 7.40E+02 |
| | 1.58 | 1.21E+03 | 8.38E+01 | 1.30E+02 | 1.21E+03 | 7.66E+02 |
| | 1 | 7.96E+02 | 8.44E+01 | 7.79E+01 | 7.92E+02 | 7.96E+02 |
| 54.5 | 100 | 1.97E+04 | 7.69E+01 | 4.46E+03 | 1.91E+04 | 1.97E+02 |
| | 63.1 | 1.16E+04 | 7.85E+01 | 2.31E+03 | 1.13E+04 | 1.83E+02 |
| | 39.8 | 7.48E+03 | 8.07E+01 | 1.21E+03 | 7.38E+03 | 1.88E+02 |
| | 25.1 | 4.86E+03 | 8.37E+01 | 5.35E+02 | 4.83E+03 | 1.94E+02 |
| | 15.8 | 3.11E+03 | 8.33E+01 | 3.65E+02 | 3.09E+03 | 1.96E+02 |
| | 10 | 1.97E+03 | 8.53E+01 | 1.60E+02 | 1.97E+03 | 1.97E+02 |
| | 6.31 | 1.30E+03 | 8.58E+01 | 9.57E+01 | 1.29E+03 | 2.06E+02 |
| | 3.98 | 8.35E+02 | 8.70E+01 | 4.42E+01 | 8.34E+02 | 2.10E+02 |
| | 2.51 | 5.30E+02 | 8.82E+01 | 1.70E+01 | 5.30E+02 | 2.11E+02 |
| | 1.58 | 3.52E+02 | 8.70E+01 | 1.86E+01 | 3.52E+02 | 2.22E+02 |
| | 1 | 2.00E+02 | 8.31E+01 | 2.41E+01 | 1.98E+02 | 2.00E+02 |

**TABLE C-3 Dynamic shear modulus test results for virgin PG 70-22 binder**

| Temperature | Angular Frequency | Complex Modulus | Phase Angle | Storage Modulus | Loss Modulus | Complex Viscosity |
|---|---|---|---|---|---|---|
| [°C] | [1/s] | [Pa] | [°] | [Pa] | [Pa] | [Pa·s] |
| 4.4 | 100 | 2.26E+07 | 3.44E+01 | 1.86E+07 | 1.28E+07 | 2.26E+05 |
| | 63.1 | 1.90E+07 | 3.49E+01 | 1.56E+07 | 1.09E+07 | 3.01E+05 |
| | 39.8 | 1.60E+07 | 3.52E+01 | 1.31E+07 | 9.23E+06 | 4.02E+05 |
| | 25.1 | 1.35E+07 | 3.56E+01 | 1.10E+07 | 7.83E+06 | 5.36E+05 |
| | 15.8 | 1.13E+07 | 3.59E+01 | 9.18E+06 | 6.64E+06 | 7.15E+05 |
| | 10 | 9.49E+06 | 3.63E+01 | 7.65E+06 | 5.61E+06 | 9.49E+05 |
| | 6.31 | 7.92E+06 | 3.67E+01 | 6.35E+06 | 4.73E+06 | 1.25E+06 |
| | 3.98 | 6.60E+06 | 3.71E+01 | 5.27E+06 | 3.98E+06 | 1.66E+06 |
| | 2.51 | 5.48E+06 | 3.76E+01 | 4.35E+06 | 3.34E+06 | 2.18E+06 |
| | 1.58 | 4.57E+06 | 3.81E+01 | 3.60E+06 | 2.82E+06 | 2.89E+06 |
| | 1 | 3.84E+06 | 3.86E+01 | 3.00E+06 | 2.39E+06 | 3.84E+06 |
| 13 | 100 | 9.48E+06 | 3.80E+01 | 7.47E+06 | 5.83E+06 | 9.48E+04 |
| | 63.1 | 7.81E+06 | 3.84E+01 | 6.12E+06 | 4.85E+06 | 1.24E+05 |
| | 39.8 | 6.45E+06 | 3.89E+01 | 5.02E+06 | 4.05E+06 | 1.62E+05 |
| | 25.1 | 5.33E+06 | 3.90E+01 | 4.14E+06 | 3.36E+06 | 2.12E+05 |
| | 15.8 | 4.39E+06 | 3.93E+01 | 3.39E+06 | 2.78E+06 | 2.77E+05 |
| | 10 | 3.61E+06 | 3.97E+01 | 2.78E+06 | 2.31E+06 | 3.61E+05 |
| | 6.31 | 2.96E+06 | 4.01E+01 | 2.27E+06 | 1.91E+06 | 4.70E+05 |
| | 3.98 | 2.43E+06 | 4.06E+01 | 1.84E+06 | 1.58E+06 | 6.10E+05 |
| | 2.51 | 1.99E+06 | 4.11E+01 | 1.50E+06 | 1.31E+06 | 7.91E+05 |
| | 1.58 | 1.62E+06 | 4.17E+01 | 1.21E+06 | 1.08E+06 | 1.02E+06 |
| | 1 | 1.32E+06 | 4.24E+01 | 9.78E+05 | 8.91E+05 | 1.32E+06 |
| 21.1 | 100 | 3.53E+06 | 4.24E+01 | 2.61E+06 | 2.38E+06 | 3.53E+04 |
| | 63.1 | 2.82E+06 | 4.27E+01 | 2.07E+06 | 1.91E+06 | 4.47E+04 |
| | 39.8 | 2.28E+06 | 4.31E+01 | 1.67E+06 | 1.56E+06 | 5.73E+04 |
| | 25.1 | 1.84E+06 | 4.34E+01 | 1.33E+06 | 1.26E+06 | 7.31E+04 |
| | 15.8 | 1.48E+06 | 4.39E+01 | 1.06E+06 | 1.02E+06 | 9.31E+04 |
| | 10 | 1.18E+06 | 4.43E+01 | 8.44E+05 | 8.23E+05 | 1.18E+05 |
| | 6.31 | 9.45E+05 | 4.48E+01 | 6.71E+05 | 6.66E+05 | 1.50E+05 |
| | 3.98 | 7.53E+05 | 4.54E+01 | 5.29E+05 | 5.36E+05 | 1.89E+05 |
| | 2.51 | 6.02E+05 | 4.61E+01 | 4.18E+05 | 4.34E+05 | 2.40E+05 |
| | 1.58 | 4.81E+05 | 4.68E+01 | 3.29E+05 | 3.50E+05 | 3.03E+05 |
| | 1 | 3.84E+05 | 4.76E+01 | 2.59E+05 | 2.83E+05 | 3.84E+05 |
| 29.5 | 100 | 1.20E+06 | 4.79E+01 | 8.08E+05 | 8.92E+05 | 1.20E+04 |
| | 63.1 | 9.44E+05 | 4.82E+01 | 6.29E+05 | 7.04E+05 | 1.50E+04 |
| | 39.8 | 7.43E+05 | 4.86E+01 | 4.91E+05 | 5.57E+05 | 1.87E+04 |
| | 25.1 | 5.81E+05 | 4.91E+01 | 3.81E+05 | 4.39E+05 | 2.31E+04 |
| | 15.8 | 4.54E+05 | 4.96E+01 | 2.94E+05 | 3.46E+05 | 2.86E+04 |

| | | | | | | |
|---|---|---|---|---|---|---|
| | 10 | 3.53E+05 | 5.02E+01 | 2.26E+05 | 2.71E+05 | 3.53E+04 |
| | 6.31 | 2.73E+05 | 5.09E+01 | 1.72E+05 | 2.12E+05 | 4.33E+04 |
| | 3.98 | 2.12E+05 | 5.17E+01 | 1.32E+05 | 1.66E+05 | 5.33E+04 |
| | 2.51 | 1.64E+05 | 5.26E+01 | 9.96E+04 | 1.30E+05 | 6.52E+04 |
| | 1.58 | 1.26E+05 | 5.35E+01 | 7.49E+04 | 1.01E+05 | 7.95E+04 |
| | 1 | 9.63E+04 | 5.46E+01 | 5.57E+04 | 7.85E+04 | 9.63E+04 |
| 37.8 | 100 | 3.96E+05 | 5.35E+01 | 2.36E+05 | 3.19E+05 | 3.96E+03 |
| | 63.1 | 3.01E+05 | 5.41E+01 | 1.77E+05 | 2.44E+05 | 4.77E+03 |
| | 39.8 | 2.30E+05 | 5.47E+01 | 1.33E+05 | 1.87E+05 | 5.77E+03 |
| | 25.1 | 1.74E+05 | 5.53E+01 | 9.90E+04 | 1.43E+05 | 6.93E+03 |
| | 15.8 | 1.32E+05 | 5.61E+01 | 7.35E+04 | 1.09E+05 | 8.30E+03 |
| | 10 | 9.91E+04 | 5.69E+01 | 5.41E+04 | 8.30E+04 | 9.91E+03 |
| | 6.31 | 7.43E+04 | 5.79E+01 | 3.95E+04 | 6.29E+04 | 1.18E+04 |
| | 3.98 | 5.52E+04 | 5.90E+01 | 2.84E+04 | 4.73E+04 | 1.39E+04 |
| | 2.51 | 4.09E+04 | 6.02E+01 | 2.03E+04 | 3.55E+04 | 1.63E+04 |
| | 1.58 | 3.01E+04 | 6.16E+01 | 1.43E+04 | 2.65E+04 | 1.90E+04 |
| | 1 | 2.22E+04 | 6.30E+01 | 1.01E+04 | 1.97E+04 | 2.22E+04 |
| 46.2 | 100 | 1.42E+05 | 5.94E+01 | 7.22E+04 | 1.22E+05 | 1.42E+03 |
| | 63.1 | 1.04E+05 | 5.98E+01 | 5.24E+04 | 9.00E+04 | 1.65E+03 |
| | 39.8 | 7.67E+04 | 6.04E+01 | 3.79E+04 | 6.67E+04 | 1.93E+03 |
| | 25.1 | 5.63E+04 | 6.12E+01 | 2.71E+04 | 4.94E+04 | 2.24E+03 |
| | 15.8 | 4.10E+04 | 6.22E+01 | 1.91E+04 | 3.62E+04 | 2.58E+03 |
| | 10 | 2.98E+04 | 6.34E+01 | 1.33E+04 | 2.66E+04 | 2.98E+03 |
| | 6.31 | 2.16E+04 | 6.47E+01 | 9.22E+03 | 1.95E+04 | 3.42E+03 |
| | 3.98 | 1.55E+04 | 6.62E+01 | 6.27E+03 | 1.42E+04 | 3.90E+03 |
| | 2.51 | 1.12E+04 | 6.76E+01 | 4.25E+03 | 1.03E+04 | 4.45E+03 |
| | 1.58 | 7.99E+03 | 6.92E+01 | 2.84E+03 | 7.47E+03 | 5.04E+03 |
| | 1 | 5.66E+03 | 7.07E+01 | 1.87E+03 | 5.34E+03 | 5.66E+03 |
| 54.5 | 100 | 5.54E+04 | 6.44E+01 | 2.39E+04 | 5.00E+04 | 5.54E+02 |
| | 63.1 | 3.91E+04 | 6.49E+01 | 1.66E+04 | 3.54E+04 | 6.20E+02 |
| | 39.8 | 2.82E+04 | 6.55E+01 | 1.17E+04 | 2.57E+04 | 7.08E+02 |
| | 25.1 | 2.02E+04 | 6.65E+01 | 8.04E+03 | 1.85E+04 | 8.04E+02 |
| | 15.8 | 1.44E+04 | 6.77E+01 | 5.46E+03 | 1.33E+04 | 9.08E+02 |
| | 10 | 1.02E+04 | 6.92E+01 | 3.60E+03 | 9.49E+03 | 1.02E+03 |
| | 6.31 | 7.13E+03 | 7.07E+01 | 2.36E+03 | 6.73E+03 | 1.13E+03 |
| | 3.98 | 4.97E+03 | 7.23E+01 | 1.51E+03 | 4.73E+03 | 1.25E+03 |
| | 2.51 | 3.42E+03 | 7.39E+01 | 9.52E+02 | 3.29E+03 | 1.36E+03 |
| | 1.58 | 2.34E+03 | 7.54E+01 | 5.89E+02 | 2.26E+03 | 1.48E+03 |
| | 1 | 1.58E+03 | 7.66E+01 | 3.66E+02 | 1.54E+03 | 1.58E+03 |

# APPENDIX D

**TABLE D-1 Resilient modulus test results for subgrade of US54N**

| | | Sample 1 | Sample 2 | Sample 3 |
|---|---|---|---|---|
| **Cell Pressure, psi** | **Deviator Stress, psi** | **Mr, ksi** | **Mr, ksi** | **Mr, ksi** |
| 6 | 2 | 14.3 | 16.3 | 16.8 |
| 6 | 4 | 14.8 | 17.5 | 17.1 |
| 6 | 6 | 16.1 | 18.1 | 17.6 |
| 6 | 8 | 16.5 | 18.6 | 18.5 |
| 6 | 10 | 17.2 | 19.2 | 19.8 |
| 4 | 2 | 8.2 | 11.8 | 10.1 |
| 4 | 4 | 8.3 | 12.1 | 10.8 |
| 4 | 6 | 8.7 | 13.6 | 13.2 |
| 4 | 8 | 9.1 | 14.2 | 14.6 |
| 4 | 10 | 11.2 | 15.8 | 14.8 |
| 2 | 2 | 8.1 | 9.8 | 9.4 |
| 2 | 4 | 9.8 | 10.4 | 9.9 |
| 2 | 6 | 10.4 | 11.9 | 12.2 |
| 2 | 8 | 12.2 | 13.2 | 14.1 |
| 2 | 10 | 14.6 | 15.7 | 15.3 |

**TABLE D-2 Resilient modulus test results for subgrade of US54S**

| | | Sample 1 | Sample 2 | Sample 3 |
|---|---|---|---|---|
| **Cell Pressure, psi** | **Deviator Stress, psi** | **Mr, ksi** | **Mr, ksi** | **Mr, ksi** |
| 6 | 2 | 21.7 | 21.5 | 19.6 |
| 6 | 4 | 22.1 | 21.8 | 20.3 |
| 6 | 6 | 22.8 | 22.9 | 21.7 |
| 6 | 8 | 23.6 | 23.3 | 22.3 |
| 6 | 10 | 24.8 | 24.1 | 23.1 |
| 4 | 2 | 17.4 | 17.1 | 17.9 |
| 4 | 4 | 19.2 | 18.9 | 19.3 |
| 4 | 6 | 20.4 | 19.4 | 20.5 |
| 4 | 8 | 21.8 | 20.1 | 22.1 |
| 4 | 10 | 22.1 | 21.9 | 22.8 |
| 2 | 2 | 16.1 | 15.7 | 15.1 |
| 2 | 4 | 16.7 | 17.1 | 17.7 |
| 2 | 6 | 17.5 | 18.5 | 18.8 |
| 2 | 8 | 18.6 | 19.1 | 18.9 |
| 2 | 10 | 20.3 | 19.9 | 21.1 |

**TABLE D-3 Resilient modulus test results for subgrade of US285**

| | | Sample 1 | Sample 2 | Sample 3 |
|---|---|---|---|---|
| **Cell Pressure, psi** | **Deviator Stress, psi** | **Mr, ksi** | **Mr, ksi** | **Mr, ksi** |
| 6 | 2 | 13.5 | 13.2 | 13.1 |
| 6 | 4 | 12.1 | 11.8 | 12.6 |
| 6 | 6 | 10.6 | 10.9 | 11.1 |
| 6 | 8 | 10.9 | 10.2 | 10.8 |
| 6 | 10 | 10.3 | 9.8 | 10.1 |
| 4 | 2 | 12.1 | 11.8 | 12.3 |
| 4 | 4 | 10.4 | 11.1 | 11.8 |
| 4 | 6 | 9.2 | 10.2 | 10.6 |
| 4 | 8 | 9.5 | 9.8 | 9.9 |
| 4 | 10 | 9.2 | 9.1 | 9.4 |
| 2 | 2 | 8.3 | 7.9 | 8.5 |
| 2 | 4 | 7.3 | 7.6 | 8.1 |
| 2 | 6 | 6.5 | 7.1 | 7.4 |
| 2 | 8 | 6.4 | 6.9 | 7.1 |
| 2 | 10 | 6.6 | 6.4 | 6.7 |

**TABLE D-4 Resilient modulus test results for subgrade of I-25**

| | | Sample 1 | Sample 2 | Sample 3 |
|---|---|---|---|---|
| **Cell Pressure, psi** | **Deviator Stress, psi** | **Mr, ksi** | **Mr, ksi** | **Mr, ksi** |
| 6 | 2 | 16.1 | 16.4 | 17.8 |
| 6 | 4 | 18.1 | 17.8 | 18.6 |
| 6 | 6 | 19.1 | 19.3 | 19.6 |
| 6 | 8 | 20.2 | 20.5 | 20.9 |
| 6 | 10 | 22.3 | 21.2 | 22.4 |
| 4 | 2 | 11.8 | 12.3 | 11.9 |
| 4 | 4 | 12.5 | 13.0 | 12.5 |
| 4 | 6 | 13.1 | 13.4 | 12.9 |
| 4 | 8 | 14.2 | 14.5 | 14.5 |
| 4 | 10 | 14.8 | 15.7 | 15.1 |
| 2 | 2 | 7.8 | 8.4 | 8.1 |
| 2 | 4 | 8.2 | 8.6 | 8.6 |
| 2 | 6 | 9.2 | 9.9 | 9.5 |
| 2 | 8 | 10.2 | 11.3 | 11.6 |
| 2 | 10 | 14.2 | 13.9 | 14.5 |

**TABLE D-5 Resilient modulus test results for subgrade of US491**

| | | Sample 1 | Sample 2 | Sample 3 |
|---|---|---|---|---|
| **Cell Pressure, psi** | **Deviator Stress, psi** | **Mr, ksi** | **Mr, ksi** | **Mr, ksi** |
| 6 | 2 | 13.7 | 13.2 | 14.1 |
| 6 | 4 | 15.3 | 15.1 | 15.6 |
| 6 | 6 | 16.6 | 16.8 | 16.0 |
| 6 | 8 | 17.3 | 18.0 | 17.8 |
| 6 | 10 | 17.9 | 16.9 | 17.7 |
| 4 | 2 | 13.2 | 12.8 | 13.4 |
| 4 | 4 | 14.3 | 13.9 | 13.8 |
| 4 | 6 | 15.5 | 15.3 | 14.8 |
| 4 | 8 | 16.5 | 16.2 | 16.7 |
| 4 | 10 | 17.5 | 17.8 | 17.3 |
| 2 | 2 | 12.5 | 12.9 | 13.0 |
| 2 | 4 | 13.5 | 14.0 | 13.8 |
| 2 | 6 | 14.8 | 14.5 | 14.2 |
| 2 | 8 | 16.0 | 16.3 | 16.8 |
| 2 | 10 | 17.2 | 17.8 | 18.0 |

**TABLE D-6 Resilient modulus test results for subgrade of NM14**

| | | Sample 1 | Sample 2 | Sample 3 |
|---|---|---|---|---|
| **Cell Pressure, psi** | **Deviator Stress, psi** | **Mr, ksi** | **Mr, ksi** | **Mr, ksi** |
| 6 | 2 | 10.3 | 10.3 | 11.3 |
| 6 | 4 | 12.3 | 12.3 | 12.2 |
| 6 | 6 | 13.2 | 12.7 | 13.1 |
| 6 | 8 | 15.0 | 13.0 | 15.0 |
| 6 | 10 | 15.6 | 13.4 | 16.0 |
| 4 | 2 | 9.0 | 8.7 | 8.8 |
| 4 | 4 | 11.0 | 9.3 | 10.1 |
| 4 | 6 | 13.6 | 14.1 | 12.0 |
| 4 | 8 | 14.2 | 15.0 | 14.1 |
| 4 | 10 | 16.0 | 16.7 | 15.2 |
| 2 | 2 | 7.4 | 7.7 | 7.5 |
| 2 | 4 | 8.7 | 8.2 | 8.0 |
| 2 | 6 | 10.2 | 9.9 | 11.1 |
| 2 | 8 | 13.0 | 12.1 | 130.5 |
| 2 | 10 | 16.5 | 16.0 | 15.8 |

**TABLE D-7 Resilient modulus test results for subgrade of NM47**

| | | Sample 1 | Sample 2 | Sample 3 |
|---|---|---|---|---|
| **Cell Pressure, psi** | **Deviator Stress, psi** | **Mr, ksi** | **Mr, ksi** | **Mr, ksi** |
| 6 | 2 | 9.6 | 13.0 | 12.5 |
| 6 | 4 | 13.6 | 17.2 | 16.0 |
| 6 | 6 | 15.4 | 18.4 | 17.8 |
| 6 | 8 | 16.5 | 19.5 | 19.4 |
| 6 | 10 | 17.1 | 20.2 | 20.6 |
| 4 | 2 | 8.2 | 10.7 | 10.9 |
| 4 | 4 | 11.4 | 14.2 | 13.6 |
| 4 | 6 | 14.3 | 17.3 | 16.8 |
| 4 | 8 | 15.7 | 19.0 | 19.0 |
| 4 | 10 | 16.0 | 19.7 | 20.4 |
| 2 | 2 | 6.7 | 9.3 | 9.2 |
| 2 | 4 | 9.8 | 13.1 | 12.3 |
| 2 | 6 | 12.8 | 16.4 | 15.7 |
| 2 | 8 | 20.5 | 18.3 | 18.3 |
| 2 | 10 | 21.1 | 19.0 | 19.7 |

**TABLE D-8 Resilient modulus test results for base of US54N**

| | | Sample 1 | Sample 2 | Sample 3 |
|---|---|---|---|---|
| **Cell Pressure, psi** | **Deviator Stress, psi** | **Mr, ksi** | **Mr, ksi** | **Mr, ksi** |
| 3 | 3 | 14.7 | 17.8 | 15.2 |
| 3 | 6 | 15.4 | 18.1 | 17.1 |
| 3 | 9 | 17.1 | 19.6 | 18.7 |
| 5 | 5 | 15.2 | 18.2 | 16.8 |
| 5 | 10 | 18.4 | 20.7 | 20.1 |
| 5 | 15 | 22.2 | 22.8 | 22.2 |
| 10 | 10 | 19.4 | 22.1 | 20.8 |
| 10 | 20 | 24.9 | 32.6 | 28.9 |
| 10 | 30 | 29.4 | 38.2 | 33.6 |
| 15 | 10 | 21.2 | 24.8 | 25.2 |
| 15 | 15 | 23.3 | 27.3 | 26.8 |
| 15 | 30 | 32.2 | 40.1 | 36.6 |
| 20 | 15 | 24.5 | 26.3 | 27.3 |
| 20 | 20 | 30.6 | 31.5 | 32.4 |

**TABLE D-9 Resilient modulus test results for base of US54S**

| | | Sample 1 | Sample 2 | Sample 3 |
|---|---|---|---|---|
| **Cell Pressure, psi** | **Deviator Stress, psi** | **Mr, ksi** | **Mr, ksi** | **Mr, ksi** |
| 3 | 3 | 14.4 | 13.7 | 14.2 |
| 3 | 6 | 15.1 | 15.6 | 15.7 |
| 3 | 9 | 17.6 | 18.2 | 17.9 |
| 5 | 5 | 15.9 | 16.1 | 16.3 |
| 5 | 10 | 18.9 | 20.3 | 19.6 |
| 5 | 15 | 23.2 | 23.8 | 24.2 |
| 10 | 10 | 20.6 | 22.9 | 21.2 |
| 10 | 20 | 29.9 | 30.1 | 30.8 |
| 10 | 30 | 32.4 | 33.7 | 32.9 |
| 15 | 10 | 23.2 | 24.6 | 25.3 |
| 15 | 15 | 26.5 | 26.5 | 26.9 |
| 15 | 30 | 35.2 | 36.7 | 36.5 |
| 20 | 15 | 29.4 | 28.2 | 28.1 |
| 20 | 20 | 44.4 | 41.9 | 42.2 |

**TABLE D-10 Resilient modulus test results for base of US285**

| | | Sample 1 | Sample 2 | Sample 3 |
|---|---|---|---|---|
| **Cell Pressure, psi** | **Deviator Stress, psi** | **Mr, ksi** | **Mr, ksi** | **Mr, ksi** |
| 3 | 3 | 13.1 | 15.2 | 14.6 |
| 3 | 6 | 16.1 | 18.1 | 17.8 |
| 3 | 9 | 18.9 | 21.4 | 20.3 |
| 5 | 5 | 15.7 | 16.6 | 16.7 |
| 5 | 10 | 20.4 | 22.9 | 20.9 |
| 5 | 15 | 28.1 | 30.1 | 29.8 |
| 10 | 10 | 22.5 | 23.1 | 23.2 |
| 10 | 20 | 32.7 | 35.5 | 35.8 |
| 10 | 30 | 38.6 | 39.2 | 40.1 |
| 15 | 10 | 22.1 | 21.1 | 21.5 |
| 15 | 15 | 27.3 | 28.3 | 27.9 |
| 15 | 30 | 41.3 | 43.3 | 42.2 |
| 20 | 15 | 28.5 | 30.5 | 29.6 |
| 20 | 20 | 39.2 | 42.2 | 42.1 |

**TABLE D-11 Resilient modulus test results for base of I-25**

| | | Sample 1 | Sample 2 | Sample 3 |
|---|---|---|---|---|
| **Cell Pressure, psi** | **Deviator Stress, psi** | **Mr, ksi** | **Mr, ksi** | **Mr, ksi** |
| 3 | 3 | 14.8 | 10.8 | 13.6 |
| 3 | 6 | 17.2 | 14.6 | 16.3 |
| 3 | 9 | 19.8 | 18.3 | 19.3 |
| 5 | 5 | 18.3 | 15.4 | 17.8 |
| 5 | 10 | 23.2 | 20.8 | 20.9 |
| 5 | 15 | 24.5 | 23 | 24.3 |
| 10 | 10 | 26.6 | 24.1 | 25.9 |
| 10 | 20 | 30.3 | 31.6 | 31.8 |
| 10 | 30 | 37.2 | 38.2 | 39.2 |
| 15 | 10 | 28.7 | 27.5 | 27.9 |
| 15 | 15 | 35.3 | 29.2 | 32.5 |
| 15 | 30 | 43.3 | 35.6 | 39.8 |
| 20 | 15 | 37.9 | 33.3 | 36.1 |
| 20 | 20 | 42.9 | 40.6 | 41.5 |

**TABLE D-12 Resilient modulus test results for base of US491**

| | | Sample 1 | Sample 2 | Sample 3 |
|---|---|---|---|---|
| **Cell Pressure, psi** | **Deviator Stress, psi** | **Mr, ksi** | **Mr, ksi** | **Mr, ksi** |
| 3 | 3 | 12.3 | 12 | 11.5 |
| 3 | 6 | 12.5 | 13.2 | 12.7 |
| 3 | 9 | 13.4 | 13.9 | 13.8 |
| 5 | 5 | 13.6 | 14.9 | 15.4 |
| 5 | 10 | 15.4 | 16.7 | 17.8 |
| 5 | 15 | 17.9 | 20.2 | 20 |
| 10 | 10 | 20.5 | 22.6 | 23.2 |
| 10 | 20 | 22.8 | 24.1 | 25.6 |
| 10 | 30 | 24.5 | 25.8 | 26.3 |
| 15 | 10 | 23.8 | 26.1 | 27.6 |
| 15 | 15 | 25.4 | 26.8 | 28.3 |
| 15 | 30 | 28.6 | 29.8 | 30.7 |
| 20 | 15 | 28.0 | 33.5 | 33.3 |
| 20 | 20 | 34.0 | 36.1 | 35.7 |

**TABLE D-13 Resilient modulus test results for base of NM14**

| | | Sample 1 | Sample 2 | Sample 3 |
|---|---|---|---|---|
| **Cell Pressure, psi** | **Deviator Stress, psi** | **Mr, ksi** | **Mr, ksi** | **Mr, ksi** |
| 3 | 3 | 12.1 | 12.5 | 12.3 |
| 3 | 6 | 14.8 | 15.7 | 14.4 |
| 3 | 9 | 17.8 | 18.4 | 18.1 |
| 5 | 5 | 16.9 | 16.9 | 17.0 |
| 5 | 10 | 20.8 | 20.8 | 20.3 |
| 5 | 15 | 23.8 | 25.0 | 24.8 |
| 10 | 10 | 25.6 | 25.0 | 24.9 |
| 10 | 20 | 29.8 | 29.0 | 28.9 |
| 10 | 30 | 36.0 | 35.1 | 35.3 |
| 15 | 10 | 28.6 | 27.0 | 27.8 |
| 15 | 15 | 34.5 | 33.7 | 33.9 |
| 15 | 30 | 40.3 | 38.8 | 39.4 |
| 20 | 15 | 37.9 | 36.4 | 36.2 |
| 20 | 20 | 39.2 | 38.0 | 39.0 |

**TABLE D-14 Resilient modulus test results for base of NM47**

| | | Sample 1 | Sample 2 |
|---|---|---|---|
| **Cell Pressure, psi** | **Deviator Stress, psi** | **Mr, ksi** | **Mr, ksi** |
| 3 | 3 | 11.3 | 10.3 |
| 3 | 6 | 15.9 | 16.1 |
| 3 | 9 | 20.3 | 19.2 |
| 5 | 5 | 15.7 | 16.3 |
| 5 | 10 | 22.2 | 21.5 |
| 5 | 15 | 25.3 | 24.6 |
| 10 | 10 | 23.8 | 23.8 |
| 10 | 20 | 27.3 | 28.5 |
| 10 | 30 | 35.9 | 35.1 |
| 15 | 10 | 29.3 | 28.3 |
| 15 | 15 | 35.6 | 36.1 |
| 15 | 30 | 40.3 | 39.9 |
| 20 | 15 | 38.3 | 38.2 |
| 20 | 20 | 39.2 | 40.0 |

# APPENDIX E

**Important Field Notes**

Several crucial issues have been observed in some of the selected pavement construction sites during field testing and materials collection that needs to be documented for future use. Figure E-1 shows the compacted base course of US491 construction site. It was observed that even though the base course was compacted to the optimum level, the materials looked very loose. When the field Clegg Hammer test was performed on it, it was noticed that the base course was crushing easily. It might be an issue for the early failure of the pavement.

**FIGURE E-1 Compacted base course of US491**

Similar compaction issue was also observed on the subgrade and base course of NM47 construction site. Figure E-2 shows the compacted subgrade and base course of NM47 construction site. It is seen from Figure E-2 that the subgrade and base course materials are not well compacted. In addition, the subgrade layer does not seem to be very even.


(a) Compacted subgrade (b) Compacted base

**FIGURE E-2 Compacted subgrade and base of NM47**


New Mexico Department of Transportation
RESEARCH BUREAU
7500B Pan American Freeway NE
PO Box 94690
Albuquerque, NM 87199-4690
Tel: (505) 841-9145